MODELING, ANALYSIS AND DESIGN OF FIXED FREQUENCY SERIES-PARALLEL RESONANT DC/DC CONVERTERS USING THE EXTENDED DESCRIBING FUNCTION METHOD

JI XIE

Modeling, Analysis and Design of Fixed Frequency Series-Parallel Resonant DC/DC Converters Using the Extended Describing Function Method

By

© Ji Xie

A thesis submitted to the School of Graduate Studies

in partial fulfillment of the requirements for the degree of

Master of Engineering

Faculty of Engineering and Applied Science

Memorial University of Newfoundland

November, 1999

St. John's Newfoundland Canada

Abstract

The fixed frequency series-parallel resonant dc/dc converter is used in high current and low voltage power supplies in telecommunication applications. The frequency domain analysis technique has been the preferred method for the modeling and analysis of the converter. However, the modeling and analysis technique results in a complex set of equations from which it is difficult to establish systematic design procedure for selecting the component values of the converter.

This thesis proposes a generalized modeling, analysis and design approach of the fixed frequency series-parallel resonant dc/dc converter. A systematic approach to modeling the behavior of the converter based on extended describing function technique is presented. By employing this technique, both continuous-time large-signal and small-signal models of the converter are developed. A new set of design criterion and procedure aimed at minimizing the cost and size of the converter is developed from the large-signal model. A design example is presented to illustrate the use of the design procedure. Finally, a Pspice implementation of the converter is provided to validate the extended describing function technique.

Acknowledgement

I wish to thank my supervisor, Dr. John E. Quaicoe, for his invaluable advice and financial support. I extend my thanks to the School of Graduate Studies and Faculty of Engineering and Applied Science for providing the financial support, in the form of Graduate Fellowship and Teaching assistantships, which made this thesis possible.

I thank all my colleagues and friends for the useful discussions and suggestions. Special thanks go to the C-CAE staff for providing great help in solving computer-related problems.

Finally, I would like to take this chance to express my profound gratitude to my family for their continuous encouragement and help during my studies in Memorial University of Newfoundland.

Contents

Abstract i

Acknowledgement ii

Contents iii

List of Symbols vii

List of Figures x

List of Tables xx

Chapter 1 Introduction 1

1.1 PWM DC/DC Converters 2

1.2 Resonant DC/DC Converters 4

1.2.1 Series Resonant Converter 5

1.2.2 Parallel Resonant Converter 7

1.2.3 Series-Parallel Resonant Converter 8

1.3 Modeling and Analysis of Resonant Converters 9

1.4 Thesis Objective and Outline 11

Chapter 2 Extended Describing Function Analysis of Fixed- Frequency Series Parallel Resonant Converters 14

2.1 Circuit Description and Operating Principle 14

2.1.1 The Series-Parallel Resonant Converter with a Two-winding HF Transformer 15

2.1.2 The Series-Parallel Resonant Converters with a Three-winding HF Transformer 16

Equivalent Circuit Models of the Series-Parallel Resonant DC/DC Converters 19

2.1.4 Ideal Circuit Waveforms of the Series-Parallel Resonant DC/DC Converter 21

2.2 Extended Describing Function Modeling of the Converter 22

2.2.1 Assumptions 22

2.2.2 State-space Approach Analysis 23

2.2.3 Extended Describing Function Concept [32] 24

2.2.4 Model of the Series-Parallel Resonant DC/DC Converter Using the Extended Describing Function 27

2.2.5 Steady-State Solution 31

2.3 Small-Signal Modeling of the Series-Parallel Resonant converter 31

2.3.1 Perturbation and linearization 32

2.3.2 Circuit Implementation of Small-Signal Model 33

2.4 Summary 34

Chapter 3 Steady-State Performance of the Series-Parallel Resonant DC/DC Converter 36

3.1 Frequency-domain Analysis 36

3.1.1 Control Parameters 37

3.2 Characteristics of the Fixed Frequency Series-Parallel Converter 38

3.2.1 Steady-state Waveforms 38

3.2.2 Effect of Control Parameters on the Output Voltage and State Variables of the Converter 47

3.3 Pspice Software Simulation 52

3.3.1 Pspice Simulation of the Converter with Tuned Series Branch 54

3.3.2 Simulation of the Converter with Inductive Series Branch 60

3.3.3 Simulation of the Converter with Capacitive Series Branch 63

3.4 Summary 66

Chapter 4 Design of the Series-Parallel Resonant DC/DC Converters 67

4.1 Development of Design Equations 67

4.2 Performance of the Converter as a Function of the Resonant Circuit Parameters 70

4.2.1 Effect of Resonant Circuit Parameters on the KVA/KW Rating 70

4.2.2 Effect of Resonant Circuit Parameters on the Voltage Transfer Ratio, Transformer Primary Voltage, and Series Resonant Circuit Current 78

4.2.3 Effect of the Resonant Circuit Parameters on the Peak Voltage across the Series Capacitor 86

4.3 Design Procedure 93

4.4 Design Examples 94

4.5 Design Verifications Using Pspice 100

4.6 Summary 101

Chapter 5 Conclusion 102

5.1 Summary 102

5.2 Recommendations for Future Work 103

References **105**

Appendix A Frequency Domain Analysis of the Series-Parallel Resonant DC/DC Converter **110**

Waveforms of the Series-Parallel Resonant DC/DC Converter Using Two-Winding HF Transformer **114**

Design Plots of the Series-Parallel Resonant DC/DC Converter with $\delta = 175^{\circ}$ **116**

List of Symbols

L_{in}	Input filter inductor
L_o	Output filter inductor
L_s	Inductor at the series branch
L_p	Inductor at the parallel branch
L_{pr}	Primary leakage inductance of matching transformer
L_{se}	Secondary leakage inductance of matching transformer
L_t	Tertiary leakage inductance of matching transformer
C_{in}	Input filter capacitor
C_o	Output filter capacitor
C_1-C_4	Snubber capacitors of the input inverter
C_s	Capacitor at the series branch
C_p	Capacitor at the parallel branch
R_L	Load resistance
R_b	Load resistance reflected to the primary circuit
D_1-D_4	Inverter diodes
S_1-S_4	Inverter MOSFETs
f_s	Switching frequency
ω_{rs}	Angular resonant frequency of the series branch

ω_{rp} Angular resonant frequency of the parallel branch

ω_{sn} Normalized series branch angular resonant frequency

ω_{pn} Normalized parallel branch angular resonant frequency

Z_{rs} Characteristic impedance of the series branch

Z_{rp} Characteristic impedance of the parallel branch

Z_{sn} Normalized characteristic impedance of the series branch

Z_{pn} Normalized characteristic impedance of the parallel branch

V_{in} DC input voltage to the inverter

V_o Output dc voltage

v_s Quasi-square wave input to the resonant circuit

v_{cs} Voltage across the series branch capacitor

V_{csm} The peak value of v_{cs}

v_{css} The sine term of the fundament component of v_{cs}

v_{csc} The cosine term of the fundament component of v_{cs}

v_p Voltage across the primary side of the transformer

V_{pm} The peak value of v_p

v_{cp} Voltage across the parallel branch capacitor

v_{cps} The sine term of the fundament component of v_{cp}

v_{cpc} The cosine term of the fundament component of v_{cp}

i_{Ls} Current flowing through the series branch inductor

I_{sm} The peak value of i_{Ls}

i_{Lss} The sine term of the fundament component of i_{Ls}

i_{Lsc} The cosine term of the fundament component of i_{Ls}

i_{Lp} Current flowing through the parallel branch inductor

i_{Lps} The sine term of the fundament component of the i_{Lp}

i_{Lpc} The cosine term of the fundament component of the i_{Lp}

I_o Output dc current

I_{op} The magnitude of the output current referred to the primary

X_{Lsn} Normalized reactance of the series branch inductor

X_{csn} Normalized reactance of the series branch capacitor

X_{Lpn} Normalized reactance of the parallel branch inductor

X_{cpn} Normalized reactance of the parallel branch capacitor

X_{Ltn} Normalized tertiary leakage reactance

X_{Lsepn} Normalized primary leakage reactance

X_{Lse} Reactance of the secondary leakage at the secondary side

X_{Lt} Reactance of the tertiary leakage at the tertiary side

X_{Lsep} Equivalent reactance of the secondary leakage at the primary side

X_{Ltp} Equivalent reactance of the tertiary leakage at the primary side

P_o Output power

δ Pulse width

ϕ Phase shift between v_p and v_s

μ Commutation angle

List of Figures

Figure 1.1: Basic PWM dc/dc converter topology 2

Figure 1.2: The block diagram of the load resonant converter 4

Figure 1.3: Full-bridge series resonant dc/dc converter 5

Figure 1.4: Full-bridge parallel resonant dc/dc converter 7

Figure 1.5: Full-bridge series-parallel resonant dc/dc converter 8

Figure 2.1: Basic circuit diagram of the series-parallel resonant dc/dc converter using two-winding HF transformer 17

Figure 2.2: Basic circuit diagram of the series-parallel resonant dc/dc converter using three-winding HF transformer 18

Figure 2.3: Primary side equivalent circuit of the series-parallel resonant dc/dc converter using two-winding transformer 19

Figure 2.4: Primary side equivalent circuit of the series-parallel resonant converter with a three-winding HF transformer 20

Figure 2.5: Typical steady-state waveforms of the series-parallel resonant dc/dc converter 21

Figure 2.6: Equivalent circuit of the series-parallel resonant converter with state variables referred to the primary side 23

Figure 2.7: The traditional describing function concept 26

Figure 2.8: Extended describing function concept 27

Figure 2.9: Circuit implementation of the small-signal model of the converter 35

Figure 3.1: Simulated waveforms of the converter with tuned series and parallel branches, K_l=2, (a) Frequency-domain analysis, (b) Extended describing function method 41

Figure 3.2: Simulated waveforms of the converter with tuned series and parallel branches, K_l=4, (a) Frequency-domain analysis, (b) Extended describing function method 42

Figure 3.3: Simulated waveforms of the converter with capacitive parallel branch, K_l=2, (a) Frequency-domain analysis, (b) Extended describing function method 43

Figure 3.4: Simulated waveforms of the converter with inductive parallel branch, K_l=2 (a) Frequency-domain analysis, (b) Extended describing function method 44

Figure 3.5: Simulated waveforms of the converter with larger leakage inductance, K_l=2, (a) Frequency-domain analysis, (b) Extended describing function method 45

Figure 3.6: Effect of leakage inductance on the output voltage for tuned series and parallel branches 49

Figure 3.7: Effect of leakage inductance on the output voltage for tuned series and capacitive parallel branch 49

Figure 3.8: Effect of leakage inductance on output voltage for inductive, tuned, and capacitive series branch 50

Figure 3.9: Effect of leakage inductance on the phase shift between v_P and v_s for inductive, tuned and capacitive series branch 50

Figure 3.10: Effect of leakage inductance on the commutation angle for inductive, tuned, and capacitive series branch 51

Figure 3.11: Effect of pulse width on the output voltage for inductive, tuned, and capacitive series branch 51

Figure 3.12: Pspice simulation model of the dc/dc converter 53

Figure 3.13: The Pspice model of an ideal transformer 53

Figure 3.14: Pspice simulation result of the load current $K_s = 1$ 56

Figure 3.15: Pspice simulation result of the inverter output voltage $K_s = 1$ 56

Figure 3.16: Pspice simulation result of the series resonant circuit current i_s $K_s = 1$ 57

Figure 3.17: Predicted series resonant circuit current i_s, using the EDF method $K_s = 1$ 57

Figure 3.18: Pspice simulation result of the primary side voltage v_p $K_s = 1$ 58

Figure 3.19: Predicted primary side voltage v_p, using the EDF method $K_s = 1$ 58

Figure 3.20: Pspice simulation result of the primary side voltage v_p $K_s = 0.6$ 61

Figure 3.21: Predicted primary voltage v_p, using the EDF method $K_s = 0.6$ 61

Figure 3.22: Pspice simulation result of the series resonant circuit current i_s $K_s = 0.6$ 62

Figure 3.23: Predicted series resonant circuit current i_s, using the EDF method

$K_s = 0.6$ 62

Figure 3.24: Pspice simulation result of the series resonant circuit current i_s

$K_s = 1.4$ 64

Figure 3.25: Predicted series resonant circuit current i_s, using the EDF method

$K_s = 1.4$ 64

Figure 3.26: Pspice simulation result of the primary side voltage v_p

$K_s = 1.4$ 65

Figure 3.27: Predicted primary side voltage v_p, using the EDF method

$K_s = 1.4$ 65

Figure 4.1: KVA/KW rating versus normalized frequency, ω_{sn}

$\delta = 120°$, X_{Lsepn}=0, X_{Ltn}=0.2p.u.

(a) Z_{pn}=1.5, (b) Z_{pn}=2.5 72

Figure 4.2: KVA/KW rating versus normalized frequency, ω_{sn}

$\delta = 120°$, X_{Lsepn}=0, X_{Ltn}=0.2p.u.

(a) Z_{pn}=3.5, (b) Z_{pn}=4.5 73

Figure 4.3: KVA/KW rating versus normalized frequency, ω_{sn}

$\delta = 120°$, X_{Lsepn}=0.2p.u., X_{Ltn}=0.2p.u.

(a) Z_{pn}=1.5, (b) Z_{pn}=2.5 74

Figure 4.4: KVA/KW rating versus normalized frequency, ω_{sn}

$\delta = 120°$, X_{Lsepn}=0.2p.u., X_{Ltn}=0.2p.u.

(a) Z_{pn}=3.5, (b) Z_{pn}=4.5 75

Figure 4.5: KVA/KW rating versus normalized frequency, ω_{sn}

$\delta = 120°$, X_{Lsepn}=0.4p.u., X_{Lm}=0.2p.u.

(a) Z_{pn}=1.5, (b) Z_{pn}=2.5 76

Figure 4.6: KVA/KW rating versus normalized frequency, ω_{sn}

$\delta = 120°$, X_{Lsepn}=0.4p.u., X_{Lm}=0.2p.u.

(a) Z_{pn}=3.5, (b) Z_{pn}=4.5 77

Figure 4.7: Resonant current i_s versus normalized frquency, ω_{sn}

$\delta = 120°$, X_{Lsepn}=0, X_{Lm}=0.2p.u, Z_{pn}=1.5 79

Figure 4.8: Primary side voltage, v_p versus normalized frequency, ω_{sn}

$\delta = 120°$, X_{Lsepn}=0, X_{Lm}=0.2p.u, Z_{pn}=1.5 79

Figure 4.9: Voltage transfer ratio, M versus normalized frequency, ω_{sn}

$\delta = 120°$, X_{Lsepn}=0, X_{Lm}=0.2p.u.

(a) Z_{pn}=1.5, (b) Z_{pn}=2.5 80

Figure 4.10: Voltage transfer ratio, M versus normalized frequency, ω_{sn}

$\delta = 120°$, X_{Lsepn}=0, X_{Lm}=0.2p.u.

(a) Z_{pn}=3.5, (b) Z_{pn}=4.5 81

Figure 4.11: Voltage transfer ratio, M versus normalized frequency, ω_{sn}

$\delta = 120°$, X_{Lsepn}=0.2p.u., X_{Lm}=0.2p.u.

(a) Z_{pn}=1.5, (b) Z_{pn}=2.5 82

Figure 4.12: Voltage transfer ratio, M versus normalized frequency, ω_{sn}

$\delta = 120°$, X_{Lsepn}=0.2p.u., X_{Lm}=0.2p.u.

(a) Z_{pn}=3.5, (b) Z_{pn}=4.5 83

Figure 4.13: Voltage transfer ratio, M versus normalized frequency, ω_{sn}

$\delta = 120^\circ$, X_{Lsepn}=0.4p.u., X_{Ltn}=0.2p.u.

(a) Z_{pn}=1.5, (b) Z_{pn}=2.5 84

Figure 4.14: Voltage transfer ratio, M versus normalized frequency, ω_{sn}

$\delta = 120^\circ$, X_{Lsepn}=0.4p.u., X_{Ltn}=0.2p.u.

(a) Z_{pn}=3.5, (b) Z_{pn}=4.5 85

Figure 4.15: Peak capacitor voltage, v_{cs} versus normalized frequency, ω_{sn}

$\delta = 120^\circ$, X_{Lsepn}=0, X_{Ltn}=0.2p.u.

(a) Z_{pn}=1.5, (b) Z_{pn}=2.5 87

Figure 4.16: Peak capacitor voltage, v_{cs} versus normalized frequency, ω_{sn}

$\delta = 120^\circ$, X_{Lsepn}=0, X_{Ltn}=0.2p.u.

(a) Z_{pn}=3.5, (b) Z_{pn}=4.5 88

Figure 4.17: Peak capacitor voltage, v_{cs} versus normalized frequency, ω_{sn}

$\delta = 120^\circ$, X_{Lsepn}=0.2p.u., X_{Ltn}=0.2p.u.

(a) Z_{pn}=1.5, (b) Z_{pn}=2.5 89

Figure 4.18: Peak capacitor voltage, v_{cs} versus normalized frequency, ω_{sn}

$\delta = 120^\circ$, X_{Lsepn}=0.2p.u., X_{Ltn}=0.2p.u.

(a) Z_{pn}=3.5, (b) Z_{pn}=4.5 90

Figure 4.19: Peak capacitor voltage, v_{cs} versus normalized frequency, ω_{sn}

$\delta = 120^\circ$, X_{Lsepn}=0.4p.u., X_{Ltn}=0.2p.u.

(a) Z_{pn}=1.5, (b) Z_{pn}=2.5 91

Figure 4.20: Peak capacitor voltage, v_{cs} versus normalized frequency, ω_{sn}

$\delta = 120°$, X_{Lsepn}=0.4p.u., X_{Ltn}=0.2p.u.

(a) Z_{pn}=3.5, (b) Z_{pn}=4.5 92

Figure 4.21: KVA/KW rating versus normalized frequency, ω_{sn}

$\delta = 175°$, X_{Lsepn}=0.05p.u., Z_{pn}=1.5, Z_{sn}=3.5 99

Figure 4.22: Voltage transfer ratio, M versus normalized frequency, ω_{sn}

$\delta = 175°$, X_{Lsepn}=0.05p.u., Z_{pn}=1.5, Z_{sn}=3.5 100

Figure A.1: Nth harmonics equivalent circuit of the series-parallel resonant converter. 111

Figure 0.1: Simulated waveforms of the converter with tuned series and parallel branch using two-winding HF transformer, K_i=2 115

Figure 0.2: Simulated waveforms of the converter with tuned series and parallel branch using two-winding HF transformer, K_i=4 115

Figure 0.1: KVA/KW rating versus normalized frequency, ω_{sn}

$\delta = 175°$, X_{Lsepn}=0, X_{Ltn}=0.2p.u.

(a) Z_{pn}=1.5, (b) Z_{pn}=2.5 117

Figure 0.2: KVA/KW rating versus normalized frequency, ω_{sn}

$\delta = 175°$, X_{Lsepn}=0, X_{Ltn}=0.2p.u.

(a) Z_{pn}=3.5, (b) Z_{pn}=4.5 118

Figure 0.3: KVA/KW rating versus normalized frequency, ω_{sn}

$\delta = 175°$, X_{Lsepn}=0.2p.u., X_{Ltn}=0.2p.u.

(a) Z_{pn}=1.5, (b) Z_{pn}=2.5 119

Figure 0.4: KVA/KW rating versus normalized frequency, ω_{sn}

$\delta = 175^{\circ}$, X_{Lsepn}=0.2p.u., X_{Ltn}=0.2p.u.

(a) Z_{pn}=3.5, (b) Z_{pn}=4.5 120

Figure 0.5: KVA/KW rating versus normalized frequency, ω_{sn}

$\delta = 175^{\circ}$, X_{Lsepn}=0.4p.u., X_{Ltn}=0.2p.u.

(a) Z_{pn}=1.5, (b) Z_{pn}=2.5 121

Figure 0.6: KVA/KW rating versus normalized frequency, ω_{sn}

$\delta = 175^{\circ}$, X_{Lsepn}=0.4p.u., X_{Ltn}=0.2p.u.

(a) Z_{pn}=3.5, (b) Z_{pn}=4.5 122

Figure 0.7: Voltage transfer ratio, M versus normalized frequency, ω_{sn}

$\delta = 175^{\circ}$, X_{Lsepn}=0, X_{Ltn}=0.2p.u.

(a) Z_{pn}=1.5, (b) Z_{pn}=2.5 123

Figure 0.8: Voltage transfer ratio, M versus normalized frequency, ω_{sn}

$\delta = 175^{\circ}$, X_{Lsepn}=0, X_{Ltn}=0.2p.u.

(a) Z_{pn}=3.5, (b) Z_{pn}=4.5 124

Figure 0.9: Voltage transfer ratio, M versus normalized frequency,ω_{sn}

$\delta = 175^{\circ}$, X_{Lsepn}=0.2p.u., X_{Ltn}=0.2p.u.

(a) Z_{pn}=1.5, (b) Z_{pn}=2.5 125

Figure 0.10: Voltage transfer ratio, M versus normalized frequency, ω_{sn}

$\delta = 175^{\circ}$, X_{Lsepn}=0.2p.u., X_{Ltn}=0.2p.u.

(a) Z_{pn}=3.5, (b) Z_{pn}=4.5 126

Figure 0.11: Voltage transfer ratio, M versus normalized frequency, ω_{sn}

$\delta = 175^{\circ}$, X_{Lsepn}=0.4p.u., X_{Ltn}=0.2p.u.

(a) Z_{pn}=1.5, (b) Z_{pn}=2.5 127

Figure 0.12: Voltage transfer ratio, M versus normalized frequency, ω_{sn}

$\delta = 175^{\circ}$, X_{Lsepn}=0.4p.u., X_{Ltn}=0.2p.u.

(a) Z_{pn}=3.5, (b) Z_{pn}=4.5 128

Figure 0.13: Peak capacitor voltage, v_{cs} versus normalized frequency, ω_{sn}

$\delta = 175^{\circ}$, X_{Lsepn}=0, X_{Ltn}=0.2p.u.

(a) Z_{pn}=1.5, (b) Z_{pn}=2.5 129

Figure 0.14: Peak capacitor voltage, v_{cs} versus normalized frequency, ω_{sn}

$\delta = 175^{\circ}$, X_{Lsepn}=0, X_{Ltn}=0.2p.u.

(a) Z_{pn}=3.5, (b) Z_{pn}=4.5 130

Figure 0.15: Peak capacitor voltage, v_{cs} versus normalized frequency, ω_{sn}

$\delta = 175^{\circ}$, X_{Lsepn}=0.2p.u., X_{Ltn}=0.2p.u.

(a) Z_{pn}=1.5, (b) Z_{pn}=2.5 131

Figure 0.16: Peak capacitor voltage, v_{cs} versus normalized frequency, ω_{sn}

$\delta = 175^{\circ}$, X_{Lsepn}=0.2p.u., X_{Ltn}=0.2p.u.

(a) Z_{pn}=3.5, (b) Z_{pn}=4.5 132

Figure 0.17: Peak capacitor voltage, v_{cs} versus normalized frequency, ω_{sn}

$\delta = 175^{\circ}$, X_{Lsepn}=0.4p.u., X_{Ltn}=0.2p.u.

(a) Z_{pn}=1.5, (b) Z_{pn}=2.5 133

Figure 0.18: Peak capacitor voltage, v_{cs} versus normalized frequency, ω_{sn}

$\delta = 175^{\circ}$, X_{Lsepn}=0.4p.u., X_{Lin}=0.2p.u.

(a) Z_{pn}=3.5, (b) Z_{pn}=4.5 134

List of Tables

Table 3.1: Simulated data using frequency-domain analysis and EDF method..... 46

Table 3.2: Predicted and simulations results for the two-winding transformer 59

Table 4.1: Design results for the three-winding high frequency transformer

$\delta = 120^{\circ}$, X_{Lm}=0.2p.u..... 96

Table 4.2: Design results for the two-winding high-frequency transformer

$\delta = 175^{\circ}$ 98

Table 4.3: Predicted and simulated values of the design example using three-winding high frequency transformer 100

Table 4.4: Predicted and simulated values of the design example using two-winding high frequency transformer 101

Chapter 1

Introduction

Converters are power conversion stages, which provide interfaces and power matching between the power supply and user loads. Converter circuits consist of power semiconductor devices, signal electronics, as well as energy storage elements such as inductors and capacitors. Converters are divided into four categories, ac/ac, ac/dc, dc/ac, and dc/dc, depending on the form of the power at the supply and load sides.

The dc/dc converters provide interface between dc systems of different voltage levels. They are widely used in many industrial applications which have the requirement to convert a fixed-voltage dc source into a variable-voltage dc source and in dc motor drive applications. According to the methods of power conversion, dc/dc converters are categorized as PWM dc/dc converters and resonant converters.

This thesis deals with a dc/dc power converter. As such the operating principles, modeling, analysis and control methods of the two types of dc/dc converters are reviewed in the following sections.

1.1 PWM DC/DC Converters

The basic topology and principle of operation of the PWM dc/dc converters is illustrated in Figure 1.1. When the switch is closed at time t=0, the source voltage is applied to the load directly. If the switch is opened at time t=*DT* and remains off till time t=*T*, the voltage across the load is zero. The waveform of the output voltage is shown in Figure 1.1(b). The expected average output voltage is obtained by selecting the appropriate value of the "ON" time of the switch or the duty ratio D of the switch. The control of the ripple voltage and current at the output can be implemented by adding an L-C filter. Based on the basic topology, several classic converter topologies, such as BUCK, BOOST, BUCK-BOOST, and CÚK converters, have been derived. The details of these basic converter topologies and analysis have been discussed extensively in the literature [1]-[13].

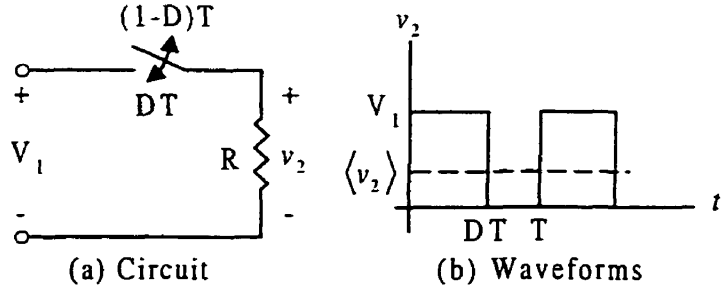

Figure 1.1: Basic PWM dc/dc converter topology

The basic PWM converters have simple circuit constructions. They are easy to control and have comparatively low cost. However, the turn-on and turn-off losses of the switch are very high resulting in low efficiencies. The switching power loss of a device

increases as a linear function of the switching frequency. Therefore, the PWM converters are usually used in low-frequency condition. Besides, the high di/dt and dv/dt values result in high voltage and current stresses on the switches.

To operate the power converter at high frequencies, the switching power loss has to be limited. The switching stresses of the switches can be released by connecting simple dissipative snubber circuits. *McMurray* [10] gives detailed analysis and design procedures for the selection of the snubber circuits. However, these dissipative sunbbers shift the switching power loss from the switch to the snubber circuit and therefore do not provide a reduction in the overall switching power loss.

In order to improve the performance of the converter, the phase-shift concept is applied. It allows all the switches to operate on zero-voltage switching and hence near zero switching power loss is obtained. *Vlatkovic and Vlatko* [11] provide a detailed discussion of the topology.

Small-signal modeling is an important issue in the analysis and design of power converters. The small-signal model provides dynamics behavior observer for power converters. It is used in analyzing the stability of the converters during small-signal perturbations. *Middlebrook* and *Cuk* [12] presented a widely used approach, state-space averaging method, for PWM converters, where the linear ripple assumption is sustained. It uses state space equations to represent a piece-wise linear switching circuit. The large-signal model is obtained by averaging the equations and the small-signal model follows the perturbation and linearization of the large-signal model.

The ripple in the output voltage is quite high in PWM converters due to the characteristics of the switching action. *Tymerski* and *Li* [13] have provided detailed

analysis of the ripple of the PWM converters which include simplified expression of the ripple for the converter operating in both continuous and discontinuous mode.

1.2 Resonant DC/DC Converters

It is clear that the low power loss can be reduced if the switching devices are turned "ON" and "OFF" when the voltage across a device and/or the current flowing through the device become zero. The zero-voltage and zero-current switching can be achieved using an LC resonant circuit. Such converters are called resonant converters. They can be categorized as follows depending upon the function of the resonant circuit and the switching strategies [1].

1. Load-resonant converters
2. Resonant-switch converters
3. Resonant dc-link converters
4. High-frequency-link integral-half-cycle converters

The load-resonant converter consists of an LC resonant tank circuit, which is used to remove the harmonics from the quasi-square wave inverted output as well as implementing the zero-voltage and zero-current switching. In load-resonant converters, the power flow to the load is controlled by the impedance of the resonant tank, which is determined by the switching frequency and the resonant frequency. A block diagram of the load resonant converter is shown in Figure 1.2.

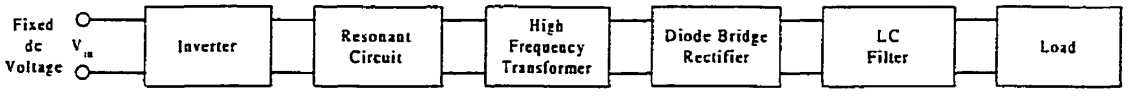

Figure 1.2: The block diagram of the load resonant converter

There are three kinds of load resonant converters depending on the form of the LC resonant tank as listed below.

Series resonant converters

Parallel resonant converters

Series-parallel resonant converters

In following sections, a brief literature review is presented for the load resonant dc/dc converters, highlighting their basic features and characteristics.

1.2.1 Series Resonant Converter

Figure 1.3 shows the full-bridge configuration of the series resonant dc/dc converter (SRC). The input inverter transforms the dc input voltage to a quasi-square wave ac input voltage, v_s, which is applied to the series resonant circuit L_s-C_s. Under the ac input stimulus, the LC resonant circuit generates an oscillatory current in the resonant circuit. The rectifier and the output filter regulate the resonant current to a dc current to the load. The ripple of the dc output is controlled by the values of L_o and C_o. The series resonant converter can operate in two modes, namely, discontinuous-conduction mode and continuous-conduction mode.

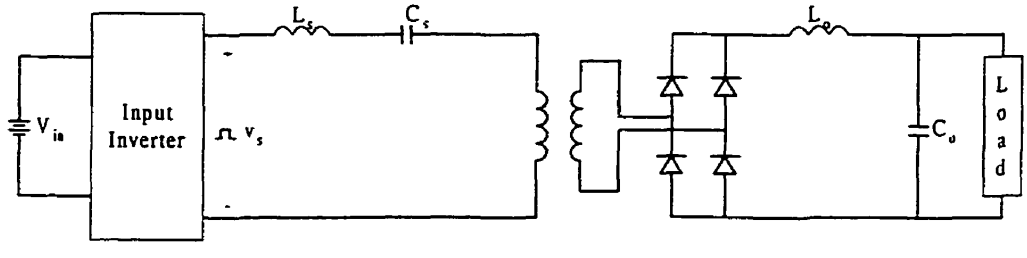

Figure 1.3: Full-bridge series resonant dc/dc converter

A number of full, quasi, multi-resonant dc/dc converter topologies have been reported in the literature [14]-[19]. The switching losses of these topologies have been reduced to near zero. However, the output voltage control is implemented by varying the operating and switching frequency. The frequency control requires a wide range variation of the switching frequency. The efficiency of the converter cannot be guaranteed under variable frequency operation. Hence, the constant frequency operation is introduced [18]. The constant frequency resonant converters offer high power densities at medium to high power levels. However, at low to medium power level, the component count is high and the power density is limited. *Jain et al* at [20] have developed an asymmetrical pulse-width-modulated resonant dc/dc converter to overcome this drawback. The experimental results show that this kind of converter can achieve high efficiency at low power and high switching frequency operation.

The main advantage of the series resonant converter is that the series resonant capacitor on the primary side acts as a dc blocking capacitor. Because of this fact the converter can easily be used in full-bridge arrangements without any additional control to eliminate the unbalance in the power FET switching times and forward voltage drops. For this reason, the SRC is suitable for high power applications where a full-bridge converter is desirable. Another advantage of the SRC is that the current flowing through the switching devices depends on the value of the load, i.e. it decreases as the load decreases. This advantage allows the power device conduction losses to decrease at light-load operations. Thus a high efficiency is obtained.

The main disadvantage of the SRC is that the output voltage cannot be regulated for the no-load case. Another disadvantage of the SRC is that the output dc filter

capacitor must carry high ripple current. This is a significant disadvantage for applications with low output voltage and high current requirement.

1.2.2 Parallel Resonant Converter

Figure 1.4 shows the full-bridge configuration of the parallel resonant dc/dc converter (PRC). The circuit configuration of the PRC is similar to that of the SRC except instead of using a series resonant circuit, the PRC uses a parallel resonant circuit which consists of a series inductor L_p and a parallel capacitor C_p. It differs from the SRC in many important respects [1]-[3], [21]-[27].

The PRC appears as a voltage source, hence they are extensively used for multiple output voltage applications.

The PRC does not provide a short circuit protection.

The PRC can operate in both step-up and step-down modes

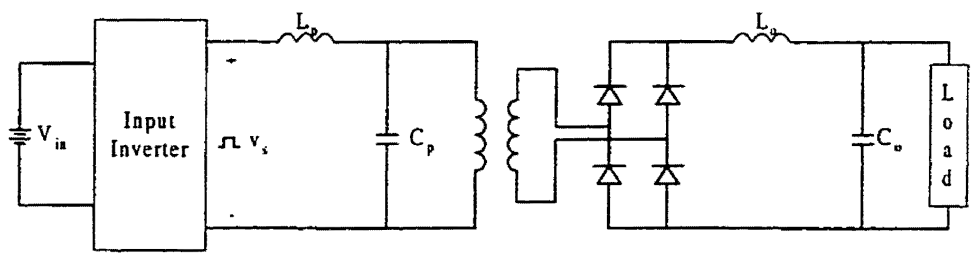

Figure 1.4: Full-bridge parallel resonant dc/dc converter

In contrast to the SRC, the PRC is suitable for low-voltage high-current applications. The load circuit of the PRC (the circuit at the secondary side of the transformer) can be modeled as a current source. The current carried by the power FETs and resonant components in the PRC is relatively independent of load. The consequence

of this behavior is that the conduction losses in the FETs and the reactive components remain constant with changing of the load. Therefore, the efficiency of the PRC operating in light-load (low output power) condition decreases.

1.2.3 Series-Parallel Resonant Converter

Figure 1.5 shows the full-bridge configuration of the series-parallel resonant converter (SPRC). A series-parallel resonant converter is the combination of the SRC and PRC. It can be seen that the resonant circuit of the converter consists of a series branch (L_s-C_s) and a parallel branch (L_p-C_p). It is clear that several different resonant circuit topologies can be derived by removing some of the resonant components. Several variations in the topology of the SPRC have been discussed in the literature [28]-[38].

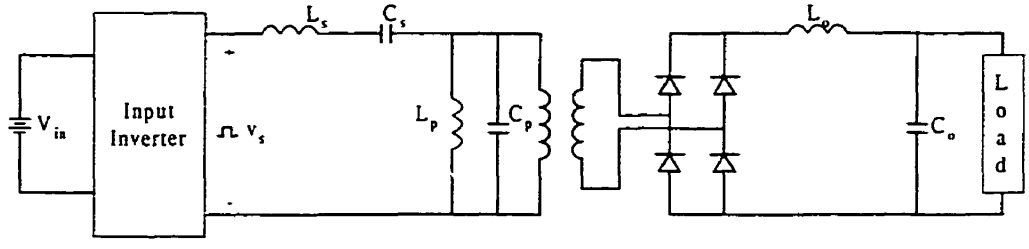

Figure 1.5: Full-bridge series-parallel resonant dc/dc converter

The series-parallel converter has the advantages of both the SRC and PRC while eliminating their weak points by properly selecting the resonant components. For example, a high-efficiency can be obtained from full-load to very small load current [28]. With a proper selection of the L_s/L_t ratio, the switch peak current can be kept almost equal to the primary-side reflected load current. It is an additional advantage compared to the standard resonant converters having high peak current through the

switches. The SPRC is best suited for applications with the requirement of low voltage, high current regulated dc output such as in telecommunication systems.

1.3 Modeling and Analysis of Resonant Converters

Recently, there has been an increased interest in the area of resonant converters due to their advantages, such as, higher operating frequency, higher efficiency, small size, light weight and low component stresses. Previously developed methods for analysis and design of resonant converters have used mainly time domain analysis, frequency domain analysis, and state-space approach.

The analysis of the converter using time-domain analysis has been reported in [24]-[26]. This method divides each switching cycle into several distinct time intervals. In each time interval, a set of differential equations is obtained. Numerical integration of the appropriate set of differential equations can be used to simulate the switching converter and thereby determine steady-state information. This method is, however, very inconvenient and consumptive of computer time.

The frequency domain analysis approach [28]-[30] represents the inverter output voltage, v_s, and the primary current, i_p, as the sum of harmonics. A harmonic equivalent circuit excited by the voltage and current harmonics yields state variables that can be represented as the sum of the responses of each individual harmonic component. This method has its simplicity but it cannot be used to obtain the small-signal model of the converter.

The state-space approach and discrete time domain modeling technique focus on the behaviors of those variables that are central to describing the dynamic performance of a system. The state-space model can describe the behavior of the converter precisely. However, it has difficulties to describe the discrete actions of switches. The system has to be analyzed at each switching interval and different state-space equations have to be solved to complete the analysis. Especially when the system is a high-order system, for example, series-parallel resonant converter, the analysis and design procedure can be very time-consuming. *Agarwal* and *Bhat* [37] have presented such a model of the series-parallel resonant converter to show the effectiveness in predicting the steady-state and transient behavior of the converter. Although only the initial condition at the beginning of every half cycle of the operating frequency are sufficient to predict the peak component stresses and the state behaviors, the derivation of the model and the solution of the equations involve complex mathematical computations.

From the previous discussions, it is shown that most of the previous work do not provide an easy-to- use model that is readily understood and applicable by most power converter design engineers. *Yang, et al* [32] have presented a systematical modeling method (extended describing function method) for resonant converters. Under the appropriate assumptions, this method can be employed in both large and small signal modeling, which result in a set of simple linear equations. The method has been applied to the analysis of SRC and PRC. However, the modeling and analysis using this technique for SPRC is not available in the literature.

The effect of transformer leakage inductance on the behavior of the converter is another important issue in converter design. Generally speaking, the leakage inductance

will lead to a commutation interval during the operation, which in turn decreases the output voltage. However, including the effect of the leakage inductance increases the complexity of the model. As a result, very few analysis methods have addressed this problem. The effects of the leakage inductance of the transformer on the performance of the series-parallel converter need further investigation.

1.4 Thesis Objective and Outline

The objective of this thesis is to develop generalized state-space models to analyze and design the series-parallel resonant converters taking the leakage inductance of the high-frequency transformer into consideration. The extended describing function concept is introduced to linearize the state-space model. Simple equations are obtained to study the steady-state performance of the converter.

The design procedures reported in the literature are normally aimed at meeting the output requirement of the converter only. Typically the design procedure involves the selection of circuit parameters to meet the output requirements and certain performance criteria (e.g. maximum load current) [37]. The cost and size of the converter is usually neglected. A new set of design criteria is developed not only to meet the output and performance requirements, but also to minimize the cost and size of the converter. The design curves are presented and the design results are verified by simulation.

The main objective of this thesis can be summarized as follows.

1. Development of a generalized state-space large-signal model for the analysis of the series-parallel resonant dc/dc converters, specifically, the fixed frequency

series-parallel resonant converters, taking into the account the effect of the leakage inductance of the high-frequency transformer on the performance of the converter.

2. Analysis of the steady-state performance of the converter.

3. Development of a generalized small-signal model of the series-parallel resonant converter.

4. Development of a generalized design model of the series-parallel resonant converter.

5. Development of a design procedure for selecting the resonant components and high-frequency transformer.

6. Verification of the models and design examples of the converter using Pspice.

The thesis is organized as follows:

In Chapter 2, the state-space model of the basic series-parallel resonant converter is presented. The Extended Describing Function (EDF) is introduced to linearize the state-space model and derive a set of linear equations which describe the performance of the converter.

In Chapter 3, the performance of the converter using the EDF model is studied. Both simulated waveforms and characteristic curves are presented. Frequency-domain analysis and Pspice software simulation results are employed to verify the accuracy of the EDF model.

In Chapter 4, a design model is developed based on the EDF model. The performance of the converter is investigated by changing frequency or changing the

values of resonant components. A design procedure is developed, which focuses on minimizing the cost and size of the converter. Pspice simulation results are provided and a comparison is made between the simulation results and predicted values.

In Chapter 5, a summary of the thesis and recommendations for the future work are provided.

Chapter 2

Extended Describing Function Analysis of Fixed- Frequency Series Parallel Resonant Converters

In this chapter, the fixed frequency series-parallel resonant dc/dc converter is analyzed using the state-space method. Due to the difficulties of describing discrete actions of switches, the Extended Describing Function (EDF) concept is introduced to linearize the state-space model. General models of the converter based on the EDF concept for both large-signal model and small-signal operation are developed. The leakage inductance of the output high-frequency transformer is included in both models.

2.1 Circuit Description and Operating Principle

In this section, two topologies of the series-parallel resonant converter are introduced. The basic series-parallel converter uses a two-winding high-frequency (HF)

transformer. The other topology uses a three-winding high-frequency transformer. The advantages of using the three-winding HF transformer are discussed.

2.1.1 The Series-Parallel Resonant Converter with a Two-winding HF Transformer

The basic circuit topology of the fixed-frequency, series-parallel resonant converter using a high-frequency transformer is shown in Figure 2.1. The function blocks of this circuit are described as follows.

Input Filter: The input filter consists of an inductor, L_{in}, and a capacitor, C_{in}. They are used to remove the high-frequency noise in the input voltage, V_{in}.

Full-bridge Inverter: The full-bridge inverter consists of four MOSFETS, S_1 to S_4, and four diodes, D_1 to D_4. The Phase-Shift-Modulation control technique [1] is used to convert the DC source voltage V_{in} to a high frequency quasi-square waveform, v_s, which becomes the input to the resonant circuit. The capacitors, C_1 to C_4, make up the snubber circuit to release the switching stress.

Resonant Circuit: The resonant circuit contains a series branch and a parallel branch. The series branch is made up of an inductor and a capacitor, namely, L_s and C_s. Similarly the parallel branch is made up of an inductor and a capacitor, namely, L_p and C_p. The resonant circuit produces a quasi-sinusoidal voltage across the capacitor C_p. The arrangement forms a generalized resonant circuit. Several different resonant circuit topologies can be derived by removing some of the resonant components. For example, the basic series resonant converter (SRC) is obtained by removing C_p and L_p. Similarly, the parallel resonant converter (PRC) is obtained by removing C_s and L_p.

Output Transformer: The high-frequency transformer is used to provide isolation as well as voltage matching between the resonant circuit and the output. In this thesis, the transformer is assumed to be ideal except for the leakage inductance.

Full-bridge Rectifier: The full-bridge rectifier is composed of four diodes, which converts the quasi-sinusoidal ac voltage to a dc output voltage. However, due to the leakage reactance of the transformer, there is a voltage reduction at the output.

Output Filter: The output filter is composed of an inductor, L_o, and a capacitor, C_o. They are large enough to provide almost ripple-free current and voltage to the load. Hence, the output of the resonant circuit can be modeled as a current source.

2.1.2 The Series-Parallel Resonant Converters with a Three-winding HF Transformer

The basic circuit topology of the series-parallel resonant converter using a three-winding HF transformer is shown in Figure 2.2. It has the same function blocks as the two-winding converter. The only difference is that the parallel resonant branch is placed on the tertiary winding of the three-winding transformer. The arrangement provides greater flexibility in the choice of the parallel capacitor, C_p. By reducing the current carrying capacity of the parallel inductor, L_p, its size can also be reduced significantly [28].

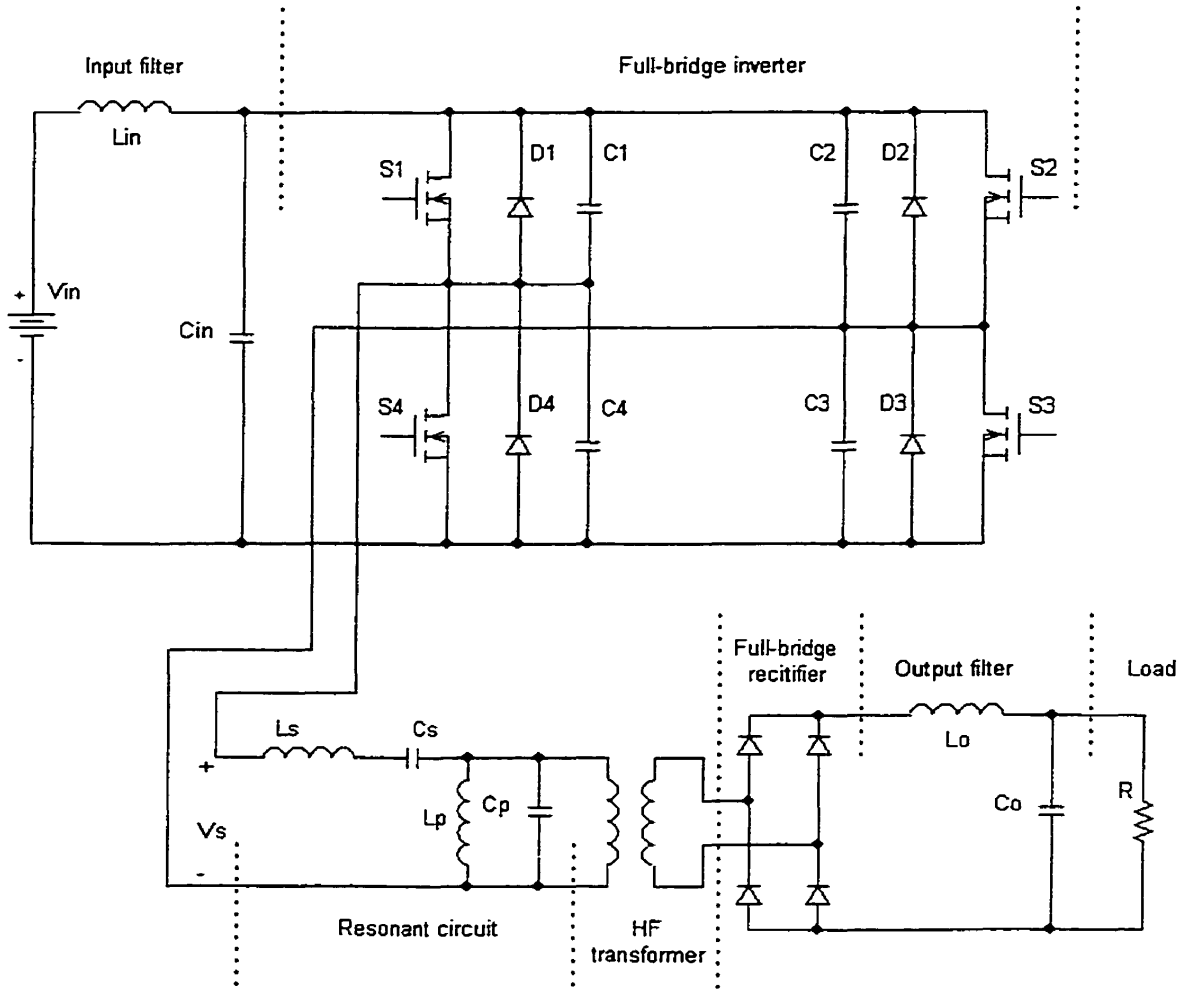

Figure 2.1: Basic circuit diagram of the series-parallel resonant dc/dc converter using two-winding HF transformer

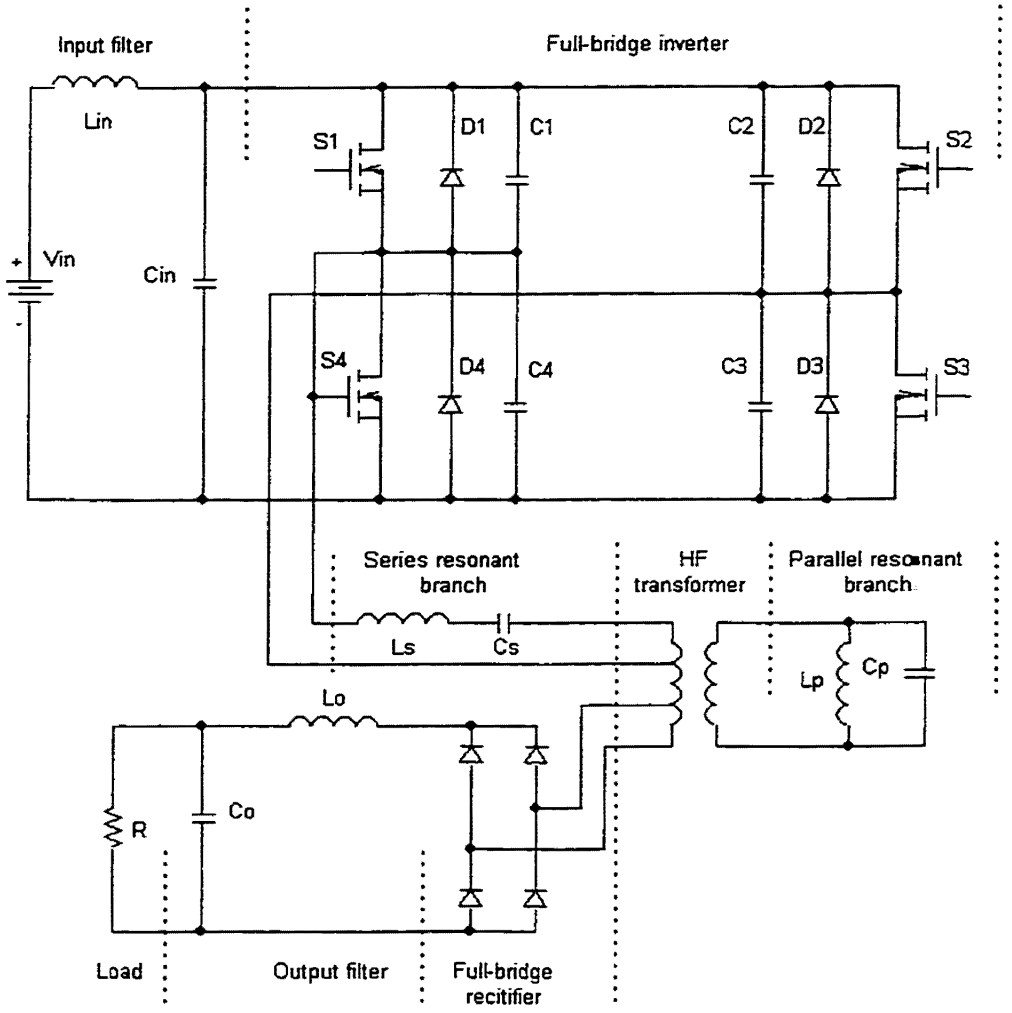

Figure 2.2: Basic circuit diagram of the series-parallel resonant dc/dc converter using three-winding HF transformer

Equivalent Circuit Models of the Series-Parallel Resonant DC/DC Converters

A simplified circuit diagram of the series-parallel resonant converter with the two-winding HF transformer referred to the primary side is shown in Figure 2.3. The input voltage v_s is a single-pulse width modulated voltage. With the output of the bridge rectifier represented as a constant current source, I_o, the transformer-bridge rectifier arrangement is represented, at the primary side, as the leakage inductance L_{sep} and the alternating source, i_p.

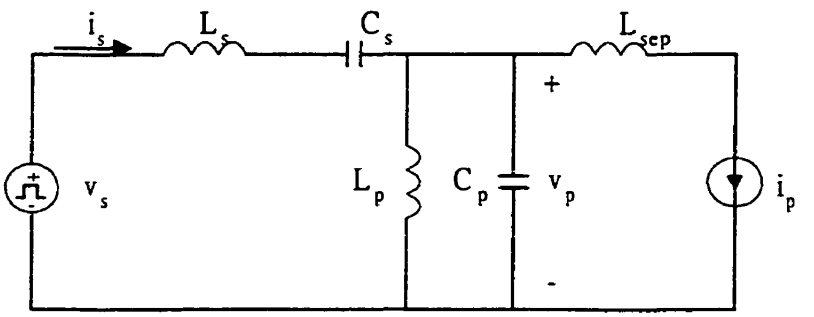

Figure 2.3: Primary side equivalent circuit of the series-parallel resonant dc/dc converter using two-winding transformer

The equivalent circuit of the series-parallel resonant converter with the three-winding HF transformer referred to the primary side is shown in Figure 2.4. The leakage inductance of the transformer consists of three parts, the primary leakage L_{pr}, the secondary leakage L_{sep}, and the tertiary leakage L_t. The primary leakage can be included in the series inductor, so it will not affect the circuit performance [28]. The secondary

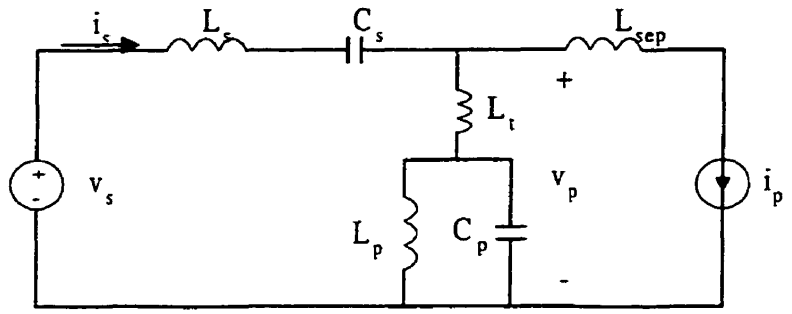

Figure 2.4: Primary side equivalent circuit of the series-parallel resonant converter with a three-winding HF transformer

leakage is the main reason for the voltage drop at the output because it causes the commutation overlap. The turns ratio of the primary to secondary winding is given by N_P:N_S, and the turns ratio of primary to tertiary winding is given by N_P:N_T. Assuming that the tertiary leakage has the same value as the secondary leakage, the equivalent reactance ratio of the tertiary and secondary winding is obtained as

$$X_{Lsep} = \left(\frac{N_P}{N_S}\right)^2 \cdot X_{Lse} \qquad (2.1)$$

$$X_{Ltp} = \left(\frac{N_P}{N_T}\right)^2 \cdot X_{Lt} \qquad (2.2)$$

$$\frac{X_{Ltp}}{X_{Lsep}} = \left(\frac{N_P}{N_T}\right)^2 \cdot \left(\frac{N_S}{N_P}\right)^2 \cdot \frac{X_{Lt}}{X_{Lse}} = \left(\frac{N_S}{N_T}\right)^2 \cdot \frac{X_{Lt}}{X_{Lse}} \qquad (2.3)$$

where

X_{Lse}: the reactance of the secondary leakage at the secondary side

X_{Lt}: the reactance of the tertiary leakage at the tertiary side

X_{Lsep}: the equivalent reactance of the secondary leakage at the primary side

X_{Ltp}: the equivalent reactance of the tertiary leakage at the primary side

Typically N_P:N_S is in the range 4:1-6:1, and N_P:N_T is in the range 1:2-1:3. Hence L_t/L_{se} is less than unity.

2.1.4 Ideal Circuit Waveforms of the Series-Parallel Resonant DC/DC Converter

The equivalent circuit models of the two resonant converters are very similar, and with the appropriate choice of circuit parameters, the waveforms in the converters are expected to be similar. A single-pulse width modulated voltage applied to the resonant circuit results in a nearly sinusoidal voltage across the parallel resonant circuit. Since the output of the bridge rectifier is represented by a constant current source, the current in the primary winding of the HF transformer will be a trapezoidal waveform. The trapezoidal nature is a result of the commutation overlap caused by the leakage inductance of the HF transformer.

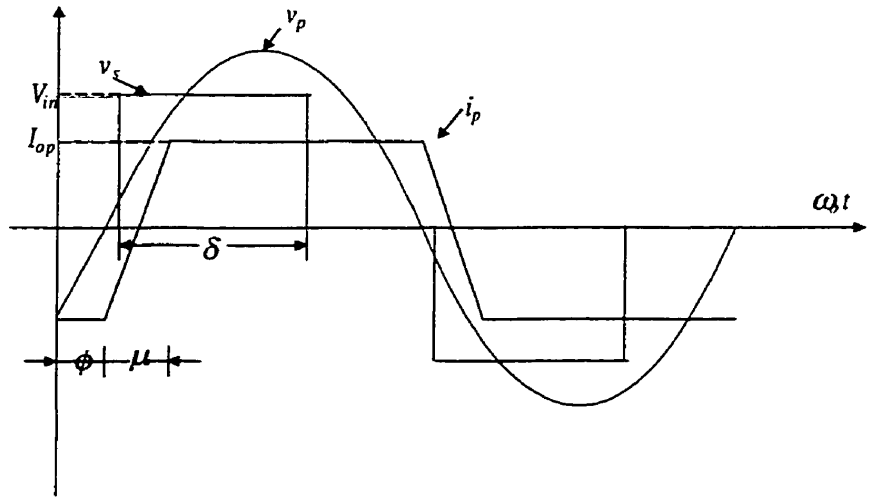

Figure 2.5: Typical steady-state waveforms of the series-parallel resonant dc/dc converter

The typical steady-state waveforms of the series-parallel resonant converter are presented in Figure 2.5. The phase shift angle, ϕ, is the phase difference between the fundamental component of the input quasi-square wave and the transformer primary voltage, v_p. The pulse width of the voltage applied to the resonant circuit is indicated as δ, and the commutation overlap angle is shown as μ. With a constant inverter switching frequency ω_s, the converter waveforms are periodic.

2.2 Extended Describing Function Modeling of the Converter

State-space approach is a method, which focuses on the behaviors of those variables that are central to describing the dynamic performance of a system. State-space provides a uniform and convenient starting point for such diverse tasks as steady-state computation, linearization, stability evaluation, control design, and simulation. In this section, the state-space model of the fixed frequency dc/dc converter is developed. The extended describing function (EDF) technique is used to obtain a set of linear state-space equations that describe the system.

2.2.1 Assumptions

To simplify the analysis, the following assumptions are used.

All the switches and circuit components are ideal.

The voltage across the parallel branch capacitor is in continuous mode.

The input current is in continuous mode.

The current at the primary side of the transformer changes linearly during the commutation period, and is therefore assumed to be trapezoidal.

2.2.2 State-space Approach Analysis

Based on the assumptions and equivalent circuit discussed above, four state variables, i_{Ls}, i_{Lp}, v_{cp}, and v_{cs}, are used to describe the circuit. The general model based on the converter topology of the three-winding HF transformer is used to develop the state space model of the resonant converter. The model for the converter with the two-winding transformer is obtained by setting L_t=0. For convenience, the equivalent circuit with the state variables is redrawn in Figure 2.6.

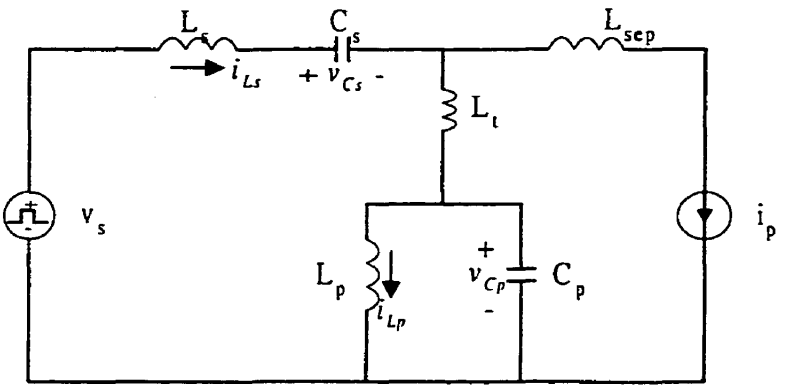

Figure 2.6: Equivalent circuit of the series-parallel resonant converter with state variables referred to the primary side

The general state-space equations for the circuit are obtained as

$$L_s \frac{di_{Ls}}{dt} + v_{Cs} + L_t\left(\frac{di_{Ls}}{dt} - \frac{di_p}{dt}\right) + v_{Cp} = v_s \qquad (2.4)$$

$$L_p \frac{di_{Lp}}{dt} = v_{Cp} \qquad (2.5)$$

$$C_p \frac{dv_{Cp}}{dt} = i_{Ls} - i_p - i_{Lp} \qquad (2.6)$$

$$C_s \frac{dv_{Cs}}{dt} = i_{Ls} \qquad (2.7)$$

2.2.3 Extended Describing Function Concept [32]

It is shown in Figure 2.5 that the typical waveforms of the switching circuit are periodic in the steady state. Thus the waveforms can be expressed in a Fourier series:

$$x = \sum_{k=-\infty}^{\infty} X_k \exp(j\omega_s kt) \qquad (2.8)$$

where $\omega_s = \frac{2\pi}{T_s}$ is the fixed switching frequency of the inverter and x represents the state variables.

It has been proved that the amplitudes of the harmonics decay at a rate $O(k^2)$ as k increases [31]. Generally speaking, the filtering property of the resonant circuits will eliminate the higher order harmonics. So it is reasonable to take the first few harmonics to approximate the periodic waveforms, in our case, the state variables:

$$x_i \approx \sum_{k \in H_i} X_{ik} \exp(j\omega_s kt) \qquad (2.9)$$

where i is the index of the state variables; $H_i = \left(\pm k_{i,1}, \ \pm k_{i,2}, \ \cdots \ \pm k_{i,m_i}\right)$, is called the harmonic indices, and k_{i,m_i} is the index of the highest order harmonics used to approximate the state variable x_i, The real form of equation (2.9) is given by

$$x_i = \sum_{k \in H_i} a_{ik} \cos(\omega_s k t) + b_{ik} \sin(\omega_s k t) \qquad (2.10)$$

where a_{ik} and b_{ik} are the Fourier coefficients of kth harmonics. $\{H_i\}$ contains the information on how the state variables are approximated. They are determined by the nature of the nonlinear system and by experience. For DC/DC converters, it is adequate to use only dc terms for the low pass filter variables, while for the resonant variables the first few harmonic terms should be sufficient. It is important to note that the coefficients of the harmonic terms are assumed to be time varying. This allows the investigation of the dynamic behavior of these terms when the system is modulated.

The following discussion concentrates on the interactions of $\{x_{ik}\}$, inputs, and control variables through the non-linearity of the system. It is convenient to define a vector called the harmonic coefficient vector (HCV), which contains all of the harmonic terms as

$$z = \left(a_{i0},\ b_{i0},\ \cdots\ a_{ik},\ b_{ik},\ \cdots | k \in H_i\right) \qquad (2.11)$$

The elements of z are dc terms and amplitude terms of the harmonics, which are time-varying. However, in general, the local variations in the amplitude terms are slower compared to the switching frequency.

The most important step of the modeling process is to represent the nonlinear functions of the state-space model by the approximate slowly varying HCV. The extended describing function concept is introduced to tackle this task. The traditional describing function concept is illustrated in Figure 2.7. When a single input nonlinear block is excited by a sinusoidal wave, the output usually contains not only the fundamental component but also other harmonic components. If the nonlinear block is

part of a system which has low pass filter property, then all the harmonics except the fundamental component will be heavily attenuated. In this case, the output of the nonlinear block can be approximated by the fundamental component. The amplitude of the output is a nonlinear function, F(X), of the input amplitude. This F(X) is called the describing function of the nonlinear block. The fast changing input-output relation is now replaced by a slowly varying linear relationship.

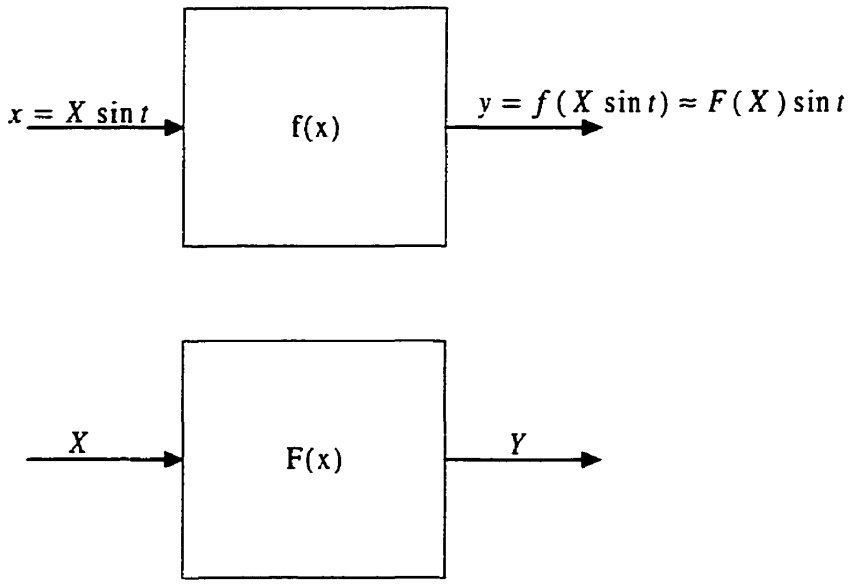

Figure 2.7: The traditional describing function concept

It is very easy to relate the above discussion and the modeling problem presented to resonant dc/dc converters. In both cases, nonlinear systems are excited by periodic inputs, and only certain harmonic components of the output are considered important. In the case of resonant converters where multiple inputs and outputs are considered, a more general approach called the extended describing function concept is used. Figure 2.8 illustrates the concept. The magnitudes of the outputs are nonlinear functions of the

inputs. Linear functions are obtained by replacing the fast changing inputs $x = (x_1 \quad x_2 \quad \cdots \quad x_n)$ by their slow time varying harmonic coefficients, $z = (a_{i0}, \ b_{i0}, \ \cdots \ a_{ik}, \ b_{ik}, \ \cdots | k \in H_i)$. By equating the sine and cosine terms separately, the nonlinear state-space model can be described by a set of linear equations.

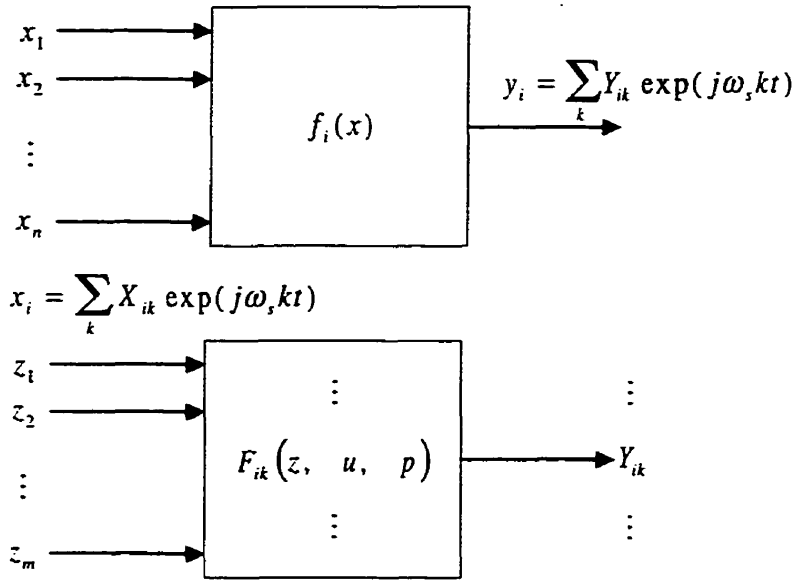

Figure 2.8: Extended describing function concept

2.2.4 Model of the Series-Parallel Resonant DC/DC Converter Using the Extended Describing Function

For the fixed frequency series-parallel resonant dc/dc converter, assume that the state variables $\{i_{Ls}(t) \quad i_{Lp}(t) \quad v_{Cp}(t) \quad v_{Cs}(t)\}$ can be approximated by their fundamental components. Using equation (2.10), the state variables are represented by

$$i_{Ls}(t) = i_{Lss}(t)\sin\omega_s t + i_{Lsc}(t)\cos\omega_s t \qquad (2.12)$$

$$i_{Lp}(t) = i_{Lps}(t)\sin\omega_s t + i_{Lpc}(t)\cos\omega_s t \qquad (2.13)$$

$$v_{Cp}(t) = v_{Cps}(t)\sin\omega_s t + v_{Cpc}(t)\cos\omega_s t \qquad (2.14)$$

$$v_{Cs}(t) = v_{Css}(t)\sin\omega_s t + v_{Csc}(t)\cos\omega_s t \qquad (2.15)$$

As discussed before, the envelope terms, $\{i_{Ls}(t),\ i_{Lp}(t),\ v_{Cp}(t),\ v_{Cs}(t)\}$, are slowly time varying, so the dynamic behavior of these terms can be investigated. The derivatives of $i_{Ls}(t)$, $i_{Lp}(t)$, $v_{Cp}(t)$, and $v_{Cs}(t)$ are obtained from equations (2.12) to (2.15) as

$$\frac{di_{Ls}}{dt} = \left(\frac{di_{Lss}}{dt} - \omega_s i_{Lsc}\right)\sin\omega_s t + \left(\frac{di_{Lsc}}{dt} + \omega_s i_{Lss}\right)\cos\omega_s t \qquad (2.16)$$

$$\frac{di_{Lp}}{dt} = \left(\frac{di_{Lps}}{dt} - \omega_s i_{Lpc}\right)\sin\omega_s t + \left(\frac{di_{Lpc}}{dt} + \omega_s i_{Lps}\right)\cos\omega_s t \qquad (2.17)$$

$$\frac{dv_{Cp}}{dt} = \left(\frac{dv_{Cps}}{dt} - \omega_s v_{Cpc}\right)\sin\omega_s t + \left(\frac{dv_{Cpc}}{dt} + \omega_s v_{Cps}\right)\cos\omega_s t \qquad (2.18)$$

$$\frac{dv_{Cs}}{dt} = \left(\frac{dv_{Css}}{dt} - \omega_s v_{Csc}\right)\sin\omega_s t + \left(\frac{dv_{Csc}}{dt} + \omega_s v_{Css}\right)\cos\omega_s t \qquad (2.19)$$

It is shown in Figure 2.5 that the typical waveform of the output current referred to the primary is trapezoidal because of the commutation overlap caused by the leakage reactance of the high-frequency transformer. The Fourier Series expression of the output current is given by

$$i_p = \sum_{n=1,3\cdots}^{\infty} \frac{8 I_{op}}{\pi\mu n^2}\sin\left(\frac{n\mu}{2}\right)\sin\left[n\left(\omega_s t - \phi - \frac{\mu}{2}\right)\right] \qquad (2.20)$$

which may be approximated by its fundamental component as

$$i_p = i_{ps}(t)\sin\omega_s t + i_{pc}(t)\cos\omega_s t \qquad (2.21)$$

where

$$i_{ps} = \frac{8 I_{op}}{\pi\mu} \sin\left(\frac{\mu}{2}\right) \cos\left(\phi + \frac{\mu}{2}\right) \qquad (2.22)$$

$$i_{pc} = -\frac{8 I_{op}}{\pi\mu} \sin\left(\frac{\mu}{2}\right) \sin\left(\phi + \frac{\mu}{2}\right) \qquad (2.23)$$

Assuming that the voltage across the primary side of the high-frequency transformer is sinusoidal with amplitude, V_{pm}, the commutation angle is given by [2]

$$\cos(\mu) = 1 - \frac{2 X_{Lsep} I_{op}}{V_{pm}} \qquad (2.24)$$

where $V_{pm} = \sqrt{\left(v_{Cps} + \left(i_{Lss} - i_{ps}\right) \cdot X_{Lt}\right)^2 + \left(v_{Cpc} + \left(i_{Lsc} - i_{pc}\right) \cdot X_{Lt}\right)^2}$

The concept of power balance, in the converter results in the equation

$$\int_0^{2\pi} v_s i_{Ls} = \int_0^{2\pi} V_o I_o \,. \qquad (2.25)$$

Finally, from the waveforms of Figure 2.5, there exists a condition that the voltage across the parallel branch is zero at the time $\omega t = \phi$, i.e.

$$v_p|_{\omega=\phi} = 0 \,. \qquad (2.26)$$

Substituting equations (2.16)-(2.20) into equations (2.4)-(2.7), eleven equations can be obtained. Equating the coefficients of the sine and cosine terms of the resulting equations, the following set of equations is obtained. These equations are obtained by assuming that in the steady state the coefficients of the sine and cosine terms in equations (2.12) to (2.15) vary so slowly that they can be assumed to be constant in relation to the high switching frequency.

$$-(L_s + L_t)\omega_s I_{Lsc} + \omega_s L_t I_{pc} + V_{Css} + V_{Cps} = E \qquad (2.27)$$

$$(L_s + L_t)\omega_s I_{Lss} - \omega_s L_t I_{ps} + V_{Csc} + V_{Cpc} = 0 \qquad (2.28)$$

$$-L_p\omega_s I_{Lpc} = V_{Cps} \tag{2.29}$$

$$L_p\omega_s I_{Lps} = V_{Cpc} \tag{2.30}$$

$$-C_p\omega_s V_{Cpc} = I_{Lss} - I_{ps} - I_{Lps} \tag{2.31}$$

$$C_p\omega_s V_{Cps} = I_{Lsc} - I_{pc} - I_{Lpc} \tag{2.32}$$

$$-C_s\omega_s V_{Csc} = I_{Lss} \tag{2.33}$$

$$C_s\omega_s V_{Css} = I_{Lsc} \tag{2.34}$$

Equations (2.24) to (2.26) are expressed in terms of the state variables as follows:

$$\cos(\mu) = 1 - \frac{2X_{Lsep}I_{op}}{\sqrt{\left(v_{Cps} + \left(i_{Lss} - i_{ps}\right)\cdot X_{Lt}\right)^2 + \left(v_{Cpc} + \left(i_{Lsc} - i_{pc}\right)\cdot X_{Lt}\right)^2}} \tag{2.35}$$

$$\int_0^{2\pi} v_s i_{Ls} = \int_0^{2\pi} V_o I_o \Rightarrow I_o = I_{op} = \sqrt{EI_{Lss}/2} \tag{2.36}$$

$$V_{ps}\sin(\phi) + V_{pc}\cos(\phi) = 0 \tag{2.37}$$

where

$$E = \frac{4}{\pi}\sin\frac{\delta}{2} \tag{2.38}$$

The EDF model of the converter is described by the eleven equations given in equations (2.27) - (2.37), where the unknown state variables to be determined are $\{I_{Lss}\ \ I_{Lsc}\ \ V_{Css}\ \ V_{Csc}\ \ I_{Lps}\ \ I_{Lpc}\ \ V_{Cps}\ \ V_{Cpc}\ \ \phi\ \ \mu\ \ I_{op}\}$.

In the above equations, the variables are normalized with respect to the base quantities defined by

Base Voltage = Input Voltage, V_{in}

Base Reactance = Load Resistance referred to the primary circuit, R_b

Base Frequency = Switching Frequency, f_s

Base Current = V_{in}/R_b

2.2.5 Steady-State Solution

The solution of the EDF model is on per unit base normalized to the quantities given above. The steady-state solution of equations (2.27)-(2.37) gives the characteristics of the converter. The constant steady-state solution of the modulation equations corresponds to a periodic steady-state solution of the original dynamic equation. Generally, a numerical method must be employed to solve these equations. In this thesis, the function `FSOLVE ( )` in MATLAB [39] is used to solve the set of equations.

2.3 Small-Signal Modeling of the Series-Parallel Resonant converter

Small-signal modeling is critical in the analysis and design of switching power supplies. The performance of the small-signal model indicates the dynamic behavior of a highly nonlinear switching power circuit around a certain operating point. In this section, the perturbation technique is employed to derive the small-signal model of the resonant converter. The goal is to demonstrate the procedure for deriving the small-signal model from the set of linear operations obtained using the EDF method. The small-signal model can be used to investigate the performance of the converter for small variation in input voltage magnitude, switching frequency and the pulse width.

2.3.1 Perturbation and linearization

Having determined the large signal operating point of the converter, the small signal model can be obtained by employing a small perturbation to the inputs around the operating point.

Assume that the inputs and control variables are perturbed around the operating point as follows:

$$v_s = V_s + \hat{v}_s \tag{2.39}$$

$$\delta = \delta + \hat{\delta} \tag{2.40}$$

$$\omega_s = \Omega_s + \hat{\omega}_s \tag{2.41}$$

Removing the higher order terms, the small signal model is given by

$$\frac{d\hat{x}}{dt} = A\hat{x} + B\hat{u} \tag{2.42}$$

where

$$\hat{x} = \left[\hat{i}_{Lss} \quad \hat{i}_{Lsc} \quad \hat{v}_{Css} \quad \hat{v}_{Csc} \quad \hat{i}_{Lps} \quad \hat{i}_{Lpc} \quad \hat{v}_{Cps} \quad \hat{v}_{Cpc}\right]^T \tag{2.43}$$

$$\hat{u} = \left[\hat{v}_s \quad \hat{\delta} \quad \hat{\omega}_s\right]^T \tag{2.44}$$

The A and B matrices are obtained from equation (2.27) to (2.34) as

$$A=\begin{bmatrix} 0 & \Omega_s & -\frac{1}{(L_s+L_t)} & 0 & 0 & 0 & -\frac{1}{(L_s+L_t)} & 0 \\ -\Omega_s & 0 & 0 & -\frac{1}{(L_s+L_t)} & 0 & 0 & 0 & -\frac{1}{(L_s+L_t)} \\ 1 & 0 & 0 & \Omega_s & 0 & 0 & 0 & 0 \\ 0 & 1 & -\Omega_s & 0 & 0 & 0 & 0 & 0 \\ 0 & 0 & 0 & 0 & 0 & \Omega_s & \frac{1}{L_p} & 0 \\ 0 & 0 & 0 & 0 & -\Omega_s & 0 & 0 & \frac{1}{L_p} \\ \frac{1}{C_p} & 0 & 0 & 0 & -\frac{1}{C_p} & 0 & 0 & \Omega_s \\ 0 & \frac{1}{C_p} & 0 & 0 & 0 & -\frac{1}{C_p} & \Omega_s & 0 \end{bmatrix} \tag{2.45}$$

$$B=\begin{bmatrix} \frac{4\sin\left(\frac{\delta}{2}\right)}{(L_s+L_t)\pi} & I_{Lsc}-\frac{L_t I_{pc}}{(L_s+L_t)} \\ 0 & -I_{Lss}+\frac{L_t I_{ps}}{(L_s+L_t)} \\ 0 & V_{Csc} \\ 0 & -V_{Css} \\ 0 & I_{Lpc} \\ 0 & -I_{Lps} \\ 0 & V_{Cpc} \\ 0 & -V_{Cps} \end{bmatrix} \tag{2.46}$$

2.3.2 Circuit Implementation of Small-Signal Model

According to equation (2.42), the small-signal model has a linear state-space equation description. It is clear that each differential equation is either a KCL or a KVL equation. By the inverse way of writing the state equation from a linear circuit, the small-

signal equivalent circuit model is synthesized from equation (2.42), as shown in Figure 2.9.

The circuit model can be easily implemented in commonly used circuit simulation software, such as PSPICE [40] to investigate the performance and characteristics of the converter for small perturbation.

2.4 Summary

In this chapter, the series-parallel resonant dc/dc converter was analyzed using the state-space approach. The extended describing function method was employed to linearize the function and derive a set of linear equations that describe the large-signal model of the converter. The method also led to the derivation of a small-signal model of the converter based on the perturbation technique. The large-signal model is used in the next chapter to describe the performance and characteristics of the converter.

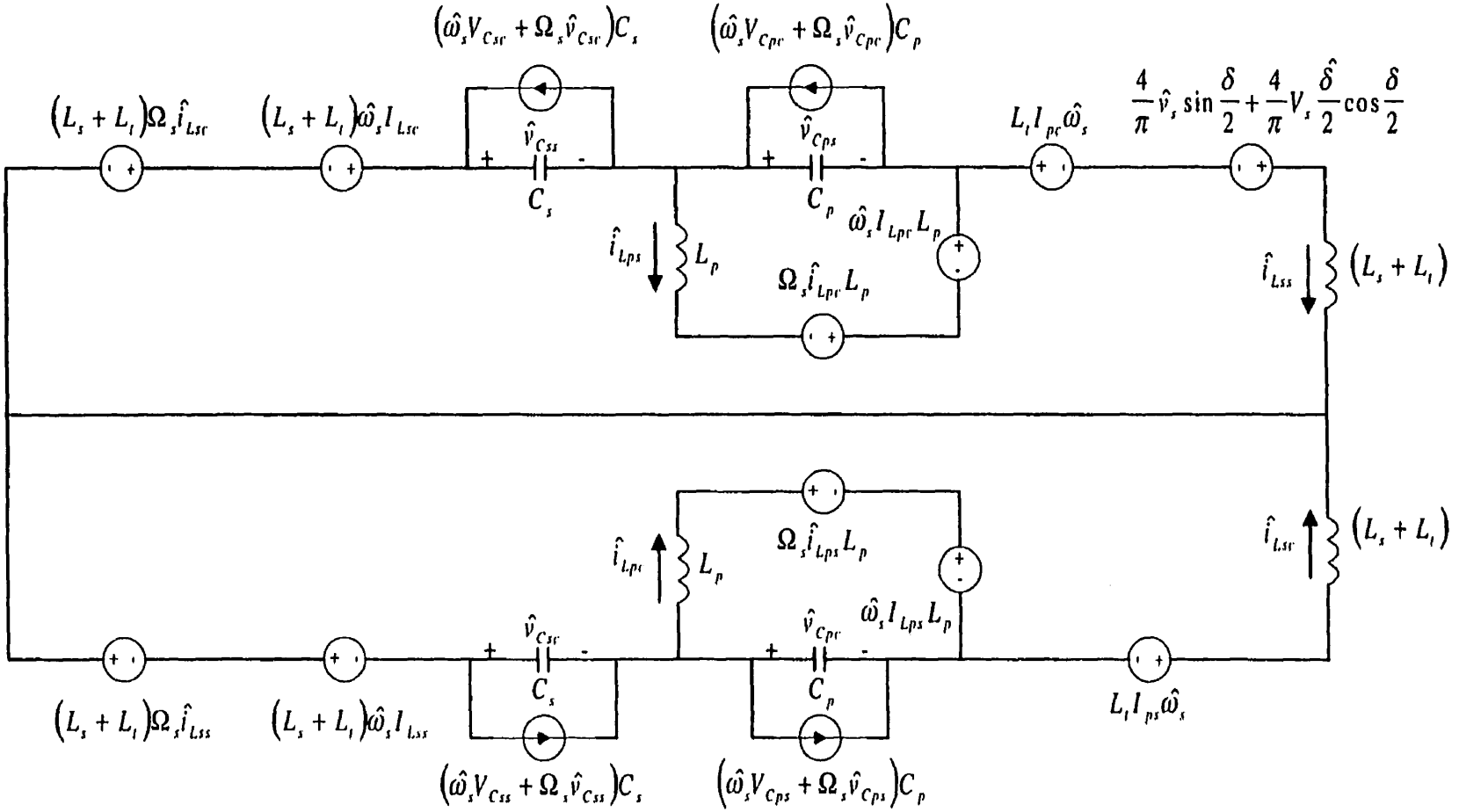

Figure 2.9: Circuit implementation of the small-signal model of the converter

Chapter 3

Steady-State Performance of the Series-Parallel Resonant DC/DC Converter

The performance characteristics of the series-parallel resonant dc/dc converter are discussed in this chapter. In order to demonstrate the validity of the models based on the extended describing function, the results are compared with those obtained from the frequency domain analysis procedure. Finally, the results from the extended describing function method and PSPICE simulation based on the parameters of an experimental converter are presented to show the accuracy of the various methods.

3.1 Frequency-domain Analysis

Frequency-domain analysis is a commonly used method for analyzing the steady-state performance of electrical and electronic circuits. The analysis is based on the harmonic analysis. As discussed previously, any periodic waveform can be expressed as a Fourier series. For any linear circuit, the outputs can be obtained as the sum of the

responses of all input harmonics. In order to analyze the multiple input-output circuit, a linear equivalent circuit is derived and the superposition theorem is applied.

The analysis of the fixed frequency series-parallel resonant dc/dc converter using the frequency domain analysis (FDM) technique has been reported in the literature [28]-[30]. However, since the results of the extended describing function (EDF) technique are to be compared with those of the frequency domain analysis technique, the derivation of the frequency domain frequency domain technique is given in Appendix A for easy reference.

3.1.1 Control Parameters

In order to describe the characteristics of the converter for a wide range of converter parameters, three normalized control parameters are introduced as follows.

The ratio of the series resonant circuit parameters is expressed as, K_s, defined as the ratio of the reactance of the series capacitor to the reactance of the series inductor, (i.e. X_{cs}/X_{Ls}). The value of K_s indicates the nature of the series resonant circuit. Specifically, if $K_s>1$, the series resonant circuit is capacitive, and if $K_s<1$, the series resonant circuit is inductive.

The ratio of the parallel resonant circuit parameters is expressed as, K_p, defined as the ratio of the reactance of the parallel capacitor to the reactance of the parallel inductor, (i.e. X_{cp}/X_{Lp}). Specifically, if $K_p>1$, the parallel resonant circuit is inductive, and if $K_p<1$, the parallel resonant circuit is capacitive.

The ratio of the inductance parameters is expressed as, K_l, defined as the ratio of the reactance of the series inductor to the reactance of the parallel inductor, (i.e. X_{Ls}/X_{Lp}).

The variations in the resonant circuit parameters are expressed in terms of variations in K_s, K_p, and K_l. The distortions in the waveforms are expressed in terms of the Total Harmonic Distortion (THD) defined as

$$THD = \left[\sum_{k\neq 1} X_k^2\right]^{1/2} \Big/ X_1 \times 100\% \qquad (3.1)$$

where X is the variable.

3.2 Characteristics of the Fixed Frequency Series-Parallel Converter

In this section, the characteristics of the converter are presented for the three-winding resonant converter. Appendix B gives the characteristics for the two-winding converter. In order to establish the validity of the extended describing function technique, the results for the frequency-domain and the extended describing function methods are compared for a wide variation in resonant circuit parameters. Harmonic terms up to the 19th harmonic have been used in the frequency-domain method.

3.2.1 Steady-state Waveforms

In this section, the steady-state waveforms of the dc/dc converter for variations in the various resonant circuit parameters are obtained and compared, using both the frequency-domain analysis and the extended describing function methods, as shown in Figures 3.1 to 3.5. The converter waveforms of interest are the input voltage to the resonant circuit, v_s, the voltage across the primary winding of the transformer v_p, the current in the series resonant circuit, i_s, and the input current to the bridge rectifier i_p.

Figures 3.1 and 3.2 show the converter waveforms for tuned series (K_s=1) and tuned parallel (K_p=1) branches, and K_l=2 and 4 respectively. The figures show that K_l has very little effect on the wave shapes, so far as the resonant circuits are tuned. As expected, the waveforms for v_p and i_s obtained by the EDF technique are sinusoidal, as assumed, while the FDM technique shows distortions. The THD of v_p and i_s are computed to be 12.05% and 8.03% for K_l=2, and 10.82% and 3.88% for K_l=4 respectively. The waveforms further show that i_s becomes more sinusoidal for a larger K_l.

Figure 3.3 shows the converter waveforms for a tuned series branch and capacitive parallel branch. The results of the two techniques show close agreement. The THD of v_p and i_s are computed to be 5.42% and 5.54% respectively. It shows that the THD of v_p and i_s are reduced and the waveforms are more sinusoidal. Both figures show that i_s leads v_p since the parallel resonant branch is capacitive.

Figure 3.4 shows the converter waveforms for a tuned series branch and inductive parallel branch. The THD of v_p and i_s are computed to be 25.51% and 22.29% respectively. Although the low-pass filter output filter reduces the distortion in the output voltage, the high THD of v_p associated with the inductive parallel branch results in increased distortion in the dc output voltage. Both figures show that i_s lags v_p.

Figure 3.5 shows the converter waveforms for tuned series and parallel branches with a larger value of leakage inductance. The THD of v_p and i_s are computed to be 10.43% and 8.38% respectively. Compared to Figure 3.1, it is observed that increasing the leakage inductance improves the wave shapes of v_p, i.e. v_p becomes more sinusoidal. However, the commutation angle increases and the magnitude of the output current decreasing, causing a decrease in the output voltage.

Some numerical results from the frequency-domain analysis and the EDF method are given in Table 3.1. V_{pm} and I_{sm} represent the peak value of the voltage across the parallel branch and the current through the series branch respectively. The Table shows that the error in V_{pm} for an inductive parallel branch voltage is about 17%, This is to be expected since the parallel branch voltage, v_p is highly distorted if the branch is inductive. In general, the discrepancy between the results of the two methods for tuned series and parallel branches is less than 10%.

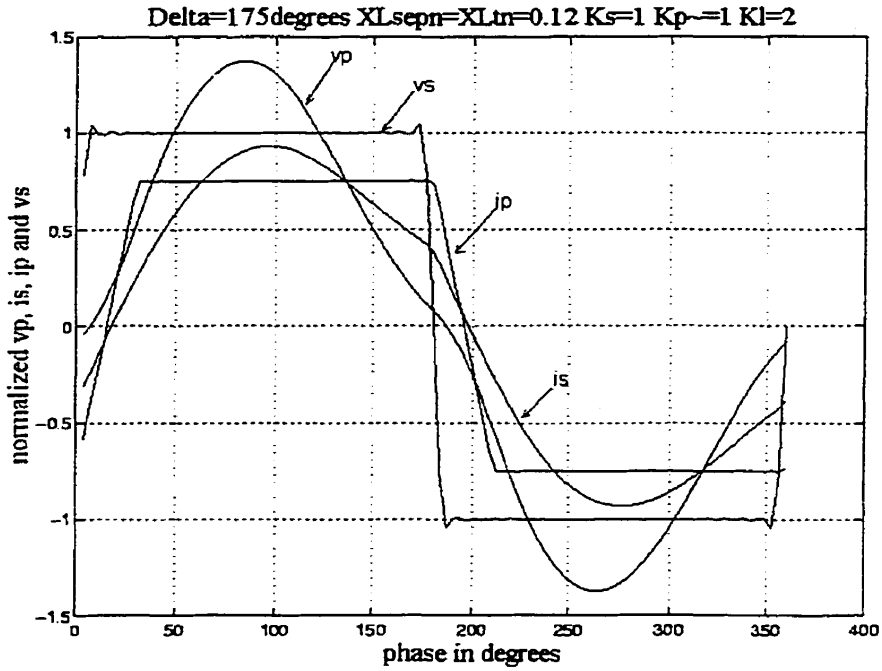

(a)

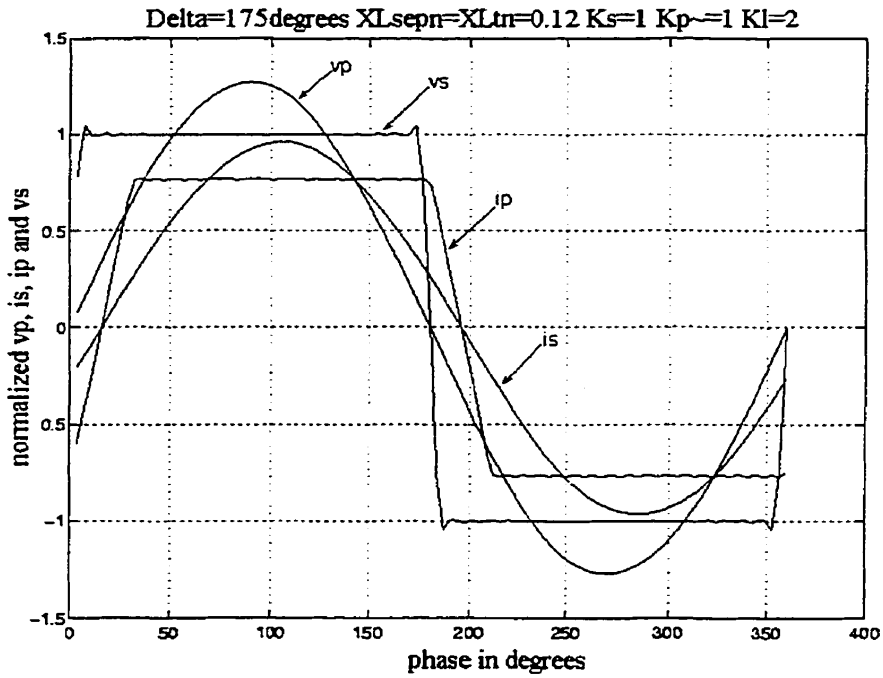

(b)

Figure 3.1: Simulated waveforms of the converter with tuned series and parallel branches, K_l=2, (a) Frequency-domain analysis, (b) Extended describing function method

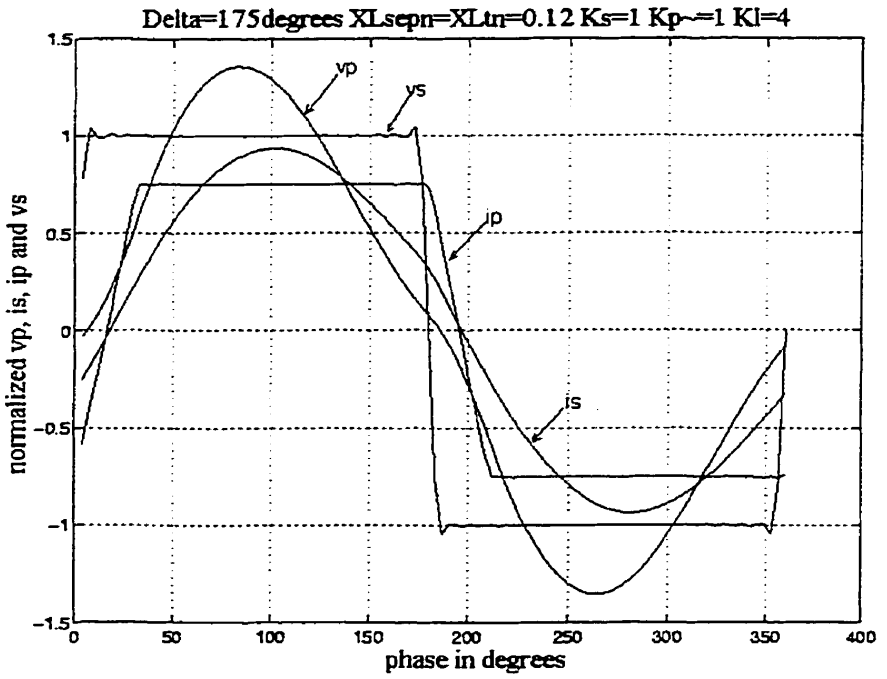

(a)

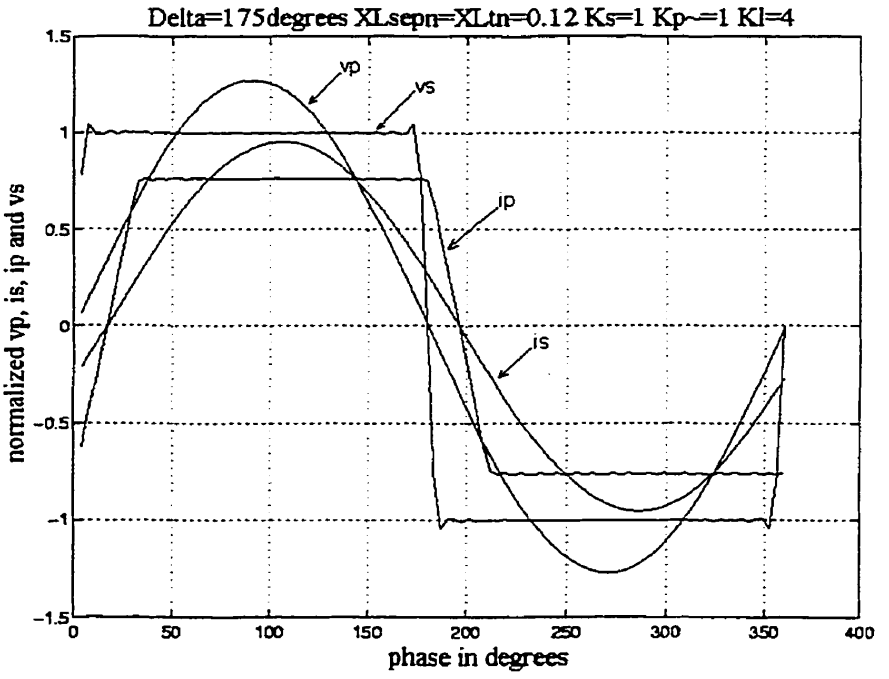

(b)

Figure 3.2: Simulated waveforms of the converter with tuned series and parallel branches, K_l=4, (a) Frequency-domain analysis, (b) Extended describing function method

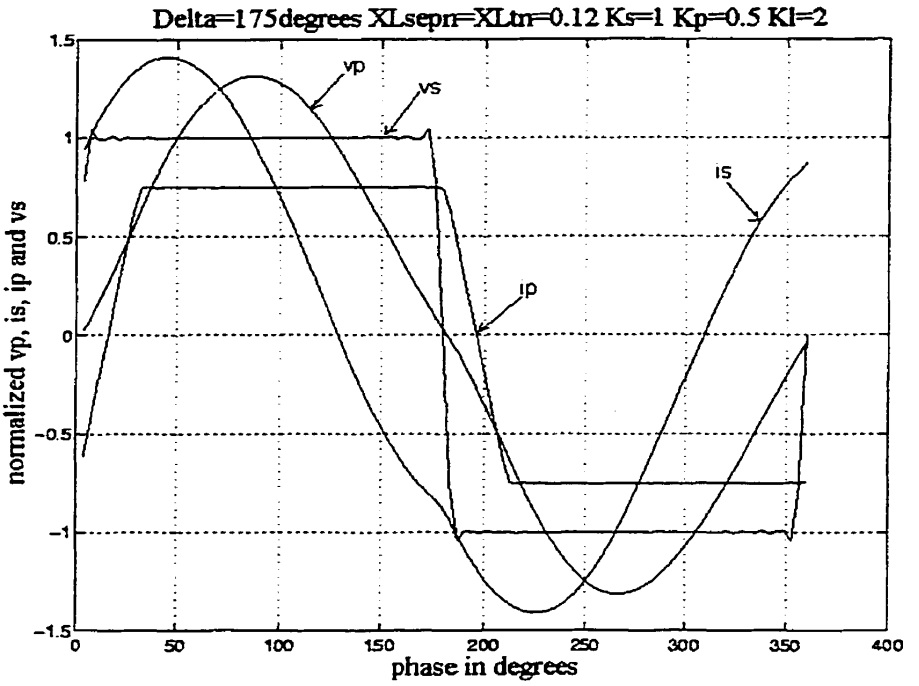

(a)

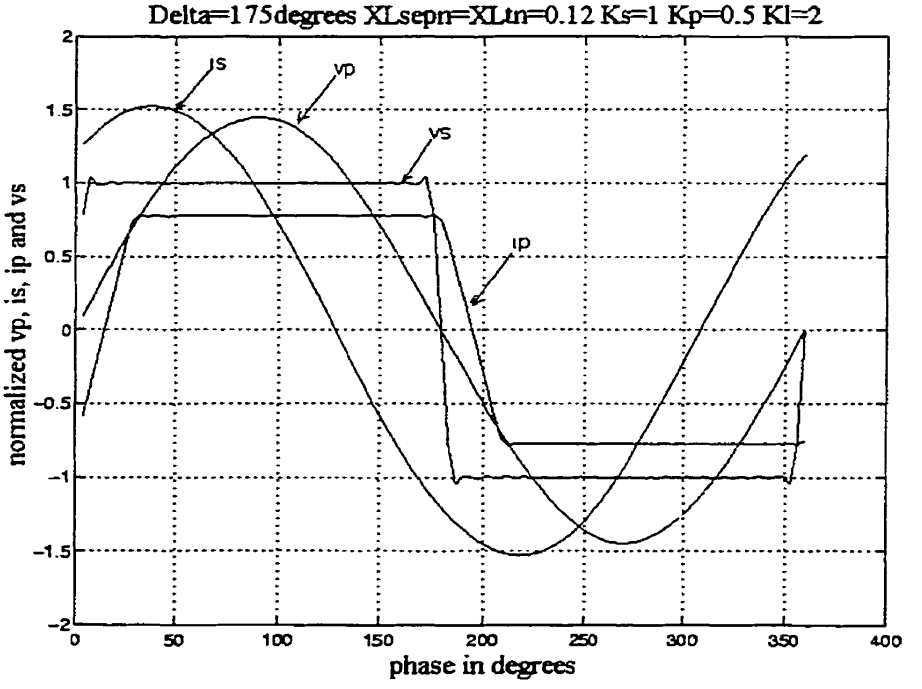

(b)

Figure 3.3: Simulated waveforms of the converter with capacitive parallel branch, K_l=2,

(a) Frequency-domain analysis, (b) Extended describing function method

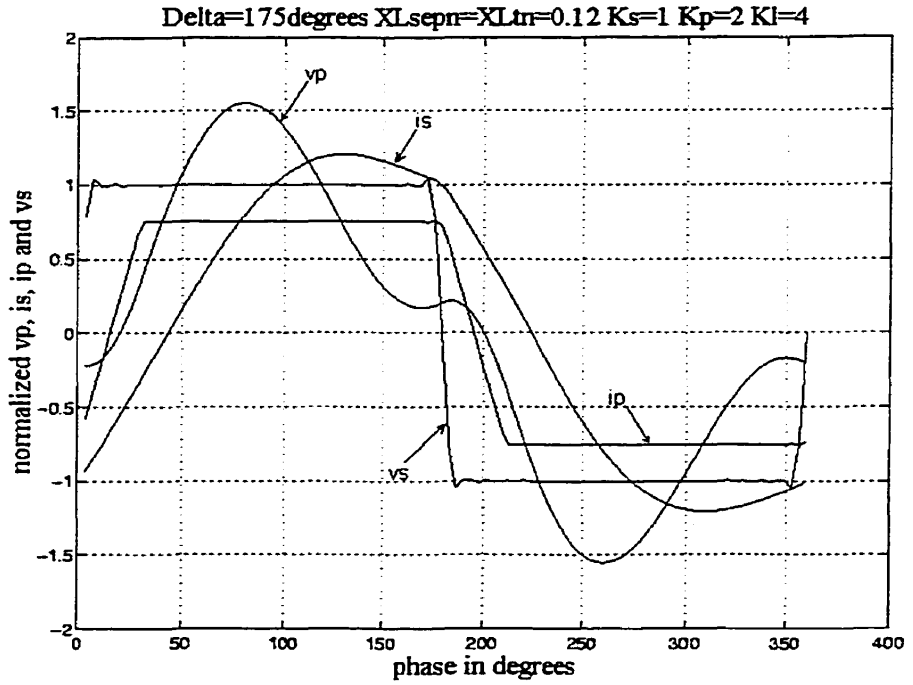

(a)

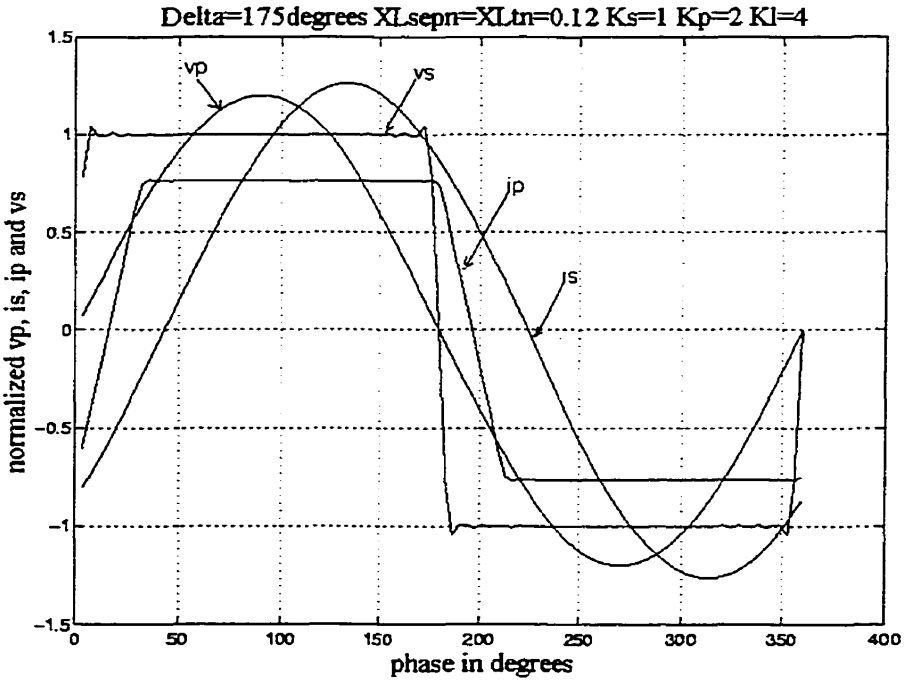

(b)

Figure 3.4: Simulated waveforms of the converter with inductive parallel branch, K_l=2

(a) Frequency-domain analysis, (b) Extended describing function method

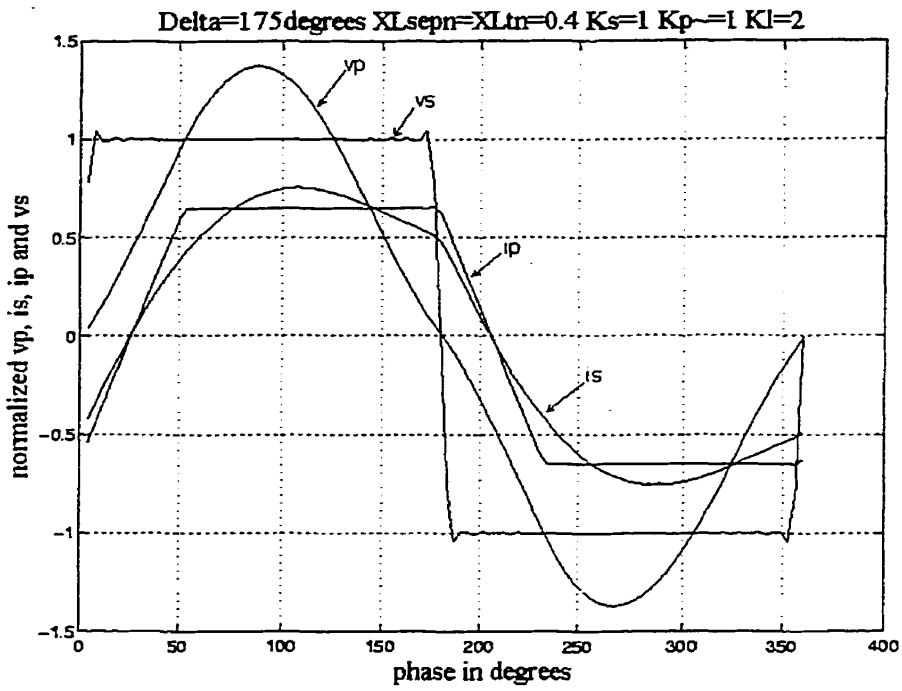

(a)

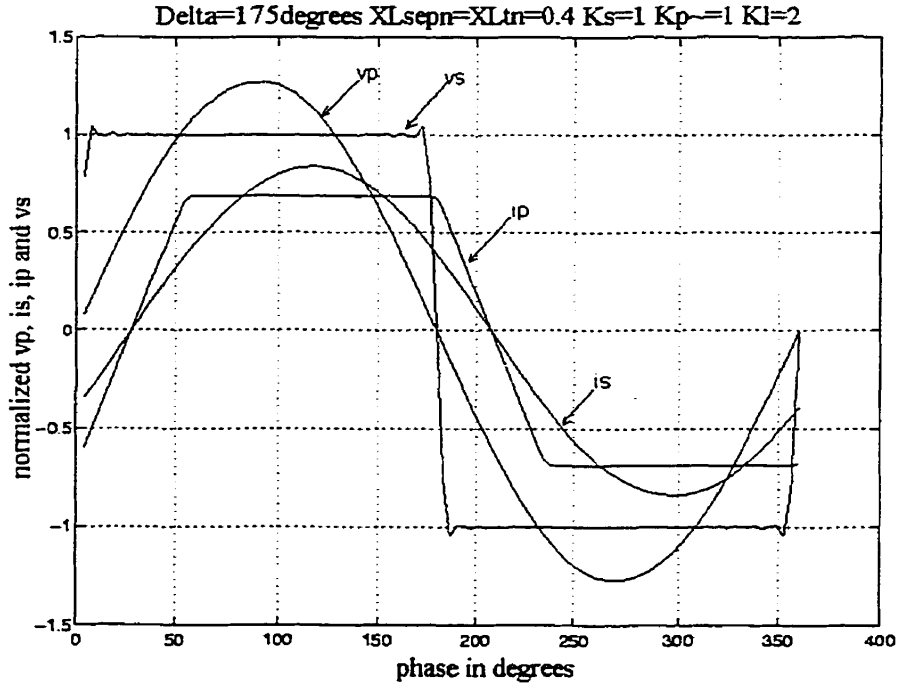

(b)

Figure 3.5: Simulated waveforms of the converter with larger leakage inductance, K_l=2,

(a) Frequency-domain analysis, (b) Extended describing function method

Table 3.1: Simulated data using frequency-domain analysis and EDF method

Specifications	Methods	V_{pm} (p.u.)	I_{sm}(p.u.)	V_o (p.u.)	ϕ (rad.)	μ (rad)
$\delta = 175°$ K_s=1 K_p=1 K_I=2 X_{Lsepn}=0.12 (p.u.) X_{Ltn}=0.12 (p.u.)	Frequency-domain Analysis	1.37	0.99	0.79	0.00	0.48
	Extended Describing Function	1.27	0.92	0.77	0.00	0.55
$\delta = 175°$ K_s=1 K_p=1 K_I=4 X_{Lsepn}=0.12 (p.u.) X_{Ltn}=0.12 (p.u.)	Frequency-domain Analysis	1.35	0.98	0.78	0.00	0.48
	Extended Describing Function	1.27	0.92	0.76	0.01	0.54
$\delta = 175°$ K_s=1 K_p=0.5 K_I=2 X_{Lsepn}=0.12 (p.u.) X_{Ltn}=0.12 (p.u.)	Frequency-domain Analysis	1.32	1.45	0.79	0.01	0.45
	Extended Describing Function	1.44	1.54	0.78	0.00	0.51
$\delta = 175°$ K_s=1 K_p=2 K_I=4 X_{Lsepn}=0.12 (p.u.) X_{Ltn}=0.12 (p.u.)	Frequency-domain Analysis	1.51	1.27	0.77	0.00	0.49
	Extended Describing Function	1.25	1.30	0.77	0.00	0.56
$\delta = 175°$ K_s=1 K_p=1 K_I=2 X_{Lsepn}=0.4 (p.u.) X_{Ltn}=0.4 (p.u.)	Frequency-domain Analysis	1.37	0.89	0.70	-0.00	0.86
	Extended Describing Function	1.27	0.82	0.69	0.00	0.97
$\delta = 120°$ K_s=1 K_p=1 K_I=2 X_{Lsepn}=0.12 (p.u.) X_{Ltn}=0.12 (p.u.)	Frequency-domain Analysis	1.17	0.83	0.66	-0.00	0.48
	Extended Describing Function	1.10	0.78	0.67	0.00	0.54
$\delta = 120°$ K_s=1 K_p=1 K_I=2 X_{Lsepn}=0.4 (p.u.) X_{Ltn}=0.4 (p.u.)	Frequency-domain Analysis	1.17	0.72	0.59	-0.00	0.86
	Extended Describing Function	1.10	0.66	0.60	0.00	0.97

3.2.2 Effect of Control Parameters on the Output Voltage and State Variables of the Converter

In the following section, the effects of X_{Lsepn} on the output voltage for the converter with a three-winding HF transformer are investigated. The tertiary leakage inductance, X_{Ltn}, is assumed to be 0.2 per unit. For a given K_p and K_l, Figure 3.6 shows the effects of different leakage inductance on the output voltage. In this case, the series branch of the converter is tuned, and the parallel branch is near the resonance point, for example, K_p=1.01. As the pulse width increases, the average input voltage increases, hence the output voltage increases. Given a fixed pulse width, an increasing leakage reactance, increases the communtation angle, and hence the voltage drop at the output increases. Similarly, the effects of different values of leakage reactance on the output voltage under the condition K_s=1.0, K_p=0.5, and K_l=2.0 are shown in Figure 3.7. It is seen that changing K_p does not affect the output voltage significantly.

Figure 3.8 shows the effect of X_{Lsepn} on the output voltage for inductive, tuned and capacitive series branch. With an increasing X_{Lsepn}, the output voltage decreases. The characteristics curves suggest that an inductive series branch will lead to higher output voltage whereas a lower output voltage is obtained with a capacitive series branch. Figure 3.9 shows the effect of the leakage reactance variation on the phase shift between v_p and v_s. With increasing leakage inductance, the phase shift between v_p and v_s decreases. When the series branch is tuned, the phase shift angle remains at zero and is independent of the leakage reactance.

Figure 3.10 shows the effect of the leakage reactance on the commutation angle. It is clear that the commutation angle increases with increasing leakage inductance.

Figure 3.11 shows the effect of the pulse-width on the output voltage with various K_S. It is observed that the relationship between the output voltage and the pulse width is approximately linear for pulse width less than 0.6 p.u. This suggests that from the point of view of a feedback control of the output voltage the converter can be approximated as a gain block for $\delta<0.6$ p.u.

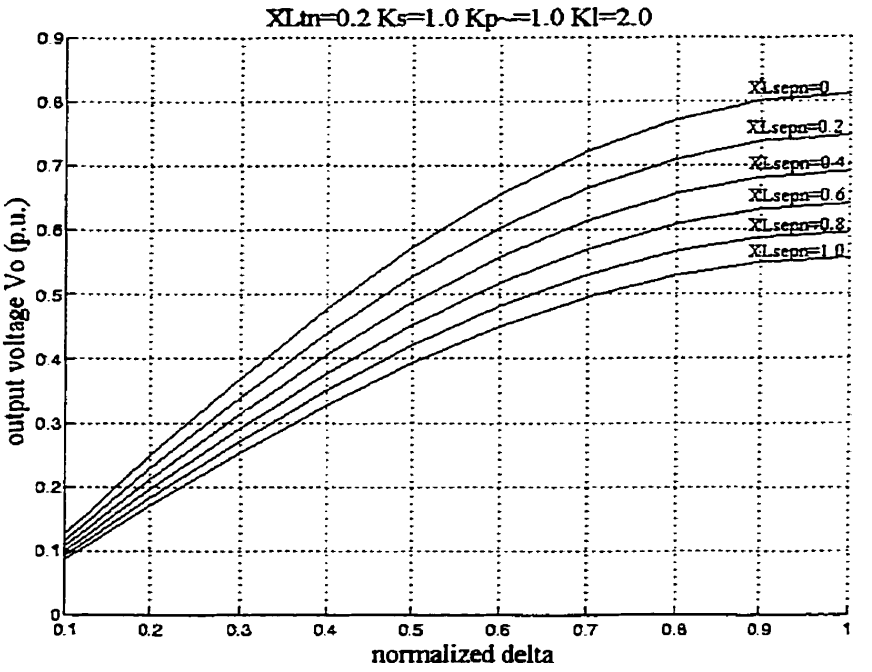

Figure 3.6: Effect of leakage inductance on the output voltage for tuned series and parallel branches

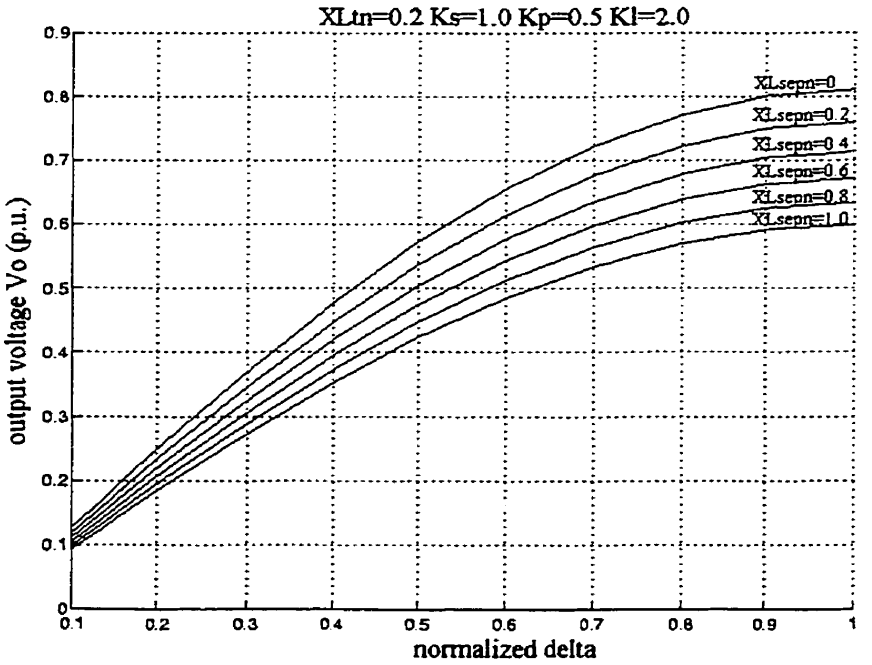

Figure 3.7: Effect of leakage inductance on the output voltage for tuned series and capacitive parallel branch

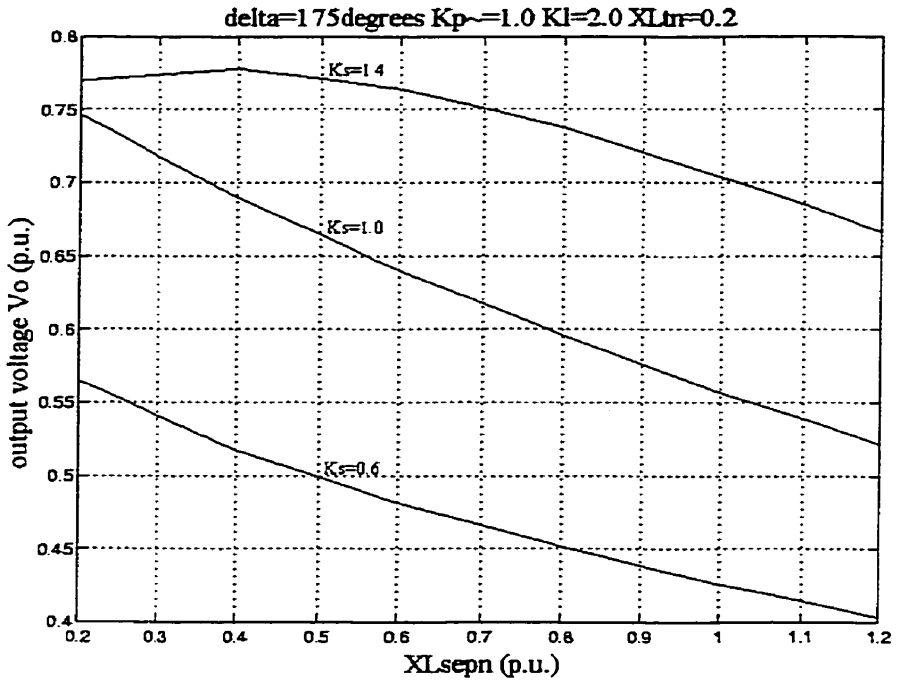

Figure 3.8: Effect of leakage inductance on output voltage for inductive, tuned, and capacitive series branch

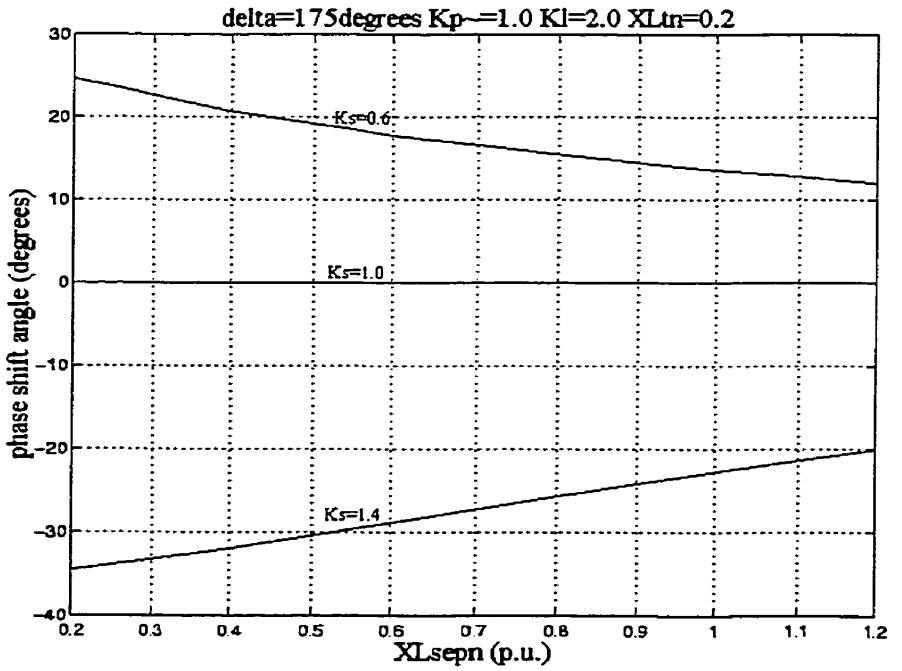

Figure 3.9: Effect of leakage inductance on the phase shift between v_P and v_S for inductive, tuned and capacitive series branch

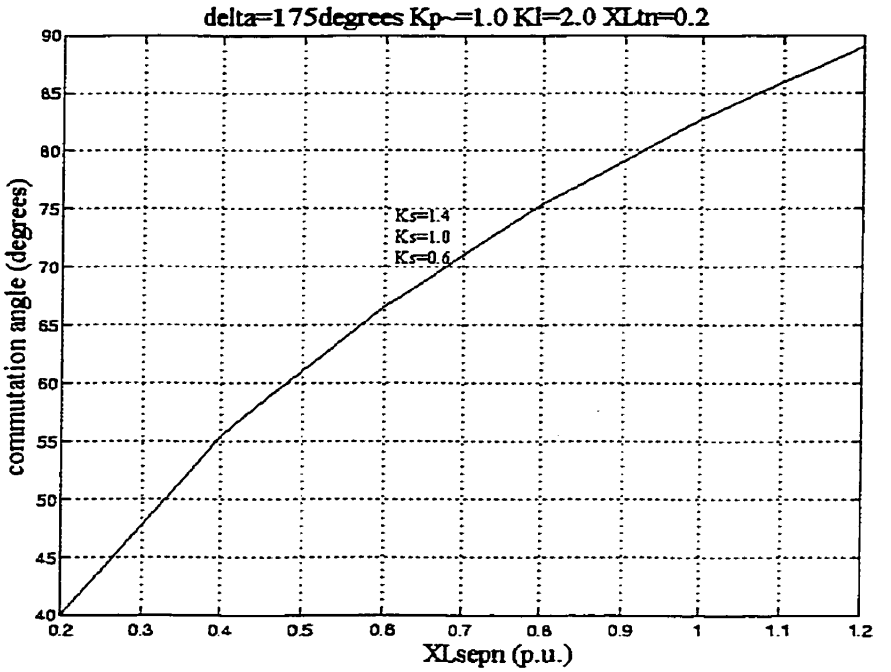

Figure 3.10: Effect of leakage inductance on the commutation angle for inductive, tuned, and capacitive series branch

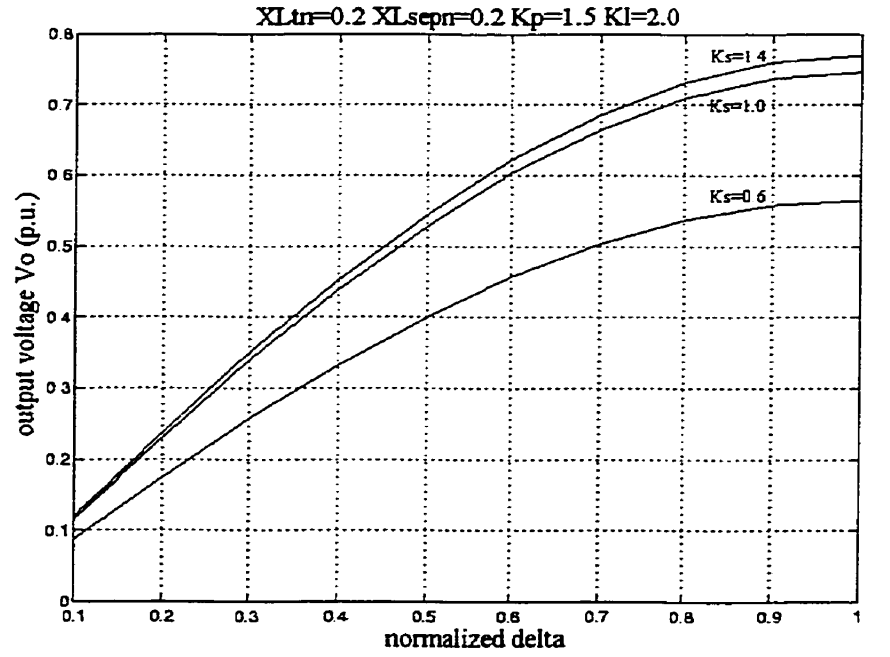

Figure 3.11: Effect of pulse width on the output voltage for inductive, tuned, and capacitive series branch

3.3 Pspice Software Simulation

Pspice is a powerful simulation tool for analyzing electrical and electronic circuits. Its prototype was SPICE (Simulation Program with Integrated Circuit Emphasis), which was developed in the early 1970s in the Department of Electrical Engineering of the University of California at Berkeley [40]. Because most of the models in Pspice are built based on the actual devices, the Pspice simulation results should be very close to the experimental results. In this thesis, the Pspice simulation results are used to validate the analysis techniques developed in the previous sections. The validation is based on the two-winding transformer model because of the availability of experimental results for the converter in the literature.

The Pspice model of the converter is shown in Figure 3.12. The voltage sources V_2 and V_3, representing the output of the inverter, provide the quasi-square wave input to the resonant circuit. The output inductance L_o and capacitor C_o make up the output filter. They must be large enough to provide the almost ripple-free output voltage and current. For the load of 0.05Ω, a 10μH inductor and 5μF capacitor can meet the ripple requirement at the switching frequency of 128kHz. Generally speaking, a larger inductor and capacitor can reduce the ripple. However, the response time to steady state will increase. Resistors with values in the range 0.01 to 0.1milliohm are added as shown in the Pspice model to avoid the convergence problems.

Figure 3.13 shows the Pspice model of the ideal transformer. The model is built based on the following characteritics of an ideal transformer.

The voltage across the secondary is 1/N times the voltage across the primary.

The current flowing out of the secondary is N times the current flowing into the primary

where N is the turns ratio. A very small resistor and a 0v DC voltage source are added to avoid the convergence problem. The leakage inductance of the transformer L_{se} is placed in the secondary circuit.

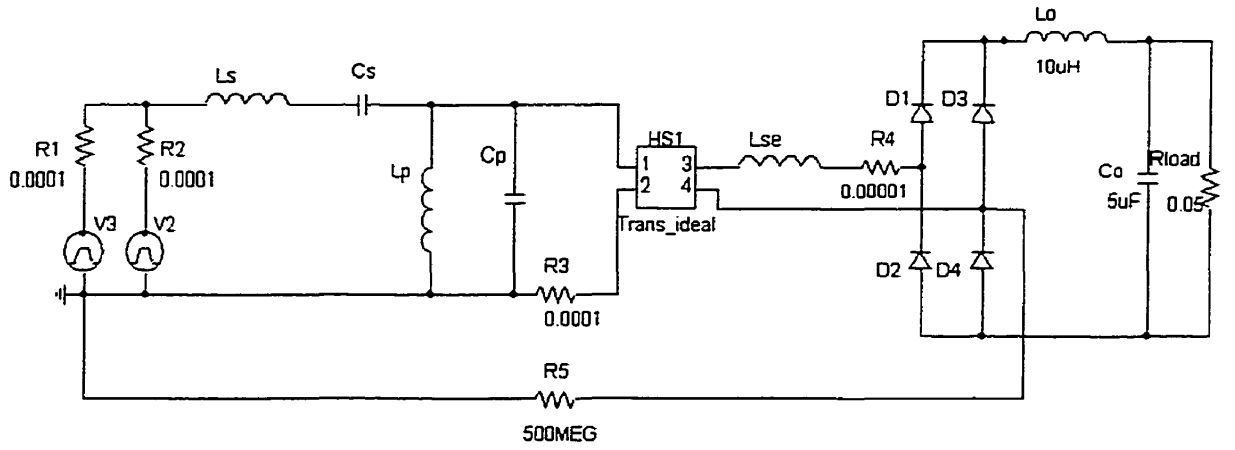

Figure 3.12: Pspice simulation model of the dc/dc converter

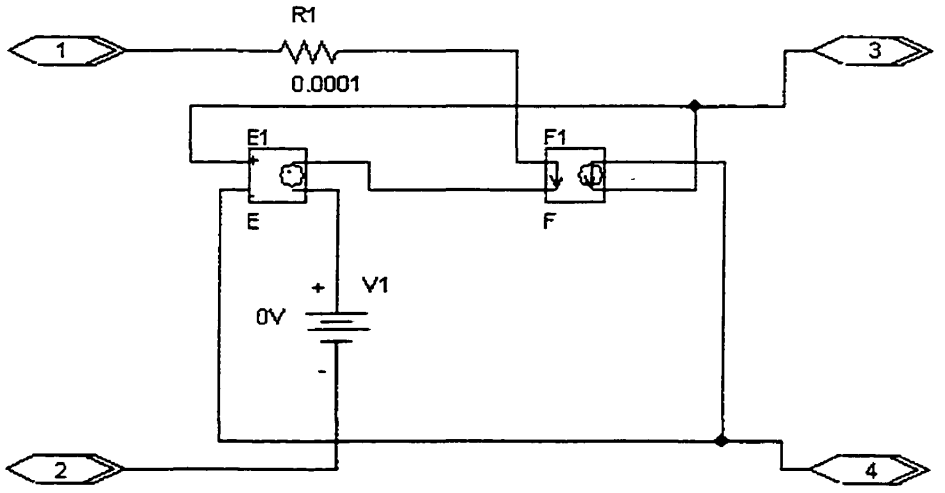

Figure 3.13: The Pspice model of an ideal transformer

The following section will compare the Pspice simulation results with those obtained using the EDF method. The values of the circuit components of an experimental converter described in [28] are used. The circuit parameters are as follows:

Series Inductor, L_s	=	3.6 μH
Series Capacitor, C_s	=	0.44 μF
Parallel Inductor, L_p	=	1.6 μH
Parallel Capacitor, C_p	=	0.88 μF
Switching Frequency, f_s	=	128 kHz
Input Voltage, V_{in}	=	60 V
Pulse Width, δ	=	114 degrees
Leakage Inductance, L_{se}	=	1 μH
Load Resistance, R_L	=	0.05 Ω

3.3.1 Pspice Simulation of the Converter with Tuned Series Branch

According to the circuit parameters listed above, the control parameters K_s, K_p, and K_l are calculated as follows:

$$K_S = X_{Cs}/X_{Ls} \cong 1.0$$

$$K_P = X_{Cp}/X_{Lp} = 1.10$$

$$K_l = X_{Ls}/X_{Lp} = 2.25$$

In this case, the series and parallel branches of the converter are slightly off tuned. Figure 3.14 shows the transient response of the output current (load current). It is

observed that the output reaches the steady state after 1.0ms. For the current parameters specified, it is assumed that all current variables reach steady state after 1.0ms.

Figure 3.15 shows the waveform of the inverter output voltage, indicating the pulse width, δ. It provides the reference point of the phase for the following plots.

Figure 3.16 shows the Pspice waveform of i_s. The THD of i_s is computed to be 11.54%. The predicted series resonant circuit current i_s obtained using the EDF method is shown in Figure 3.17. The predicted value is very close to the simulated value, in magnitude. Similarly, Figure 3.18 and Figure 3.19 show the simulated and predicted waveforms of the primary side voltage v_P. The waveforms clearly show that the predicted value of the voltage at the primary side is very close to the simulated value. The THD of v_P is computed to be 8.62%. The discrepancies in the waveshapes are due mainly to neglecting the harmonics in the EDF method.

Based on the experimental parameters, several cases with different input and transformer configurations have been calculated. The results are shown in Table 3.2. The discrepancy between the predicted and simulated results is within 10%. The Pspice results are generally lower than the EDF results because the Pspice model includes the not-ideal parameters of the diodes (e.g. the ON-state voltage drop and resistance).

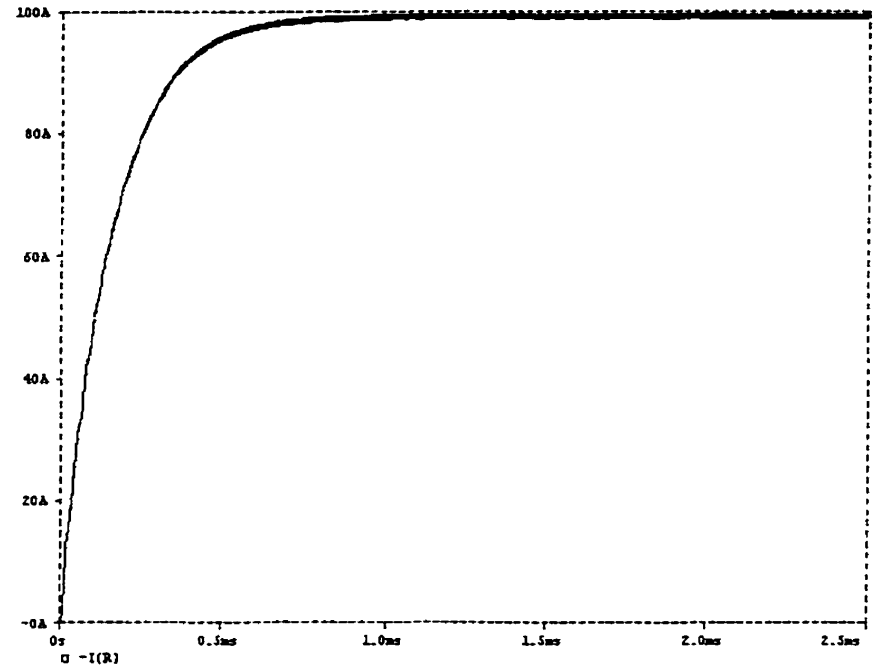

Figure 3.14: Pspice simulation result of the load current

$K_s = 1$

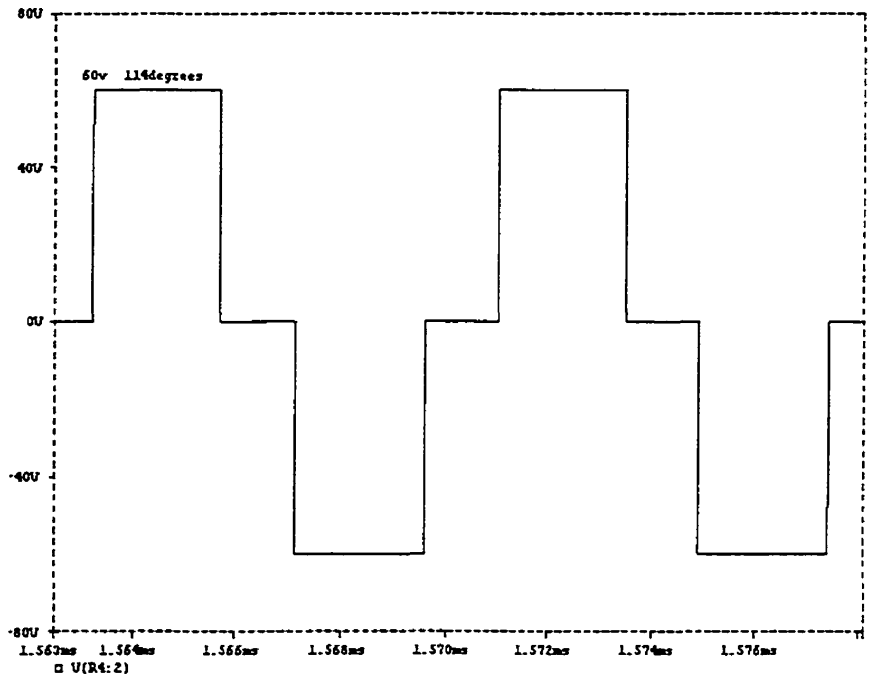

Figure 3.15: Pspice simulation result of the inverter output voltage

$K_s = 1$

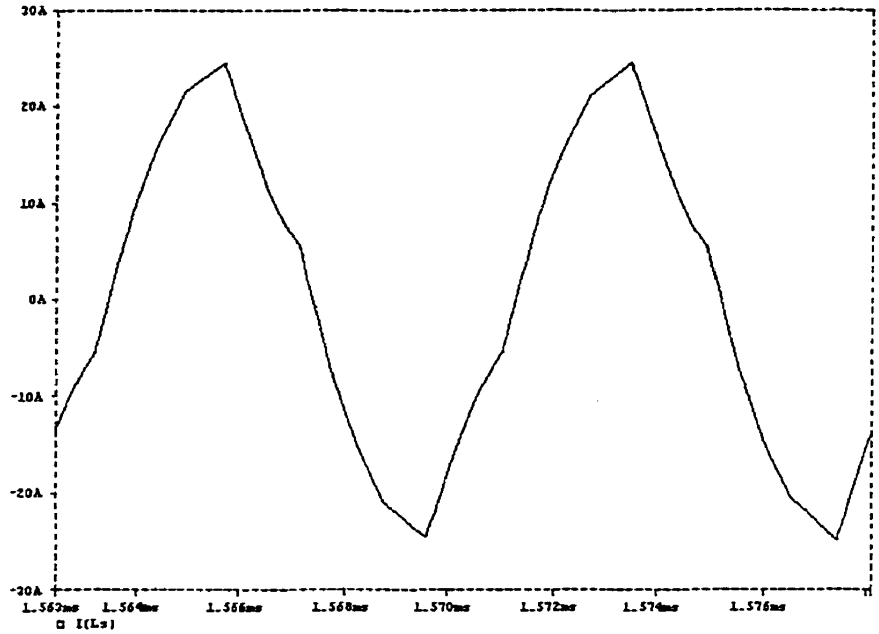

Figure 3.16: Pspice simulation result of the series resonant circuit current i_s

$K_s = 1$

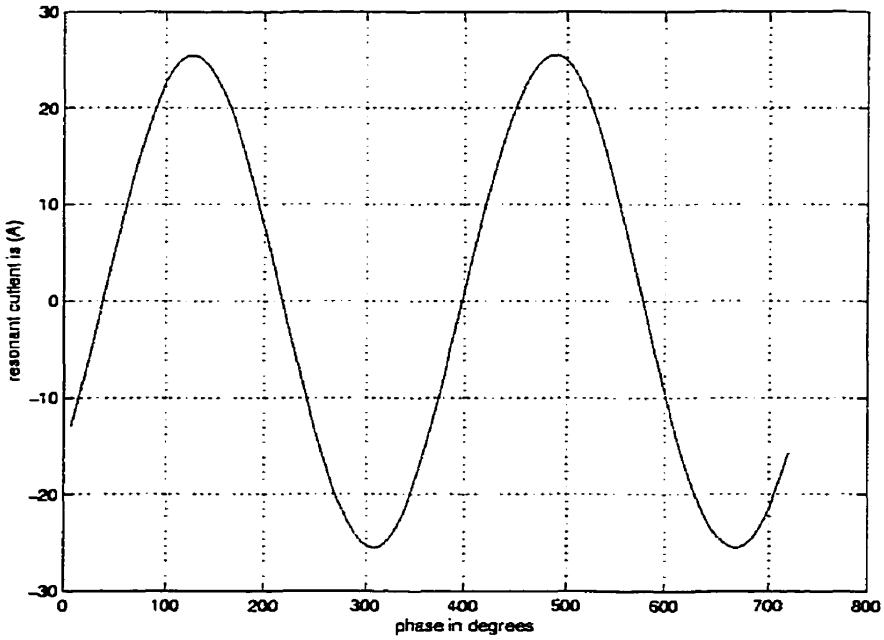

Figure 3.17: Predicted series resonant circuit current i_s, using the EDF method

$K_s = 1$

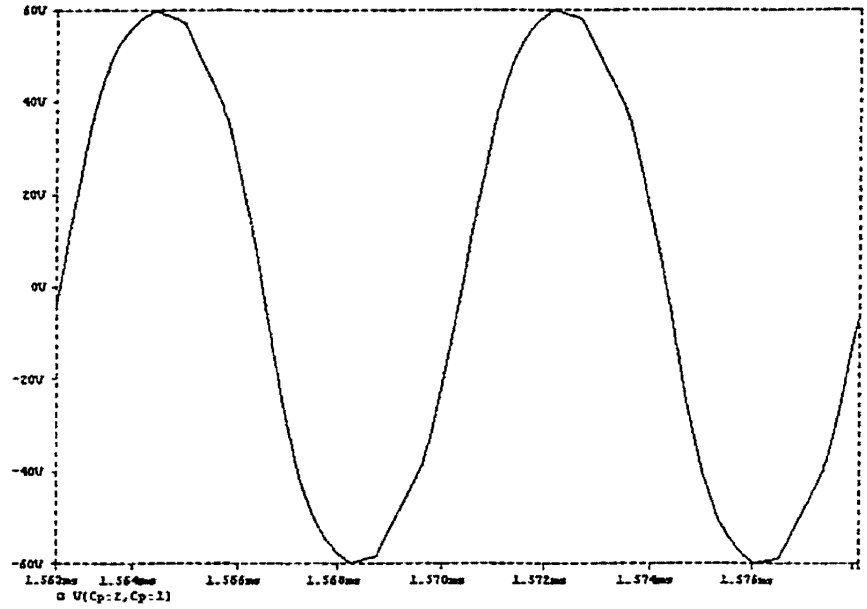

Figure 3.18: Pspice simulation result of the primary side voltage v_p

$K_s = 1$

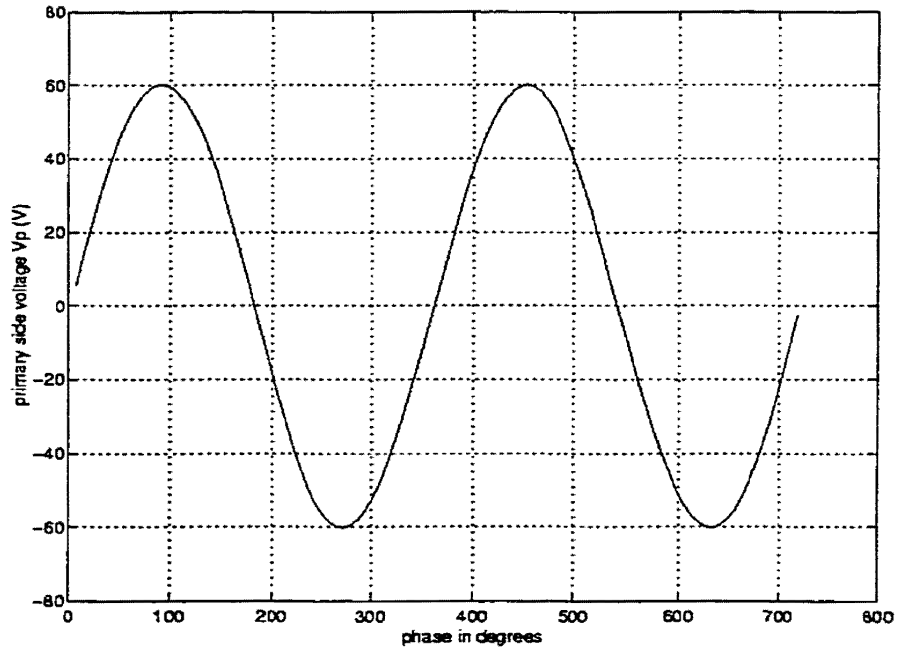

Figure 3.19: Predicted primary side voltage v_p, using the EDF method

$K_s = 1$

Table 3.2: Predicted and simulations results for the two-winding transformer

Input and Transformer Configurations	Extended Describing Function Method	Pspice Simulation Results
$V_{in} = 40$ V $N_p:N_s = 6$ $\delta = 175°$ $L_{sep} = 0$	$V_o = 5.24$ V $I_o = 104.88$ A	$V_o = 4.88$ V $I_o = 97.52$ A
$V_{in} = 60$ V $N_p:N_s = 6$ $\delta = 114°$ $L_{sep} = 1$ uH	$V_o = 5.48$ V $I_o = 109.42$ A	$V_o = 5.01$ V $I_o = 99.43$ A
$V_{in} = 48$ V $N_p:N_s = 4$ $\delta = 105°$ $L_{sep} = 1$ uH.	$V_o = 5.27$ V $I_o = 105.58$ A	$V_o = 4.76$ V $I_o = 95.37$ A
$V_{in} = 60$ V $N_p:N_s = 4$ $\delta = 80°$ $L_{sep} = 1$ uH	$V_o = 5.17$ V $I_o = 103.56$ A	$V_o = 4.58$ V $I_o = 91.57$ A

3.3.2 Simulation of the Converter with Inductive Series Branch

In this section, the parameters of the experimental example are modified to make the series branch of the converter inductive.

The values of the circuit components are as follows:

Series Inductor, L_s	=	3.6 μH
Series Capacitor, C_s	=	0.73 μF
Parallel Inductor, L_p	=	1.6 μH
Parallel Capacitor, C_p	=	0.88 μF
Switching Frequency, f_s	=	128 kHz
Input Voltage, V_{in}	=	60 V
Pulse Width, δ	=	114 degrees
Leakage Inductance, L_{se}	=	1 μH
Load Resistance, R_L	=	0.05 Ω

The control parameters K_s, K_p, and K_l are computed as follows:

$$K_S = X_{Cs}/X_{Ls} = 0.60$$

$$K_P = X_{Cp}/X_{Lp} = 1.10$$

$$K_l = X_{Ls}/X_{Lp} = 2.25$$

The simulated and the predicted results are shown in Figure 3.20 to Figure 3.23 respectively. The plots show that the predicted values of v_p and i_s are in good agreement with the simulation results.

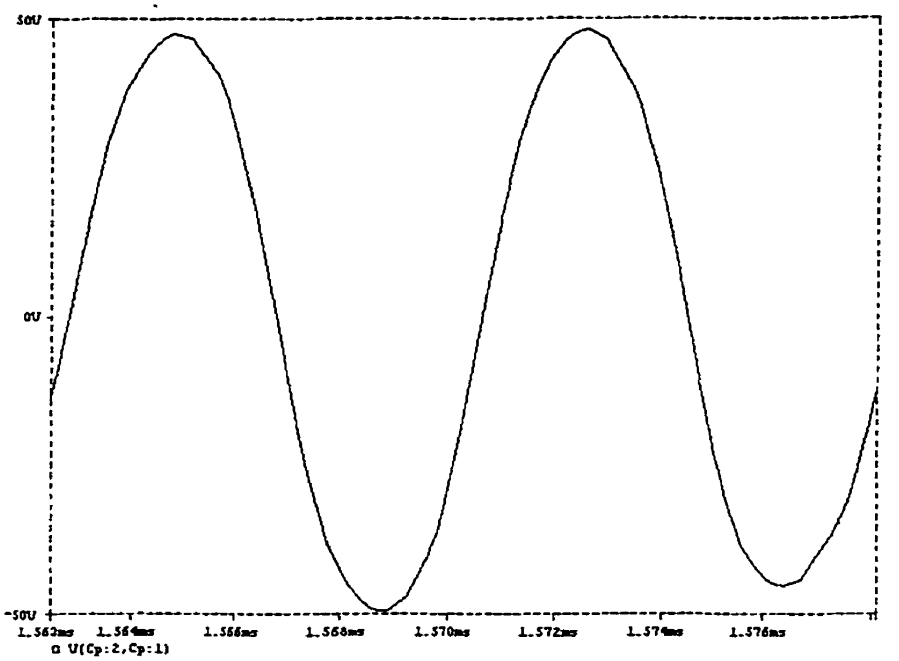

Figure 3.20: Pspice simulation result of the primary side voltage v_p

$K_s = 0.6$

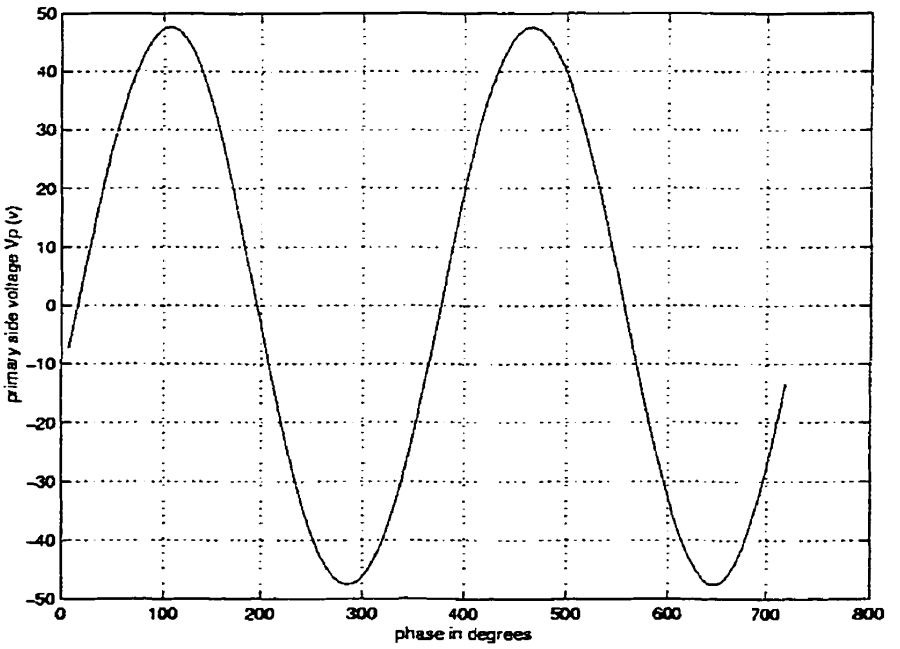

Figure 3.21: Predicted primary voltage v_p, using the EDF method

$K_s = 0.6$

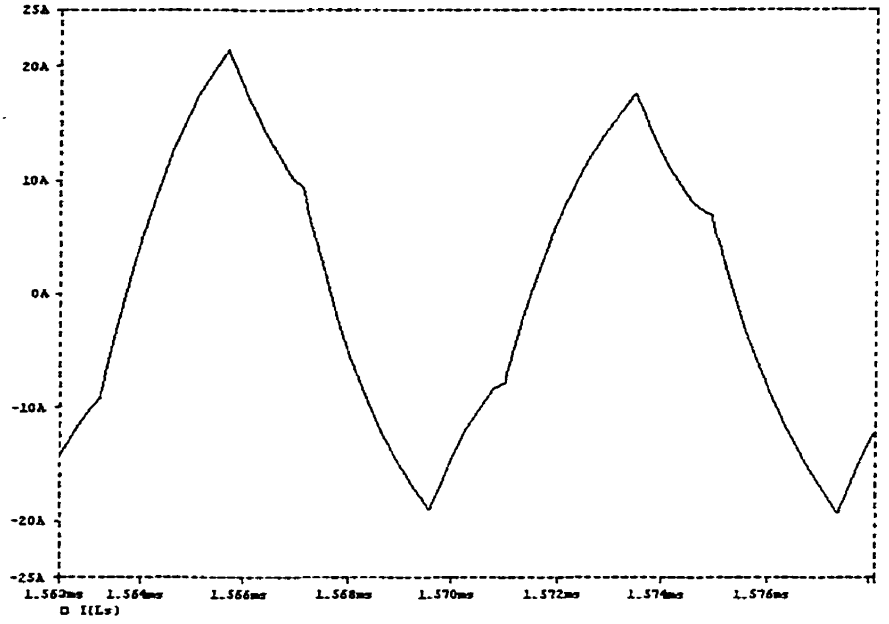

Figure 3.22: Pspice simulation result of the series resonant circuit current i_s

$K_s = 0.6$

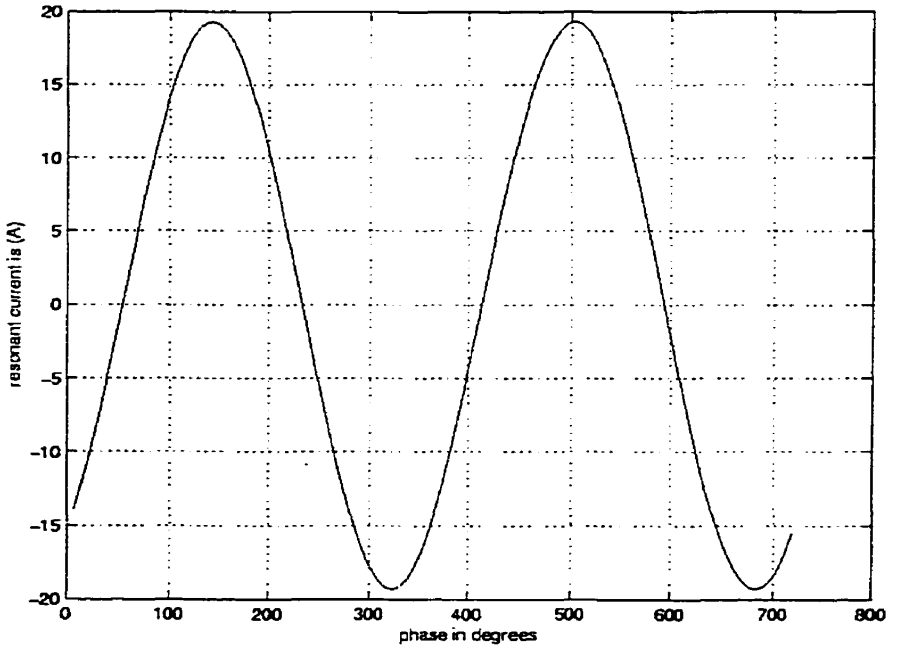

Figure 3.23: Predicted series resonant circuit current i_s, using the EDF method

$K_s = 0.6$

3.3.3 Simulation of the Converter with Capacitive Series Branch

In this section, the parameters of the experimental example are modified to make the series branch of the converter capacitive.

The values of the circuit components are as follows:

Series Inductor, L_s	=	3.6 μH
Series Capacitor, C_s	=	0.31 μF
Parallel Inductor, L_p	=	1.6 μH
Parallel Capacitor, C_p	=	0.88 μF
Switching Frequency, f_s	=	128 kHz
Input Voltage, V_{in}	=	60 V
Pulse Width, δ	=	114 degrees
Leakage Inductance, L_{se}	=	1 μH
Load Resistance, R_L	=	0.05 Ω

The control parameters K_s, K_p, and K_l are computed as follows:

$$K_S = X_{Cs}/X_{Ls} = 1.4$$

$$K_P = X_{Cp}/X_{Lp} = 1.10$$

$$K_l = X_{Ls}/X_{Lp} = 2.25$$

The simulated and the predicted results are shown in Figure 3.24 to Figure 3.27 respectively. The plots show that the predicted values of v_p and i_s are in good agreement with the simulation results.

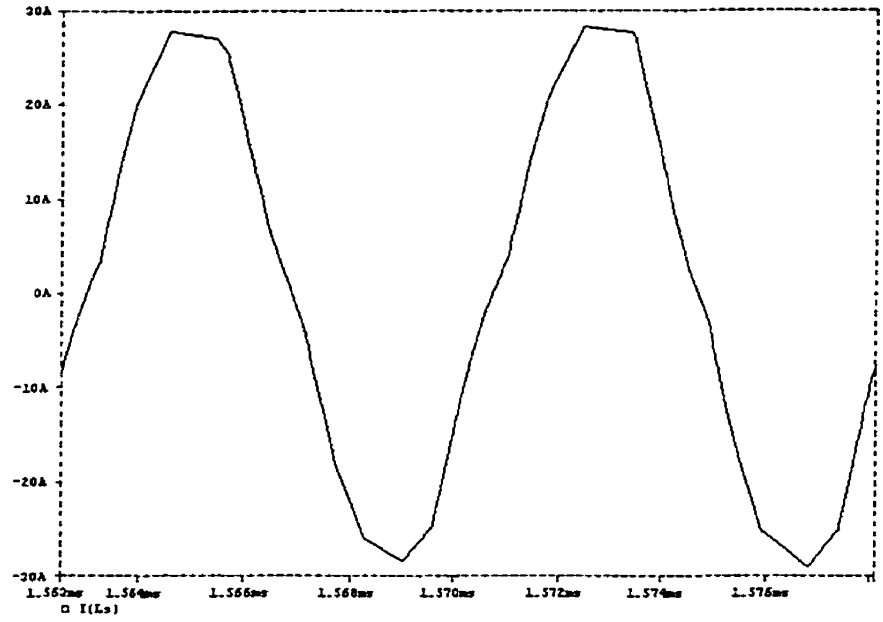

Figure 3.24: Pspice simulation result of the series resonant circuit current i_s

$K_s = 1.4$

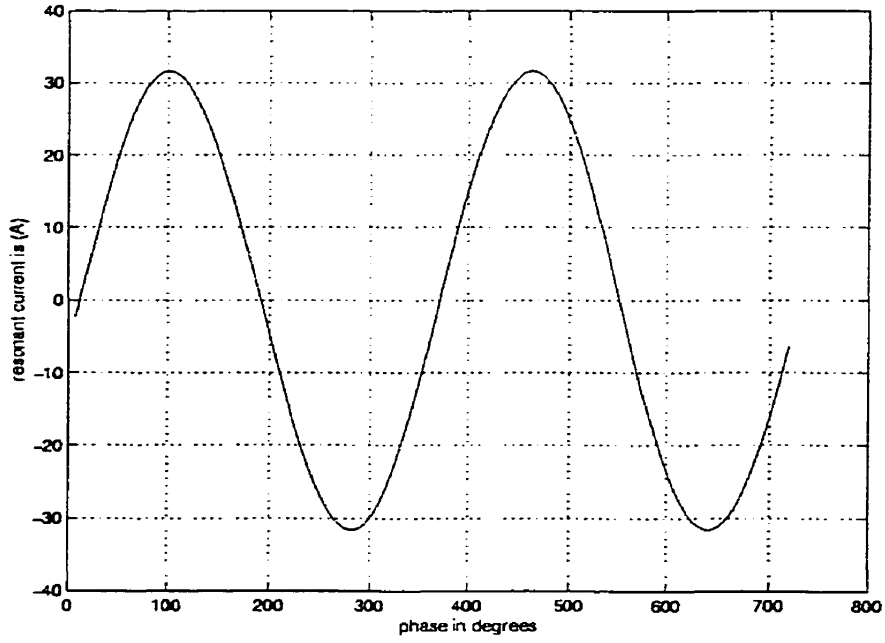

Figure 3.25: Predicted series resonant circuit current i_s, using the EDF method

$K_s = 1.4$

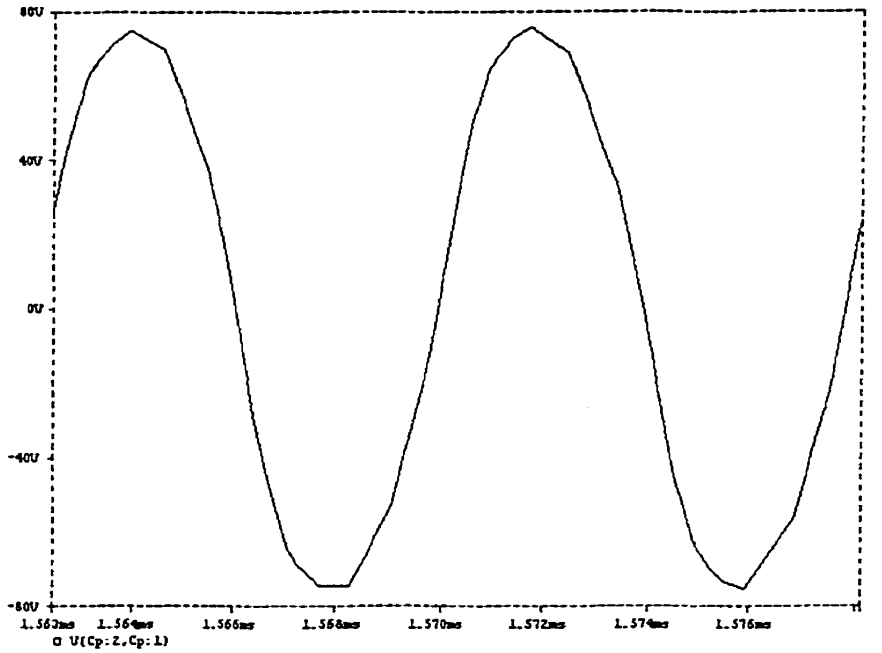

Figure 3.26: Pspice simulation result of the primary side voltage v_p

$K_s = 1.4$

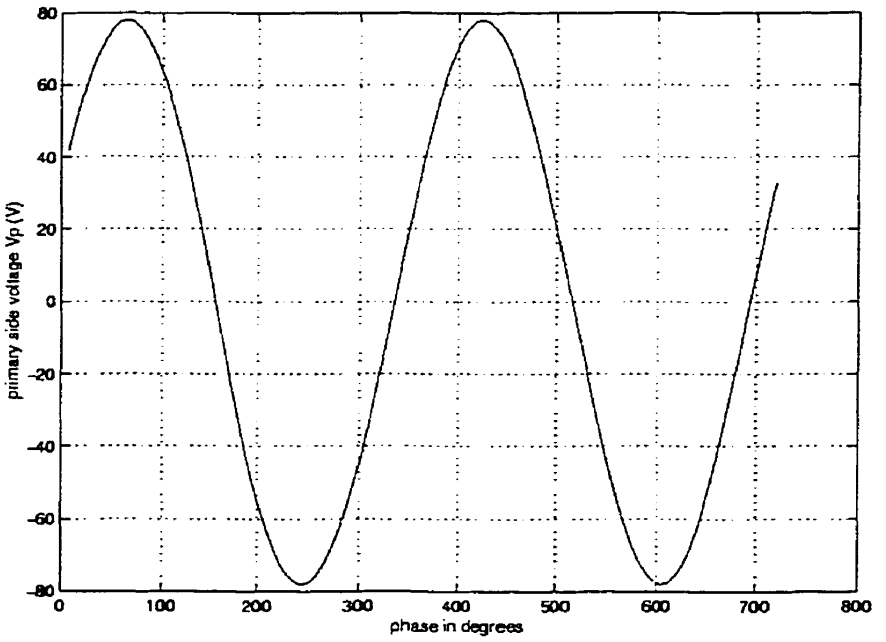

Figure 3.27: Predicted primary side voltage v_p, using the EDF method

$K_s = 1.4$

3.4 Summary

In this chapter, the converter characteristics were discussed. The frequency domain analysis and Pspice software simulation were used to validate the results from the EDF method. The results indicate that the EDF method can predict the performance of the converter accurately.

Chapter 4

Design of the Series-Parallel Resonant DC/DC Converters

In this chapter, a set of design equations based on the EDF method of the converter is developed. Four normalized parameters are derived from the equations and used to study the characteristics of the converter in order to establish design procedure that allows the resonant parameters and other circuit components to be determined. The cost and size of the converter expressed as KVA/KW rating of the resonant circuit is taken into consideration. A design procedure based on the selection of resonant parameters to minimize KVA/KW ratio is presented. Several design examples are given to illustrate the design procedure. Finally, two of the examples are verified by Pspice simulation.

4.1 Development of Design Equations

In order to establish a set of design equations for selecting the resonant parameters, the set of equations obtained by the EDF model in Chapter 2 (2.27)-(2.37)

are modified. First, four general parameters of the resonant circuits are defined as follows:

$$\omega_{rs} = 1/\sqrt{L_s C_s} \qquad (4.1)$$

$$Z_{rs} = \sqrt{L_s/C_s} \qquad (4.2)$$

$$\omega_{rp} = 1/\sqrt{L_p C_p} \qquad (4.3)$$

$$Z_{rp} = \sqrt{L_p/C_p} \qquad (4.4)$$

where ω_{rs} and Z_{rs} are the resonant frequency and characteristic impedance of the series resonant circuit, and ω_{rp} and Z_{rp} are the resonant frequency and characteristic impedance of the parallel resonant circuit respectively.

Next, the parameters in equations (4.1) to (4.4) are normalized with respect to the corresponding fixed parameters of the converter. i.e. the resonant frequencies are normalized with respect to the fixed switching frequency, ω_s, and the characteristic impedances are normalized with respect to the reflected value of the load resistance in the primary circuit, resulting in the following normalized parameters.

$$\omega_{sn} = \omega_{rs}/\omega_s \qquad (4.5)$$

$$\omega_{pn} = \omega_{rp}/\omega_s \qquad (4.6)$$

$$Z_{sn} = Z_{rs}/R_b \qquad (4.7)$$

$$Z_{pn} = Z_{rp}/R_b \qquad (4.8)$$

where R_b is the load resistance (R_L) reflected to the primary circuit.

In addition, circuit voltages are normalized with respect to the dc input voltage, V_{in}. Consequently, circuit currents are normalized with respect to the base current, $I_b=V_{in}/R_b$. Using the normalized parameters and variables, the circuit equations

developed in chapter 2 (2.27)-(2.37) for the three-winding converter can be written as follows.

$$-\left(Z_{sn}/\omega_{sn}+X_{Lln}\right)I_{Lscn}+X_{Lln}I_{pcn}+V_{Cssn}+V_{Cpsn}=E \qquad (4.9)$$

$$\left(Z_{sn}/\omega_{sn}+X_{Lln}\right)I_{Lssn}-X_{Lln}I_{psn}+V_{Cscn}+V_{Cpcn}=0 \qquad (4.10)$$

$$-\left(Z_{pn}/\omega_{pn}\right)\cdot I_{Lpcn}=V_{Cpsn} \qquad (4.11)$$

$$\left(Z_{pn}/\omega_{pn}\right)\cdot I_{Lpsn}=V_{Cpcn} \qquad (4.12)$$

$$-V_{Cpcn}/\left(\omega_{pn}\cdot Z_{pn}\right)=I_{Lssn}-I_{psn}-I_{Lpsn} \qquad (4.13)$$

$$V_{Cpsn}/\left(\omega_{pn}\cdot Z_{pn}\right)=I_{Lscn}-I_{pcn}-I_{Lpcn} \qquad (4.14)$$

$$-V_{Cscn}/\left(\omega_{sn}\cdot Z_{sn}\right)=I_{Lssn} \qquad (4.15)$$

$$V_{Cssn}/\left(\omega_{sn}\cdot Z_{sn}\right)=I_{Lscn} \qquad (4.16)$$

$$\cos(\mu)=1-\frac{2X_{Lsepn}I_{on}}{V_{pn}} \qquad (4.17)$$

$$\int_0^{2\pi} v_{sn}i_{Lsn}=\int_0^{2\pi} V_{on}I_{on} \Rightarrow I_{on}=\sqrt{EI_{Lssn}/2} \qquad (4.18)$$

$$V_{pn}\sin(\phi)+V_{pn}\cos(\phi)=0 \qquad (4.19)$$

where the subscript 'n' refers to normalized quantities. In the discussions which follow, the normalized output voltage, V_{on} is referred to as the dc voltage gain or the dc voltage transfer ratio, M.

An important consideration in the design of the resonant converter is the cost and size of the resonant circuit. An optimum design should aim at minimizing the cost and size of the resonant circuits, which is defined in terms of the KVA rating of the resonant

parameters, normalized to the KW output by the converter. The KVA/KW ratio of the resonant circuits is defined as

$$CS = \left(I_{Ls.rms}^2 \cdot X_{Ls} + V_{Cs.rms}^2 / X_{Cs} + I_{Lp.rms}^2 \cdot X_{Lp} + V_{Cp.rms}^2 / X_{Cp} \right) / P_o \qquad (4.20)$$

The normalized equations given above are general and allow the effect of the values of the circuit components on the performance of the fixed switching frequency converter to be investigated. More importantly, the equations can be used to determine the required values of the resonant circuit parameters to meet established design criteria.

4.2 Performance of the Converter as a Function of the Resonant Circuit Parameters

The normalized set of equations is used to present characteristic curves from which the preferred modes of operation of the converter and design criteria are established. In this section, the characteristics are provided for $\delta = 120^\circ$ under the condition that $\omega_{sn}=\omega_{pn}$. Similar characteristics can be obtained for other values of δ. Appendix C gives the set of characteristics for $\delta = 175^\circ$.

4.2.1 Effect of Resonant Circuit Parameters on the KVA/KW Rating

Figures 4.1 to 4.6 show the effect of the resonant parameters on the KVA/KW ratio of the resonant circuits, for three values of the transformer leakage inductance.

The figures generally show that the KVA/KW ratio of the resonant circuit decreases with decreasing Z_{sn} and increasing Z_{pn}. The cost and size function exhibits a minimum for low values of Z_{sn} and high values of Z_{pn} at different values of ω_{sn}. The effect of increasing the leakage inductance is to shift the minimum cost and size function to ω_{sn} greater than unity. In general, for a given leakage inductance, an ω_{sn} can be determined which minimizes the cost and size of the resonant circuit parameters. The figures show that to design the converter for minimum cost and size, Z_{sn} should not be more than 3.5 and Z_{pn} should not be less than 1.5p.u. However, the values of these parameters affect the performance of the converter as discussed below.

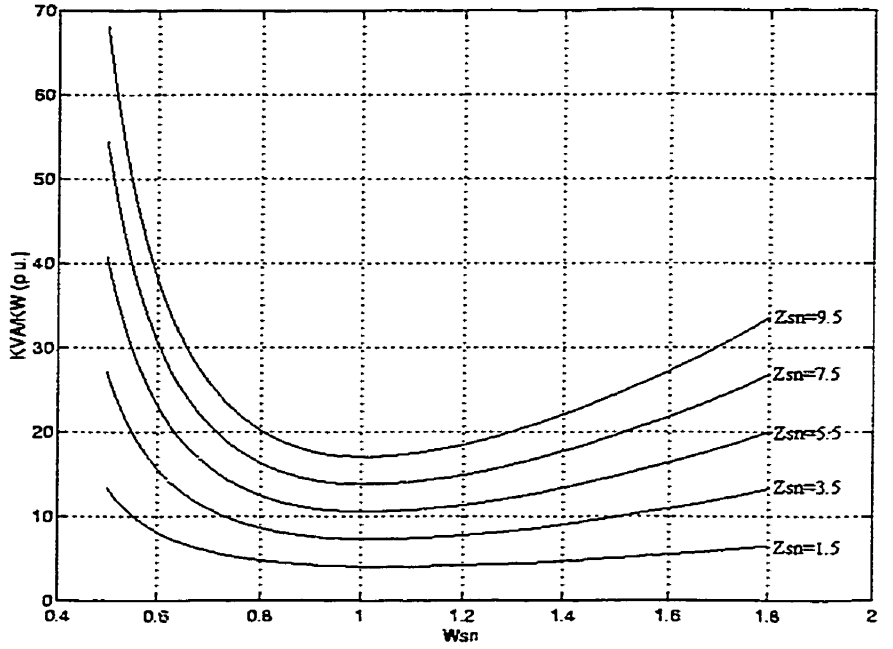

(a)

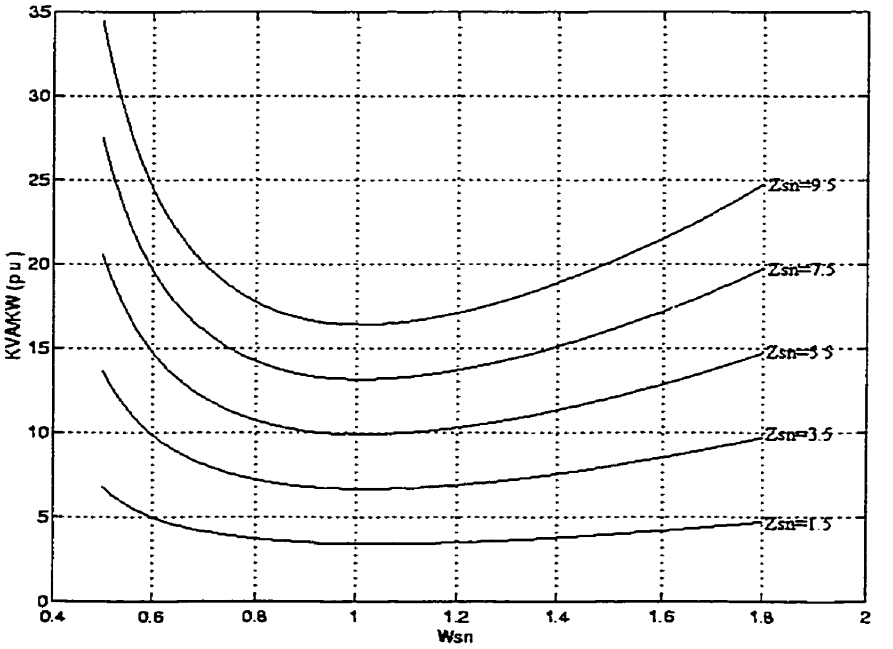

(b)

Figure 4.1: KVA/KW rating versus normalized frequency, ω_{sn}

$\delta = 120^{\circ}$, X_{Lsepn}=0, X_{Lm}=0.2p.u.

(a) Z_{pn}=1.5, (b) Z_{pn}=2.5

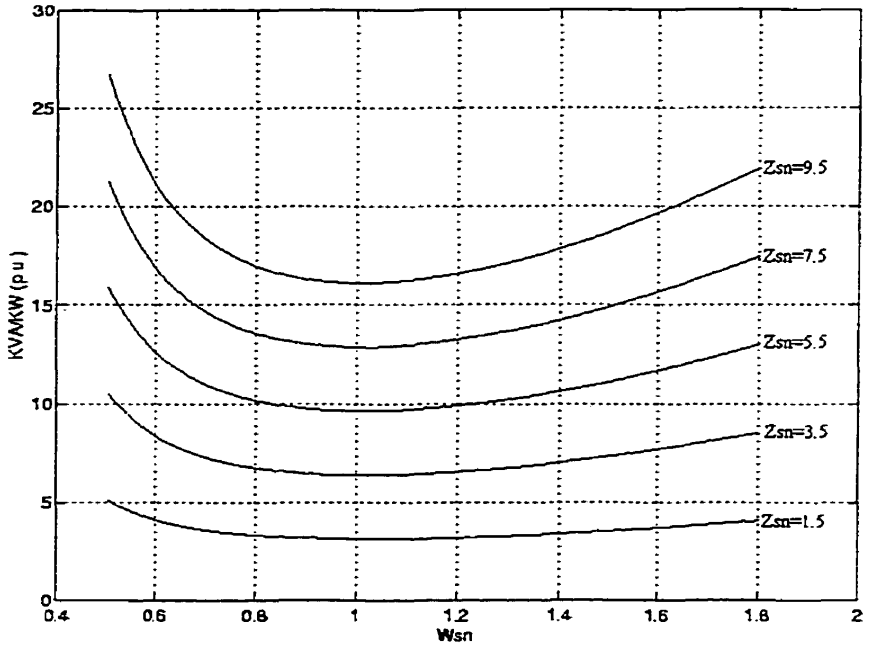

(a)

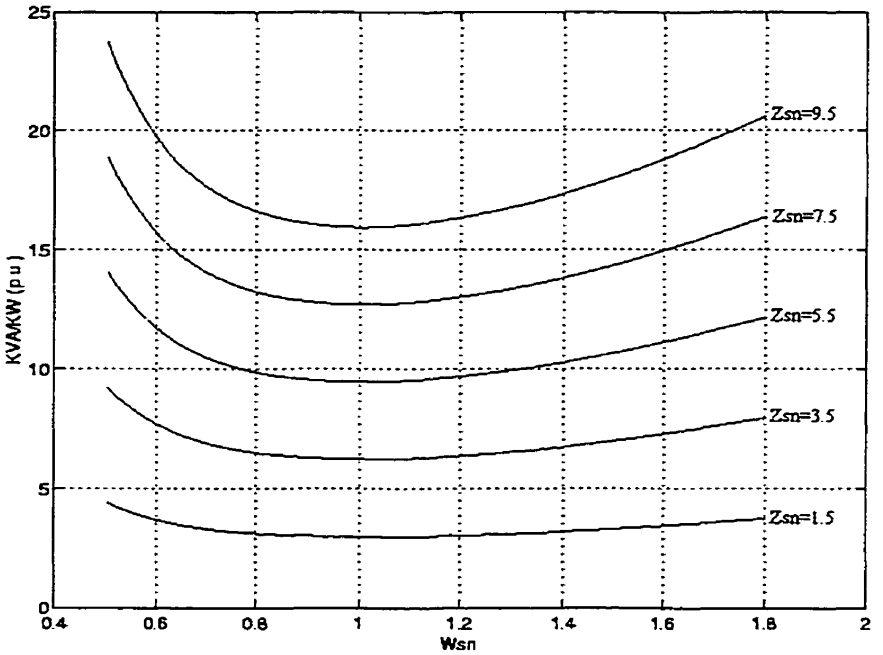

(b)

Figure 4.2: KVA/KW rating versus normalized frequency, ω_{sn}

$\delta = 120^{\circ}$, X_{Lsepn}=0, X_{Ltn}=0.2p.u.

(a) Z_{pn}=3.5, (b) Z_{pn}=4.5

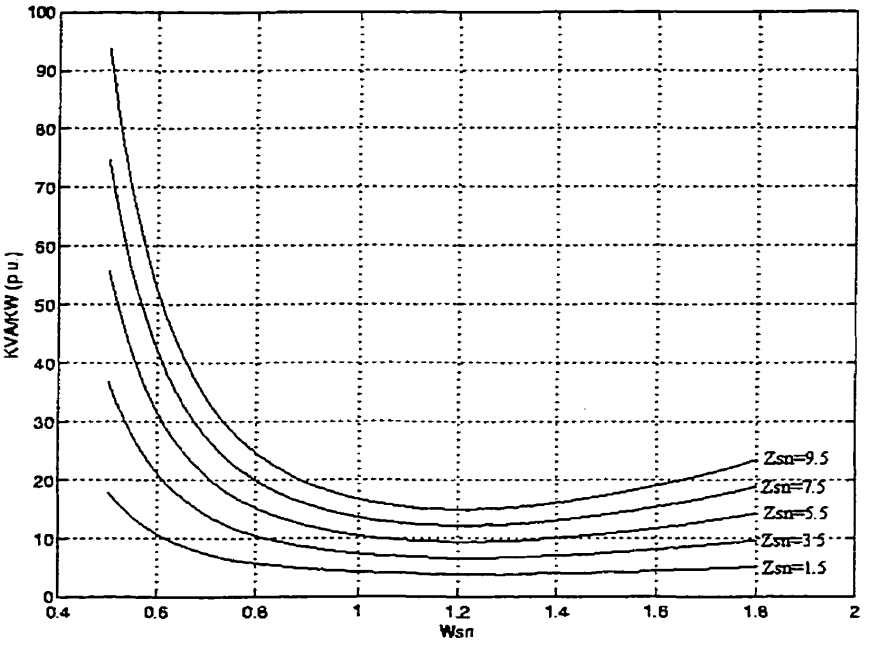

(a)

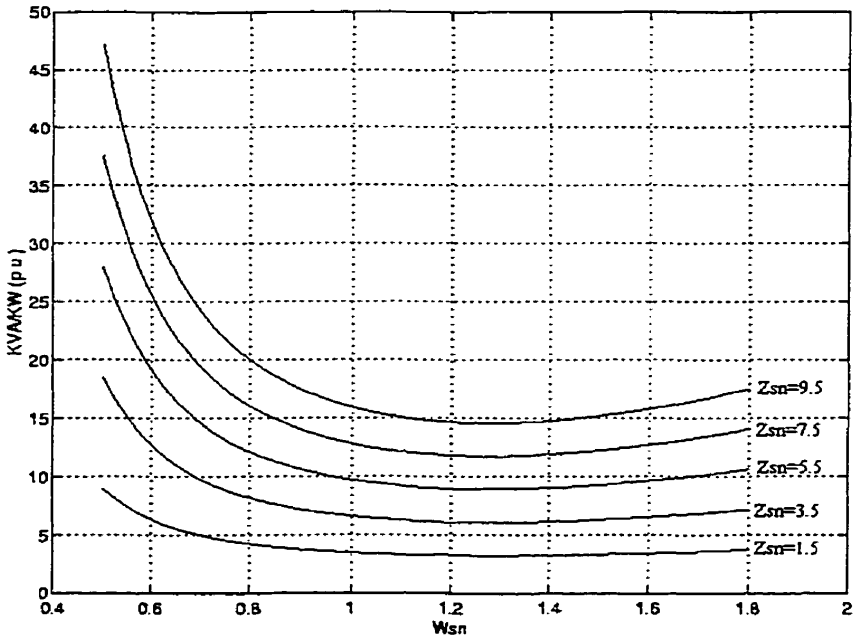

(b)

Figure 4.3: KVA/KW rating versus normalized frequency, ω_{sn}

$\delta = 120^{\circ}$, X_{Lsepn}=0.2p.u., X_{Lm}=0.2p.u.

(a) Z_{pn}=1.5, (b) Z_{pn}=2.5

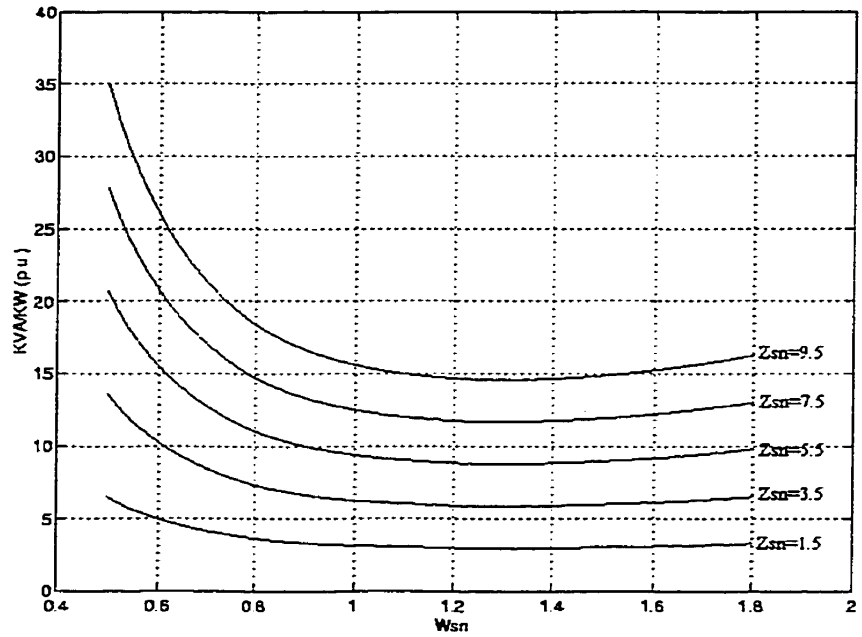

(a)

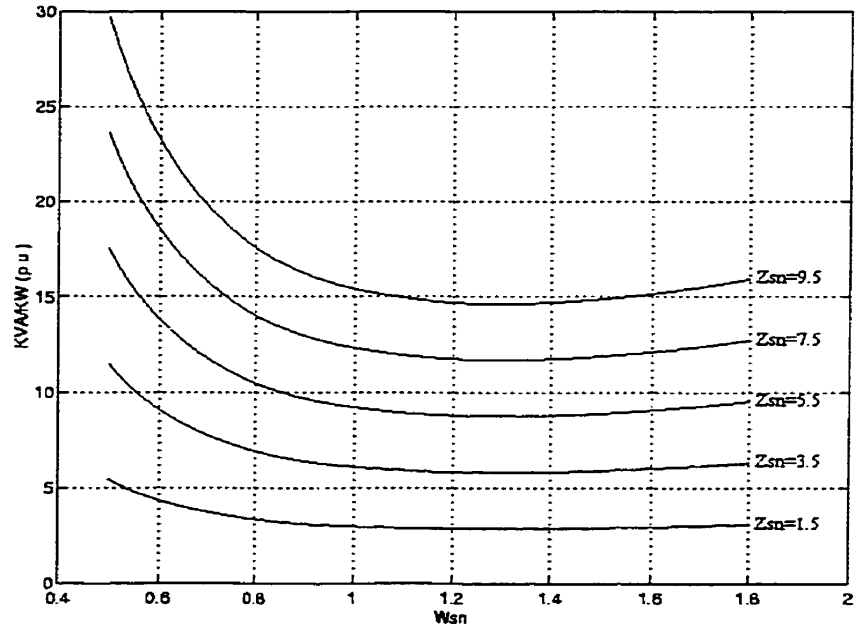

(b)

Figure 4.4: KVA/KW rating versus normalized frequency, ω_{sn}

$\delta = 120^{\circ}$, X_{Lsepn}=0.2p.u., X_{Ltn}=0.2p.u.

(a) Z_{pn}=3.5, (b) Z_{pn}=4.5

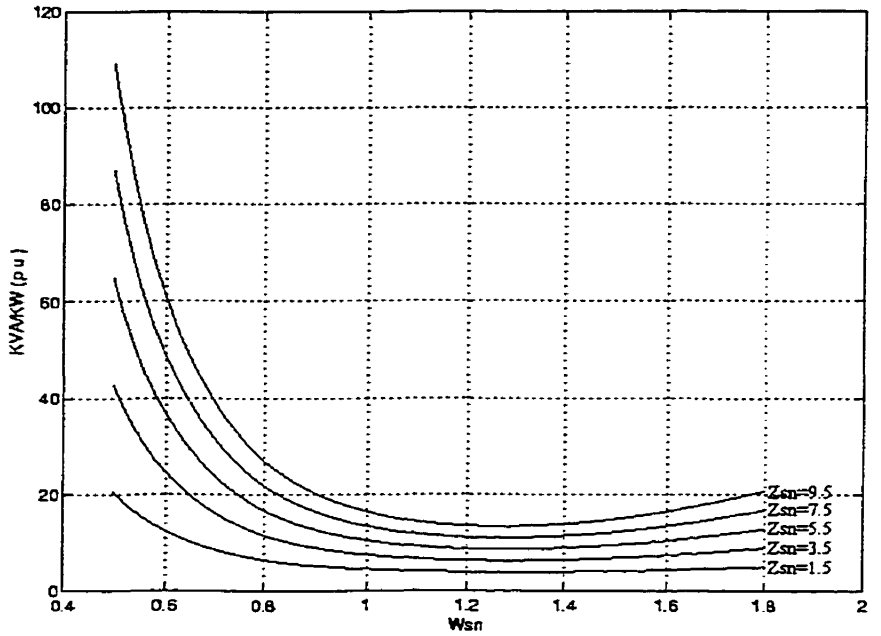

(a)

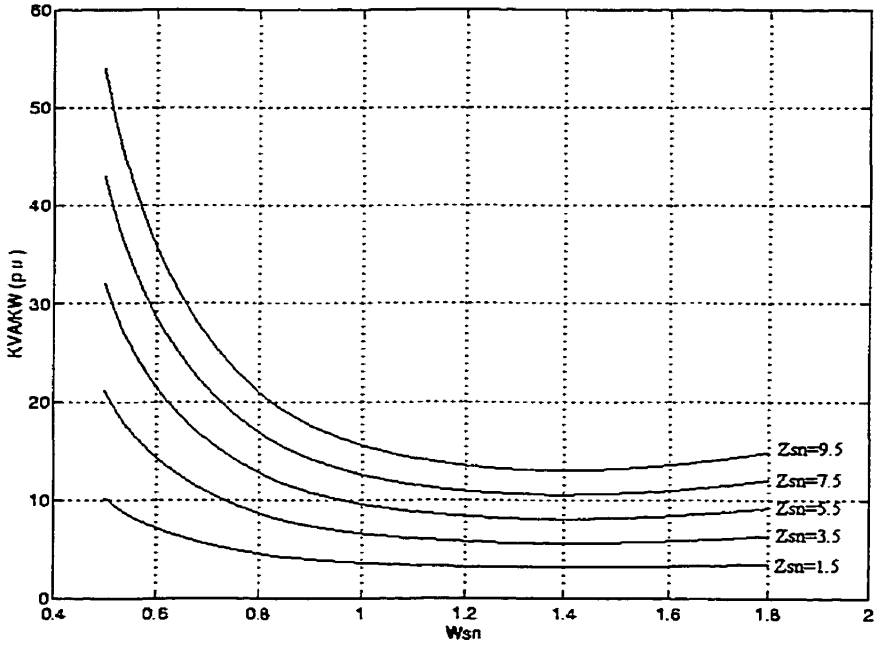

(b)

Figure 4.5: KVA/KW rating versus normalized frequency, ω_{sn}

$\delta = 120^{\circ}$, X_{Lsepn}=0.4p.u., X_{Ltn}=0.2p.u.

(a) Z_{pn}=1.5, (b) Z_{pn}=2.5

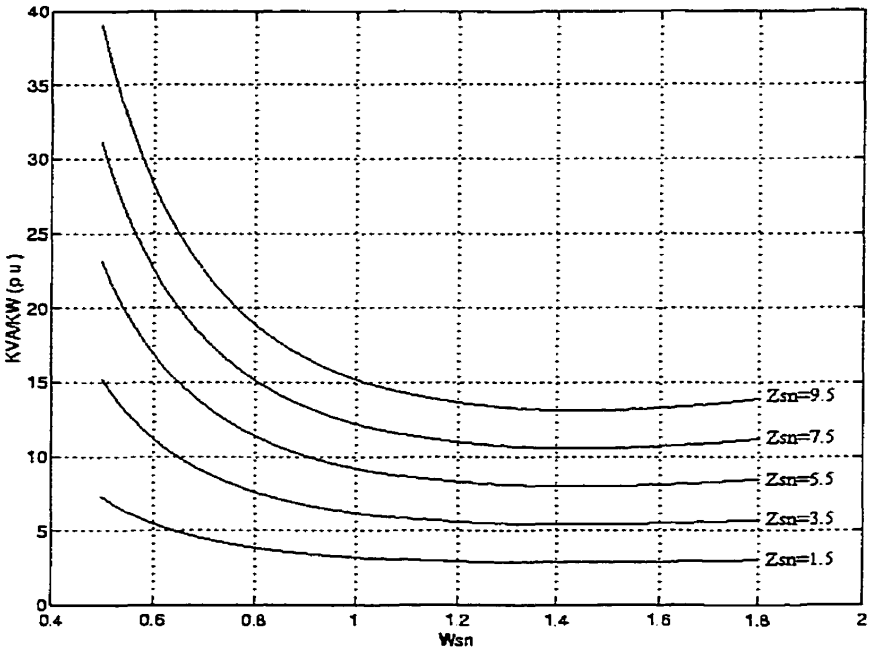

(a)

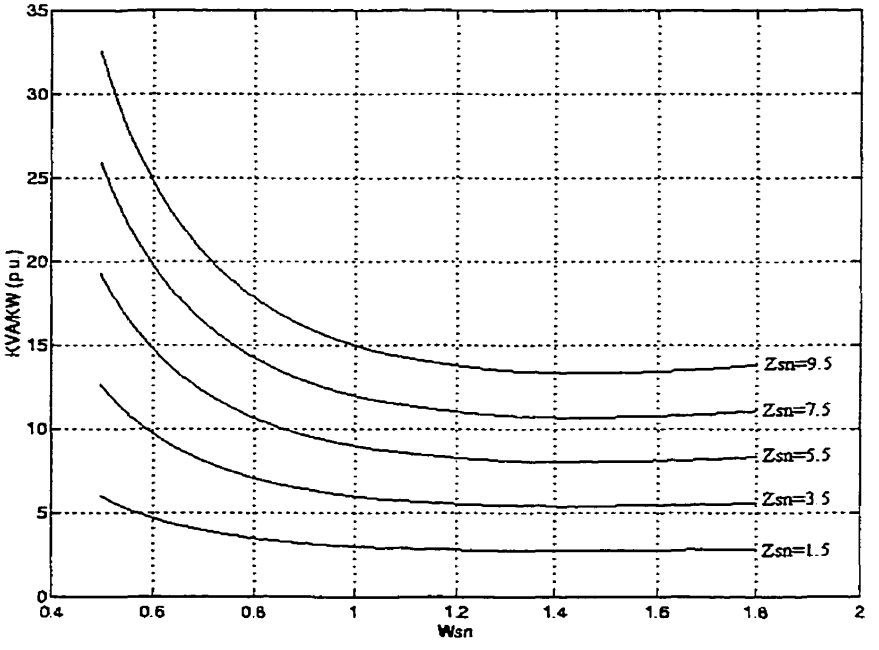

(b)

Figure 4.6: KVA/KW rating versus normalized frequency, ω_{sn}

$\delta = 120^{\circ}$, X_{Lsepn}=0.4p.u., X_{Ltn}=0.2p.u.

(a) Z_{pn}=3.5, (b) Z_{pn}=4.5

4.2.2 Effect of Resonant Circuit Parameters on the Voltage Transfer Ratio, Transformer Primary Voltage, and Series Resonant Circuit Current

The characteristic curves of Figures 4.7, 4.8 and 4.9(a) show that generally speaking, the input current i_s, the primary side voltage v_p, and the voltage transfer ratio M exhibit similar characteristics. The discussion which follows concentrates on the voltage transfer ratio. However, similar comments can be made for the series resonant circuit current i_s and the primary side voltage v_p.

The effects of the resonant parameters on the voltage transfer ratio are shown in Figures 4.9 to 4.14. The figures show that when the leakage inductance is neglected (X_{Lsepn}=0), the maximum dc voltage gain that is produced by the converter is 0.7p.u. at ω_{sn}=1.0p.u. for Z_{sn} greater than 1.5p.u. At lower value of Z_{sn} and Z_{pn}, the curves exhibit two peaks. With zero leakage inductance, the two peaks are greater than 0.7p.u. However, as Z_{sn} increases, the peak values decrease and merge into one peak at ω_{sn}=1.0p.u. for higher value of Z_{pn}. As shown in Figure 4.11 to Figure 4.14, with increasing leakage inductance, the converter still exhibits the two-peak phenomenon for lower values of Z_{sn} and Z_{pn}. However, the peaks are no longer equal; a higher peak value is obtained for ω_{sn} less than unity. Also with a non-zero leakage inductance, the peak value of the voltage transfer ratio decreases with increasing Z_{sn}, and the frequency, ω_{sn}, at which the peak occurs increases. The characteristics curves also suggest that with non-zero leakage inductance the voltage transfer ratio remains fairly constant for a wide variation in Z_{sn} if ω_{sn} is greater but very close to unity.

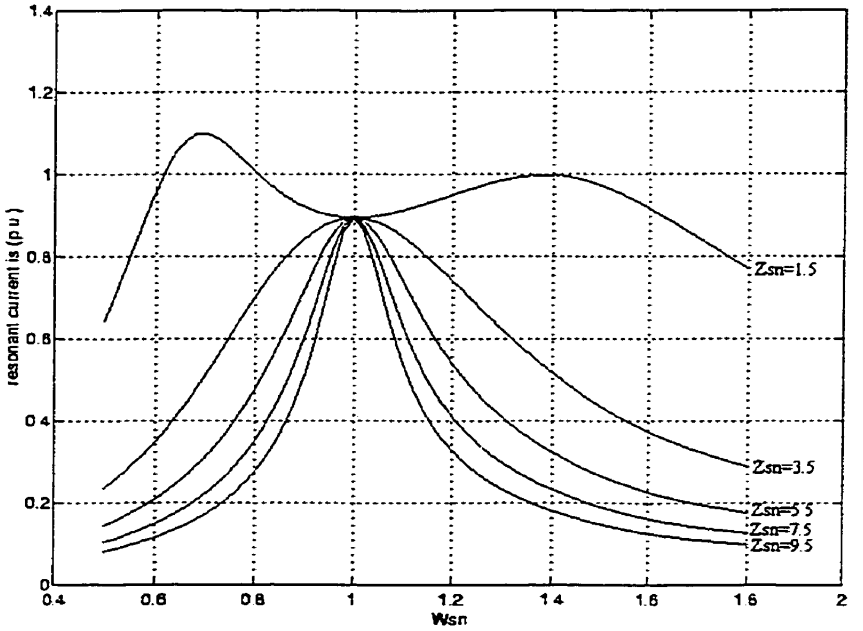

Figure 4.7: Resonant current i_s versus normalized frquency, ω_{sn}

$\delta = 120°$, X_{Lsepn}=0, X_{Ltn}=0.2p.u, Z_{pn}=1.5

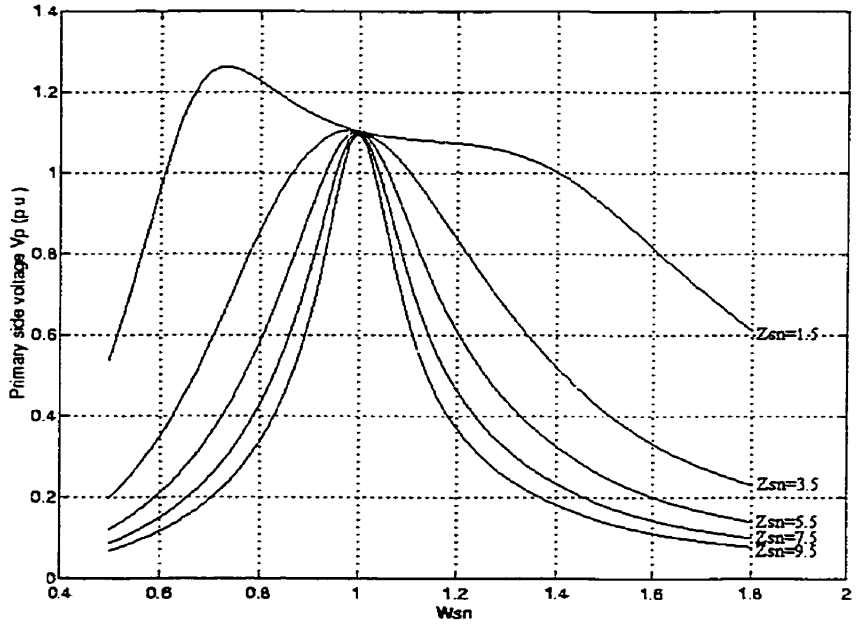

(b)

Figure 4.8: Primary side voltage, v_p versus normalized frequency, ω_{sn}

$\delta = 120°$, X_{Lsepn}=0, X_{Ltn}=0.2p.u, Z_{pn}=1.5

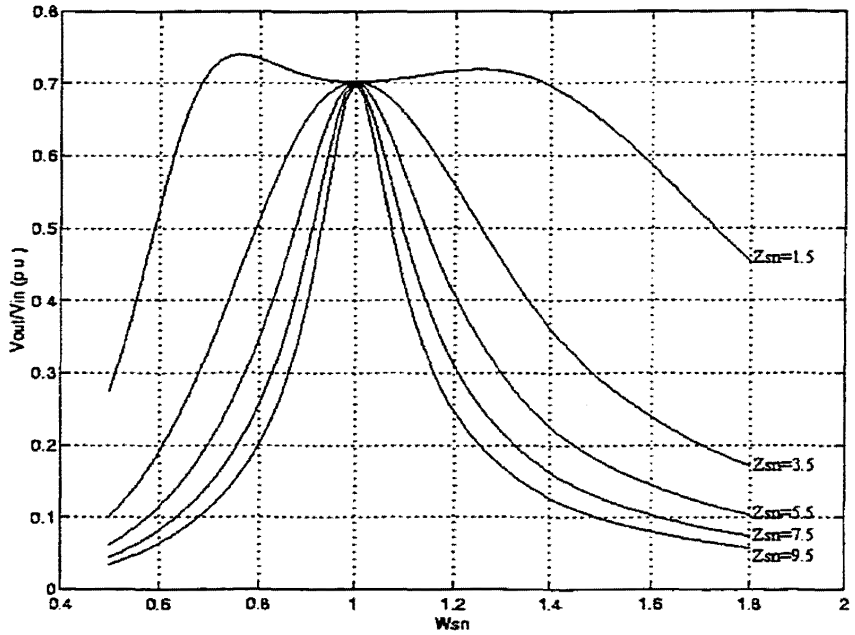

(a)

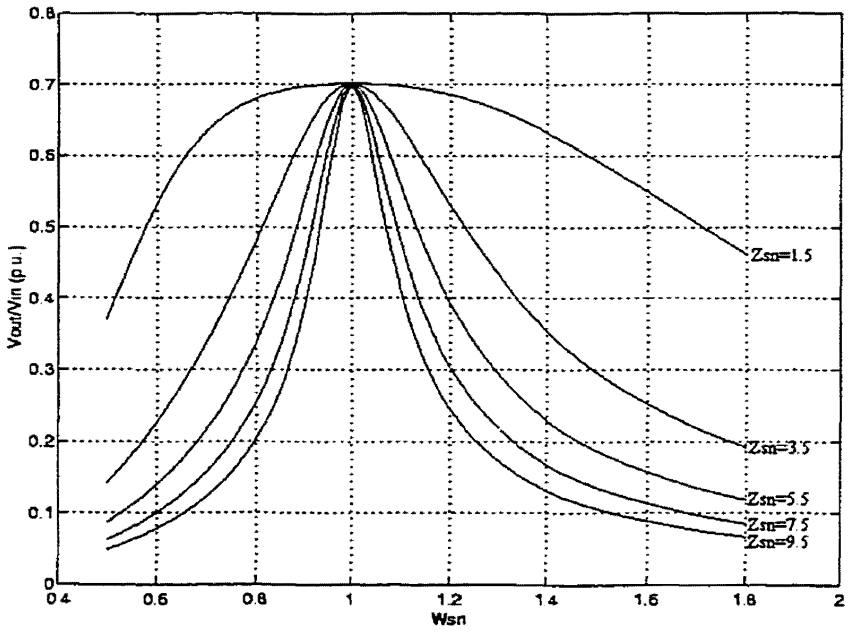

(b)

Figure 4.9: Voltage transfer ratio, M versus normalized frequency, ω_{sn}

$\delta = 120^{\circ}$, X_{Lsepn}=0, X_{Lm}=0.2p.u.

(a) Z_{pn}=1.5, (b) Z_{pn}=2.5

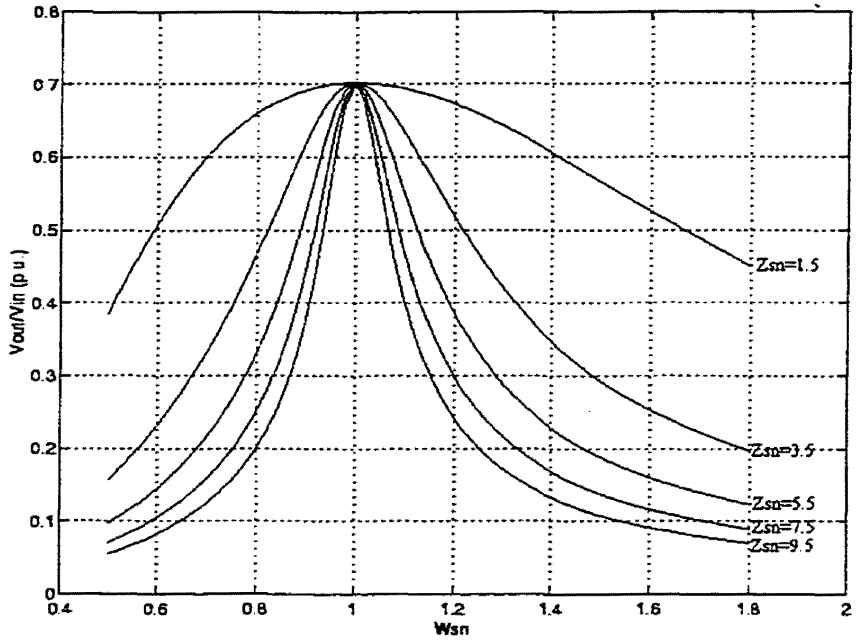

(a)

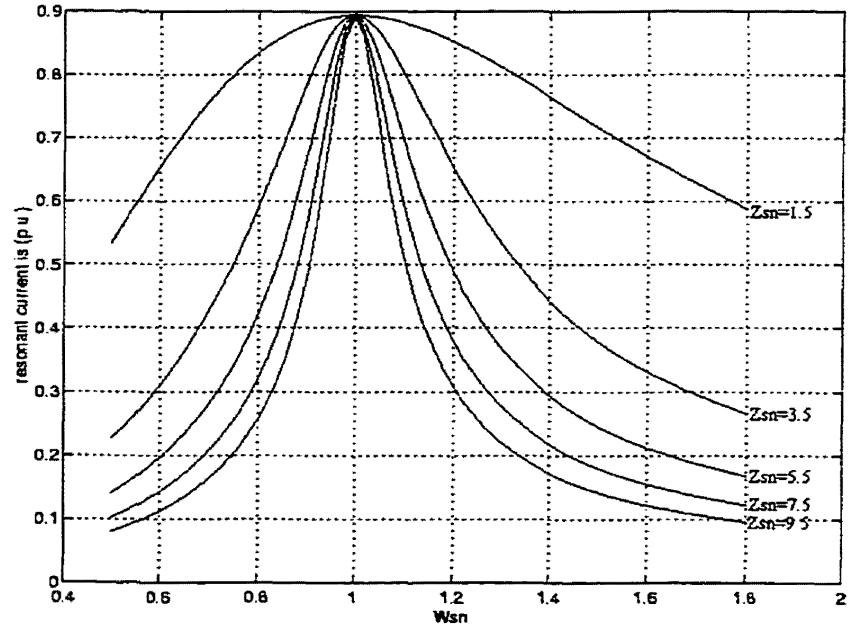

(b)

Figure 4.10: Voltage transfer ratio, M versus normalized frequency, ω_{sn}

$\delta = 120^{\circ}$, X_{Lsepn}=0, X_{Ln}=0.2p.u.

(a) Z_{pn}=3.5, (b) Z_{pn}=4.5

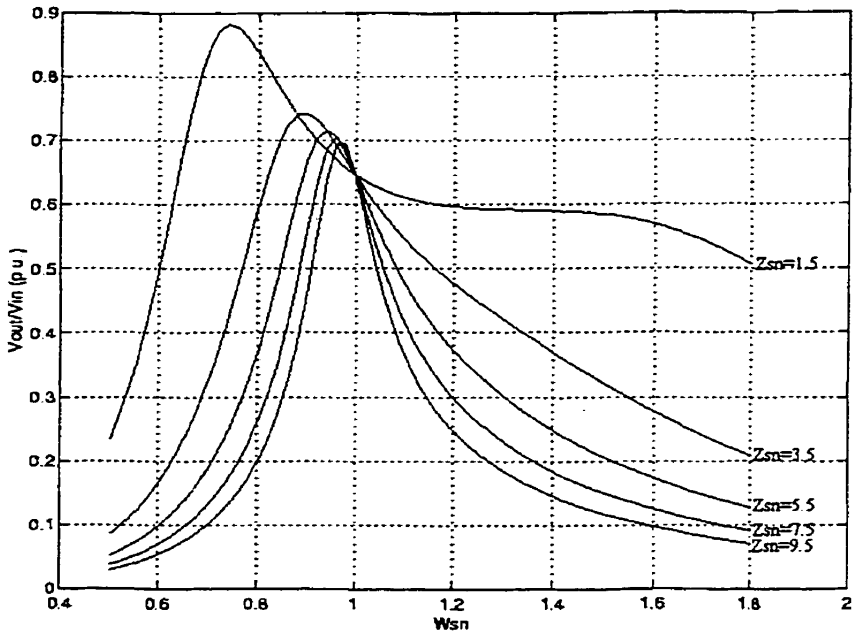

(a)

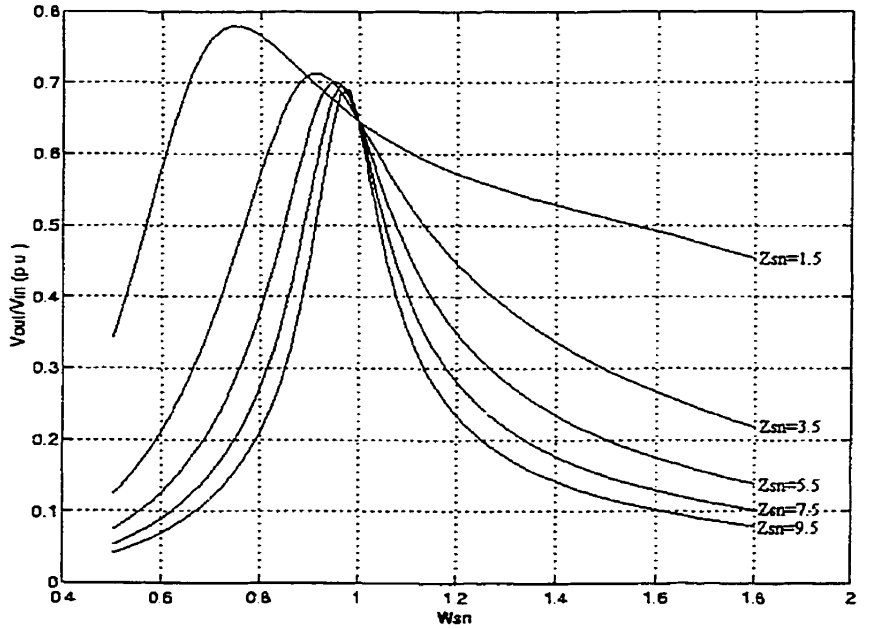

(b)

Figure 4.11: Voltage transfer ratio, M versus normalized frequency, ω_{sn}

$\delta = 120^{\circ}$, X_{Lsepn}=0.2p.u., X_{Lin}=0.2p.u.

(a) Z_{pn}=1.5, (b) Z_{pn}=2.5

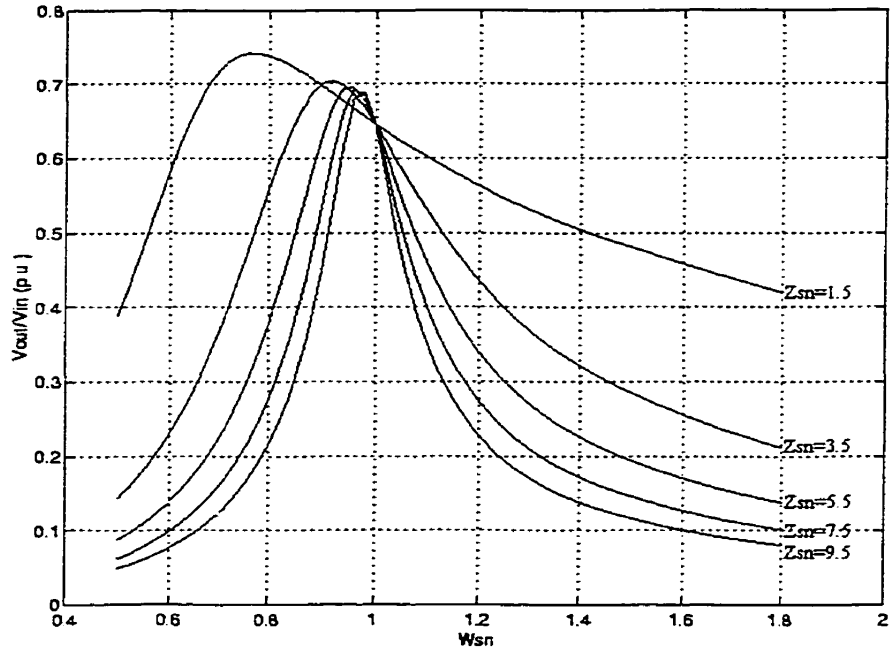

(a)

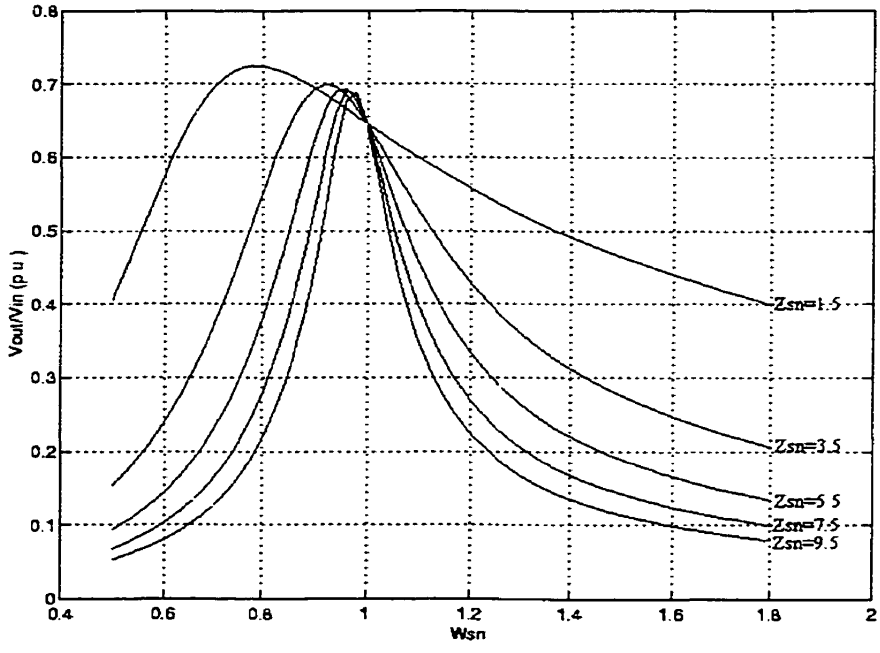

(b)

Figure 4.12: Voltage transfer ratio, M versus normalized frequency, ω_{sn}

$\delta = 120^{\circ}$, X_{Lsepn}=0.2p.u., X_{Lin}=0.2p.u.

(a) Z_{pn}=3.5, (b) Z_{pn}=4.5

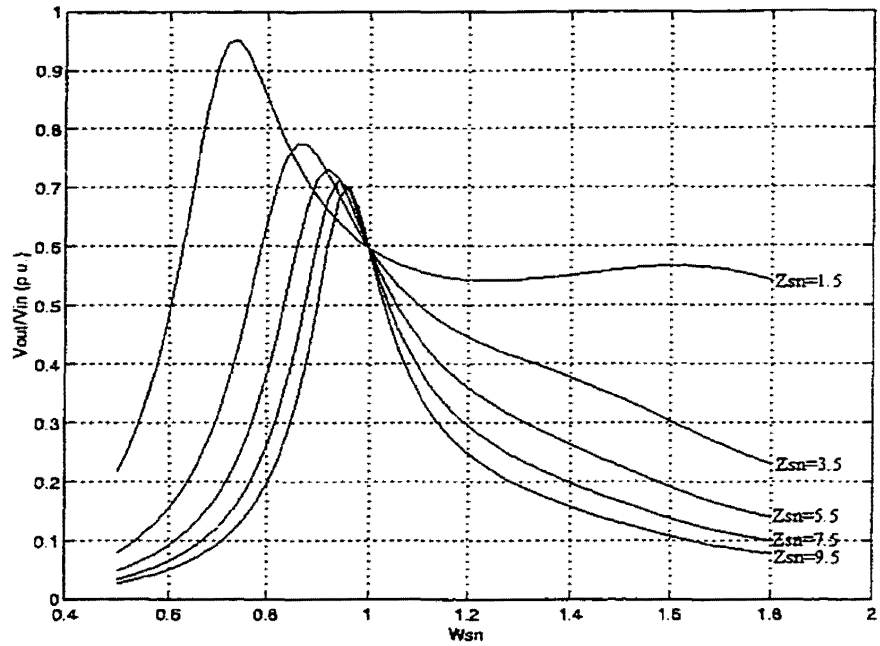

(a)

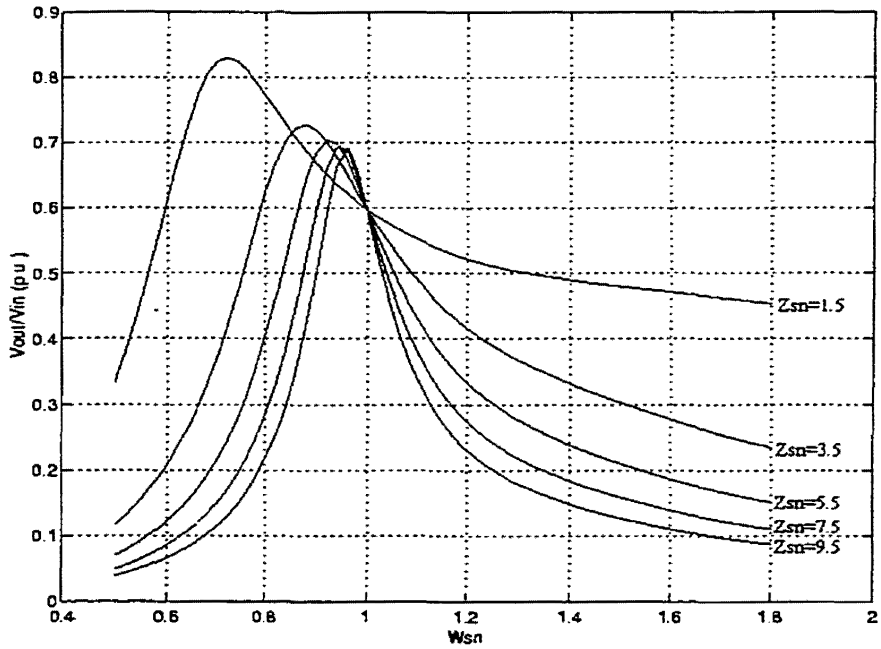

(b)

Figure 4.13: Voltage transfer ratio, M versus normalized frequency, ω_{sn}

$\delta = 120^{\circ}$, X_{Lsepn}=0.4p.u., X_{Ltn}=0.2p.u.

(a) Z_{pn}=1.5, (b) Z_{pn}=2.5

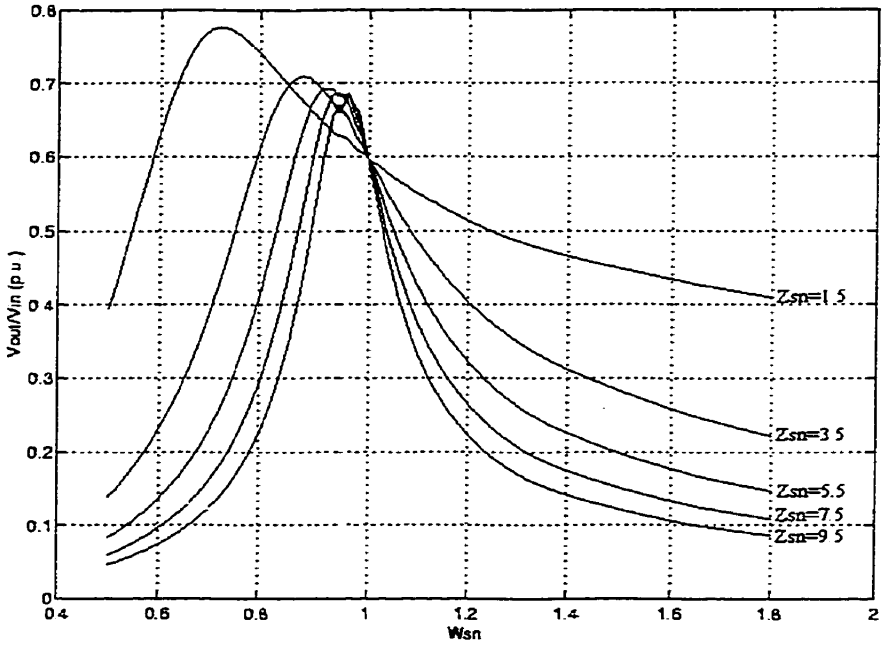

(a)

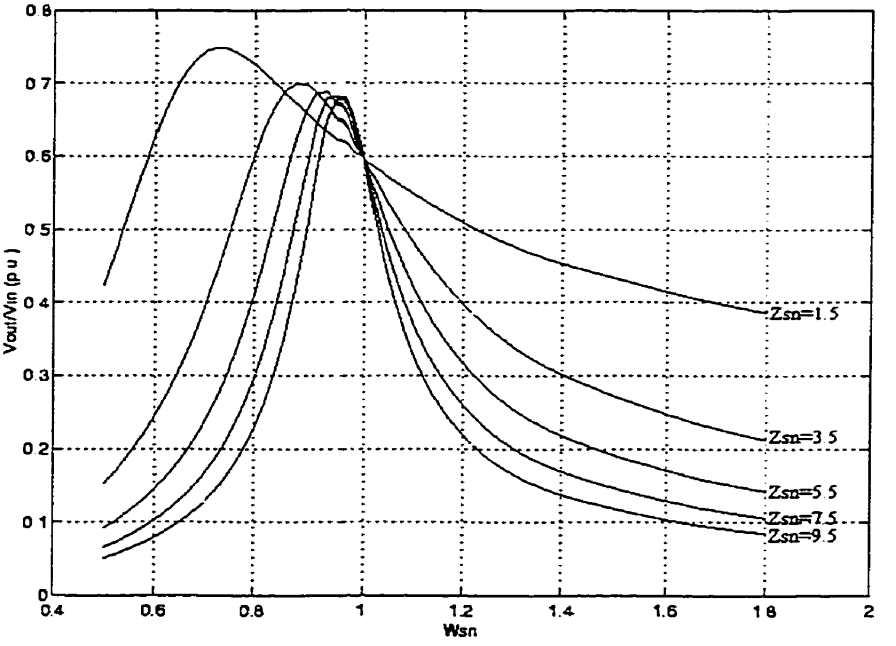

(b)

Figure 4.14: Voltage transfer ratio, M versus normalized frequency, ω_{sn}

$\delta = 120°$, X_{Lsepn}=0.4p.u., X_{Ltn}=0.2p.u.

(a) Z_{pn}=3.5, (b) Z_{pn}=4.5

4.2.3 Effect of the Resonant Circuit Parameters on the Peak Voltage across the Series Capacitor

Figures 4.15 to 4.20 show the characteristics of the peak voltage across the series capacitor, v_{cs}. Generally speaking, the peak value of v_{cs} is much higher than the peak value of v_p. The study of v_{cs} is very useful in converter design as it determines the peak voltage rating of the switching devices. It is shown in Figures 4.15 to 4.20 that the curves of v_{cs} change in an opposite trend to those of M, i_s, and v_p. With increasing Z_{sn}, the peak values of v_{cs} also increase. Therefore, a comparatively lower value of Z_{sn} should be chosen to limit the peak voltage across the series capacitor. When the leakage inductance equals to zero, the peak value of v_{cs} normally occurs at the resonant point. Moreover, with increasing values of Z_{pn}, the slope of the curves in the range from ω_{sn}=0.8 to ω_{sn}=1.2 increases. Thus a slight change in ω_{sn} can lead to a significant change in the magnitude of v_{cs}. This is harmful to the stability of the circuit. Hence, Z_{pn} cannot be very large.

With increasing values of the leakage inductance, the magnitude of v_{cs} decreases, as shown in Figure 4.18 and 4.20. This is because the output current decreases with increasing values of X_{Lsepn}.

As shown in Appendix C, a larger pulse-width will lead to a high magnitude on per unit base. However, if the voltage base (i.e. the input voltage) is much lower, the actual voltage across the series capacitor for a large pulse-width, low magnitude input voltage will not be greater than that of a low pulse-width, high magnitude input voltage. It indicates that the converter should be designed to work under the low pulse-width, high magnitude input voltage condition.

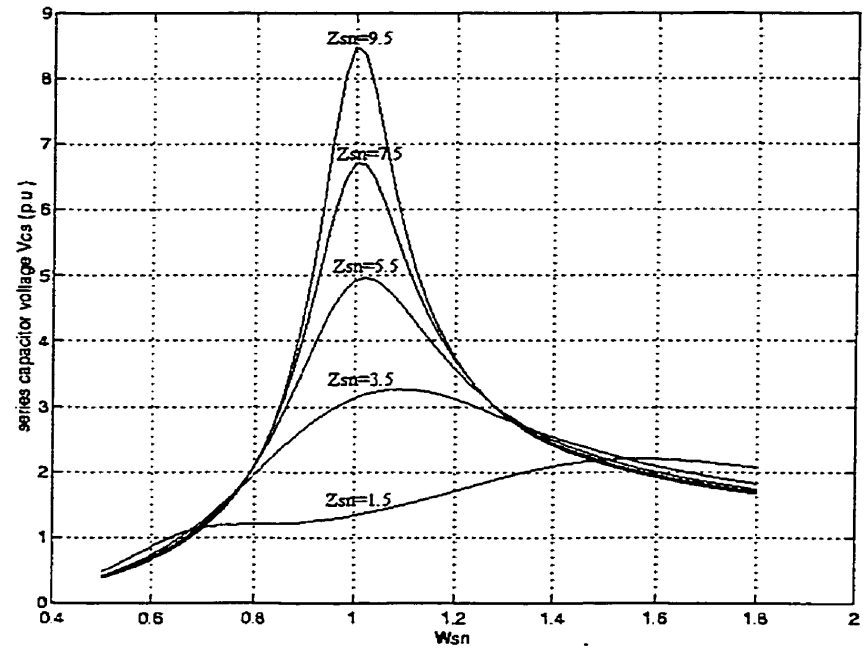

(a)

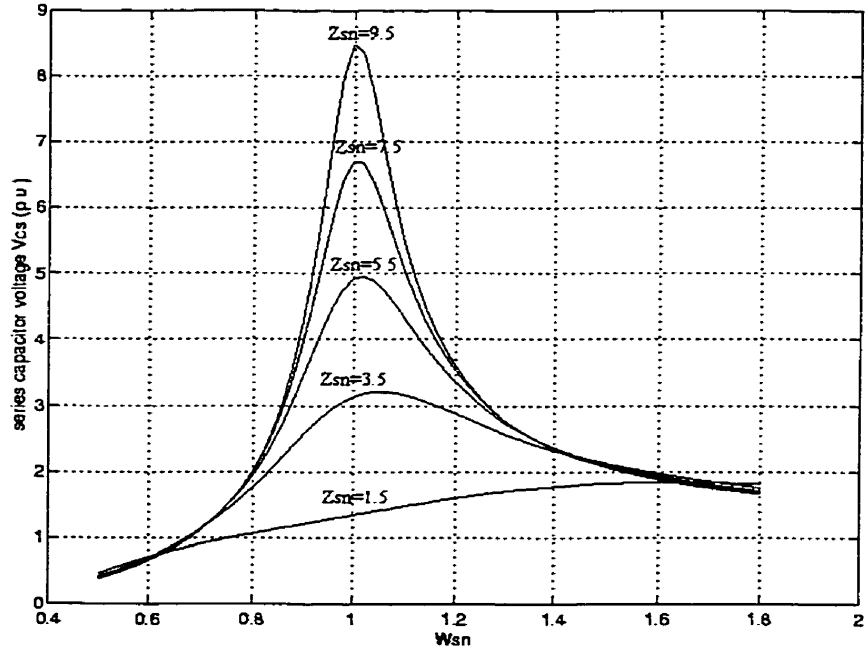

(b)

Figure 4.15: Peak capacitor voltage, v_{cs} versus normalized frequency, ω_{sn}

$\delta = 120^{\circ}$, X_{Lsepn}=0, X_{Ltn}=0.2p.u.

(a) Z_{pn}=1.5, (b) Z_{pn}=2.5

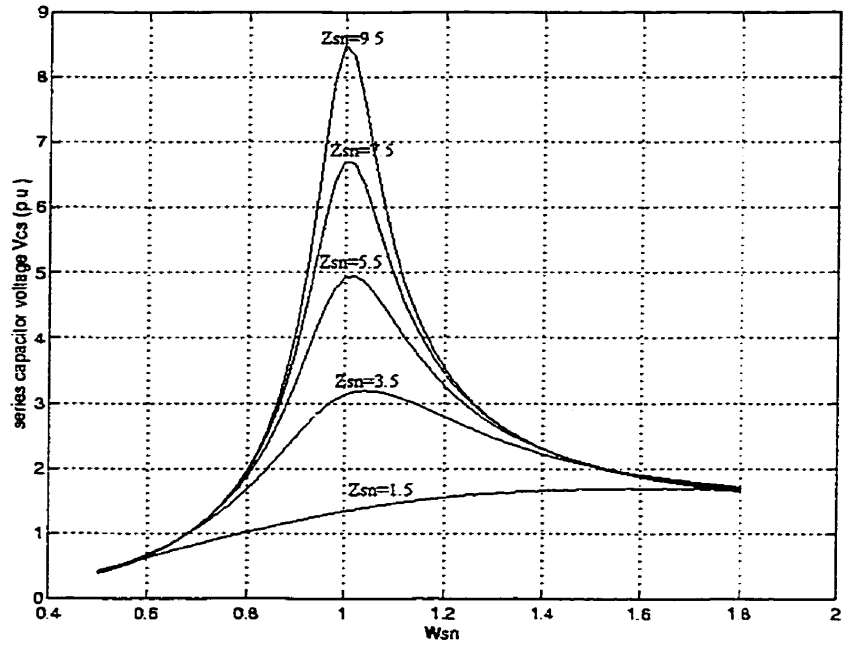

(a)

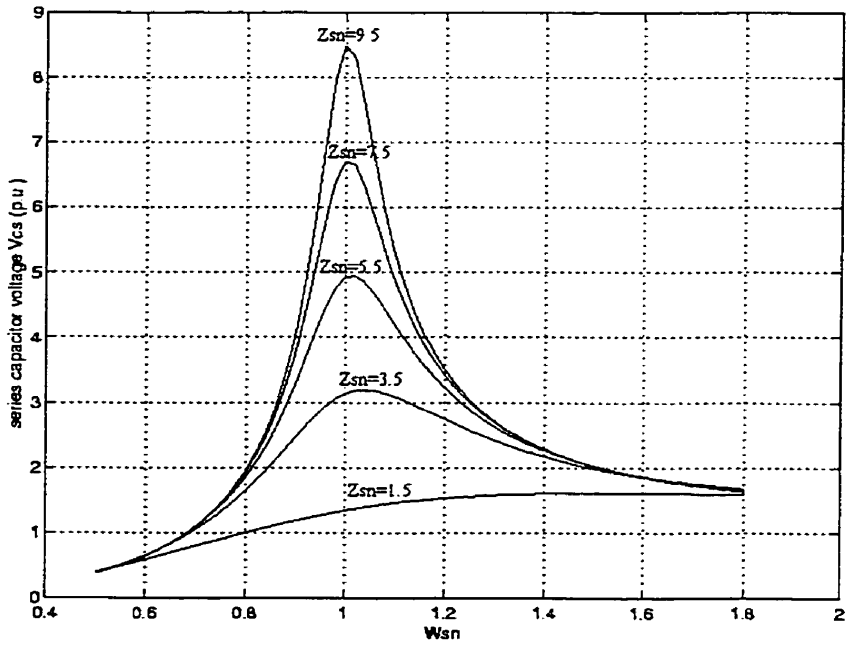

(b)

Figure 4.16: Peak capacitor voltage, v_{cs} versus normalized frequency, ω_{sn}

$\delta = 120°$, X_{Lsepn}=0, X_{Ltn}=0.2p.u.

(a) Z_{pn}=3.5, (b) Z_{pn}=4.5

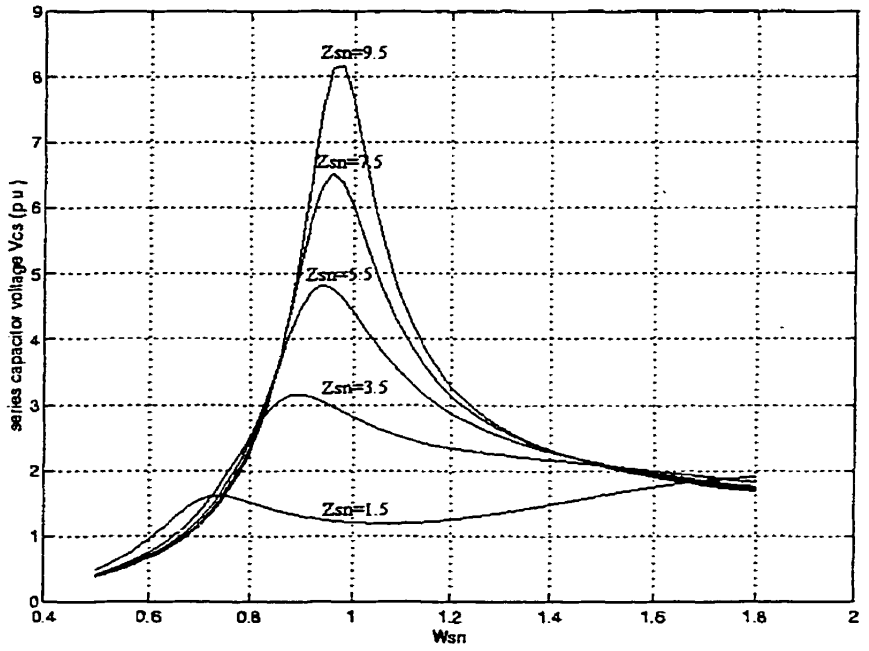

(a)

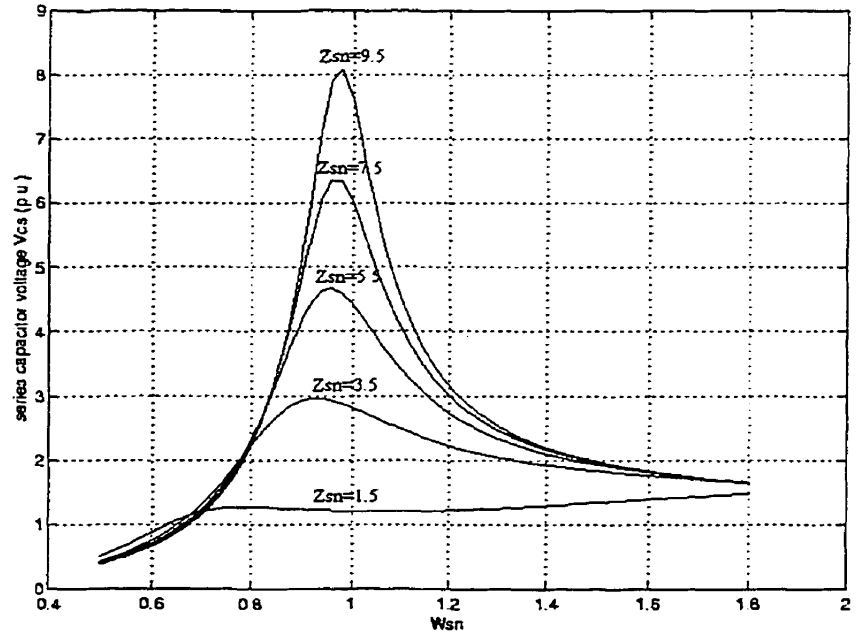

(b)

Figure 4.17: Peak capacitor voltage, v_{cs} versus normalized frequency, ω_{sn}

$\delta = 120^{\circ}$, X_{Lsepn}=0.2p.u., X_{Ltn}=0.2p.u.

(a) Z_{pn}=1.5, (b) Z_{pn}=2.5

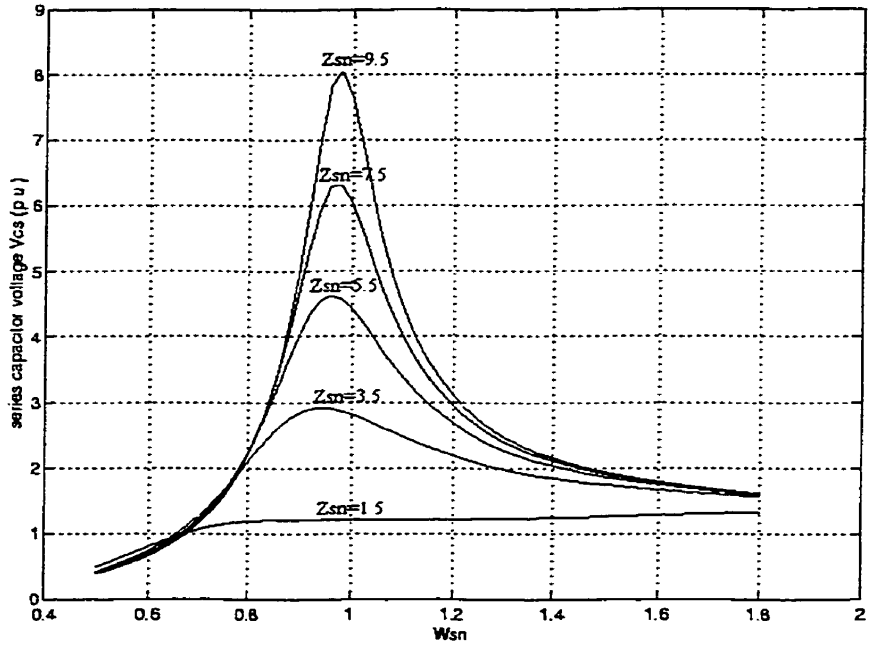

(a)

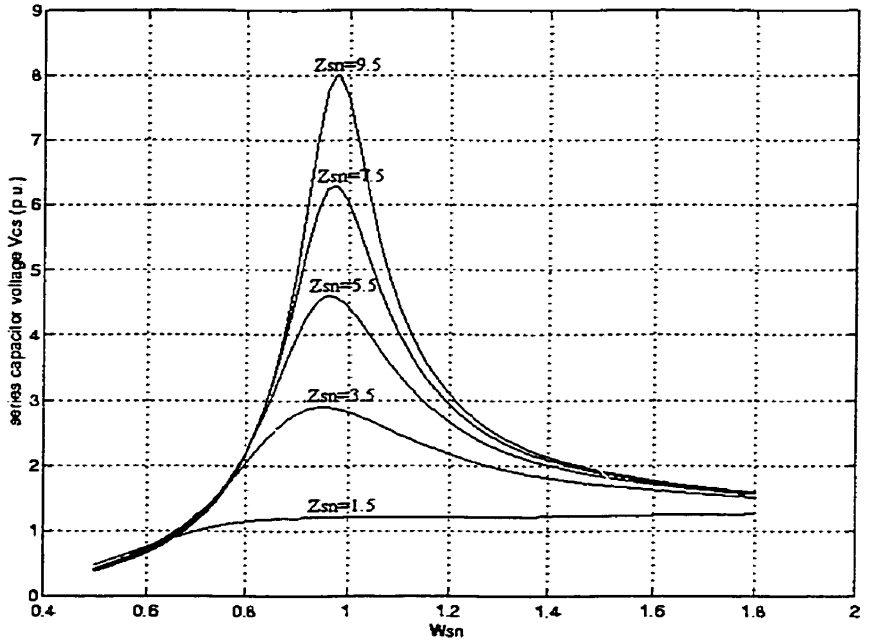

(b)

Figure 4.18: Peak capacitor voltage, v_{cs} versus normalized frequency, ω_{sn}

$\delta = 120°$, X_{Lsepn}=0.2p.u., X_{Lm}=0.2p.u.

(a) Z_{pn}=3.5, (b) Z_{pn}=4.5

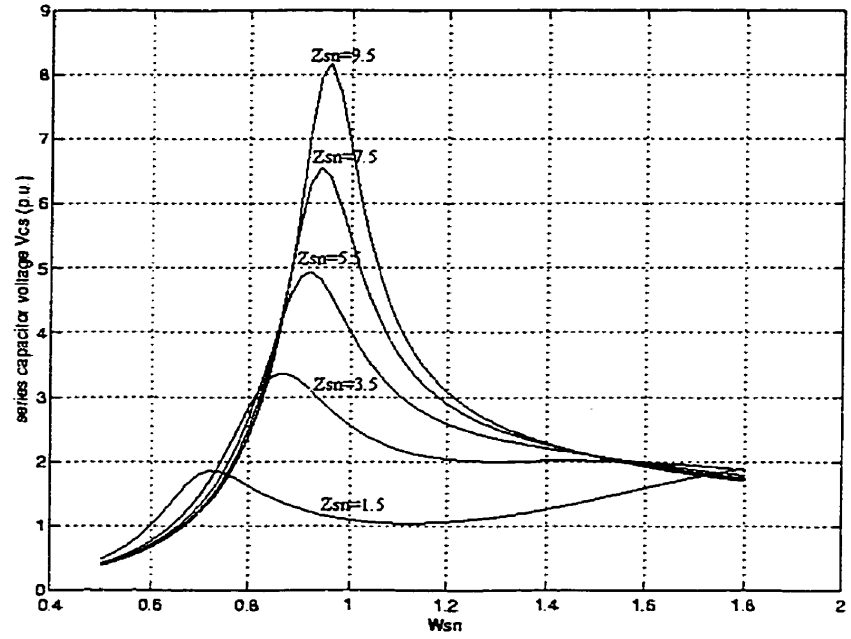

(a)

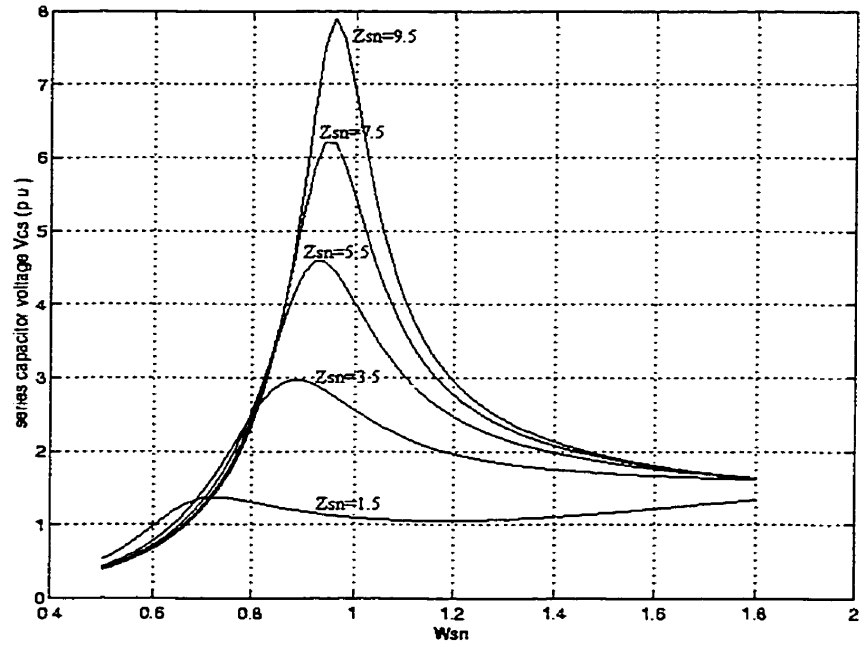

(b)

Figure 4.19: Peak capacitor voltage, v_{cs} versus normalized frequency, ω_{sn}

$\delta = 120^{\circ}$, X_{Lsepn}=0.4p.u., X_{Ltn}=0.2p.u.

(a) Z_{pn}=1.5, (b) Z_{pn}=2.5

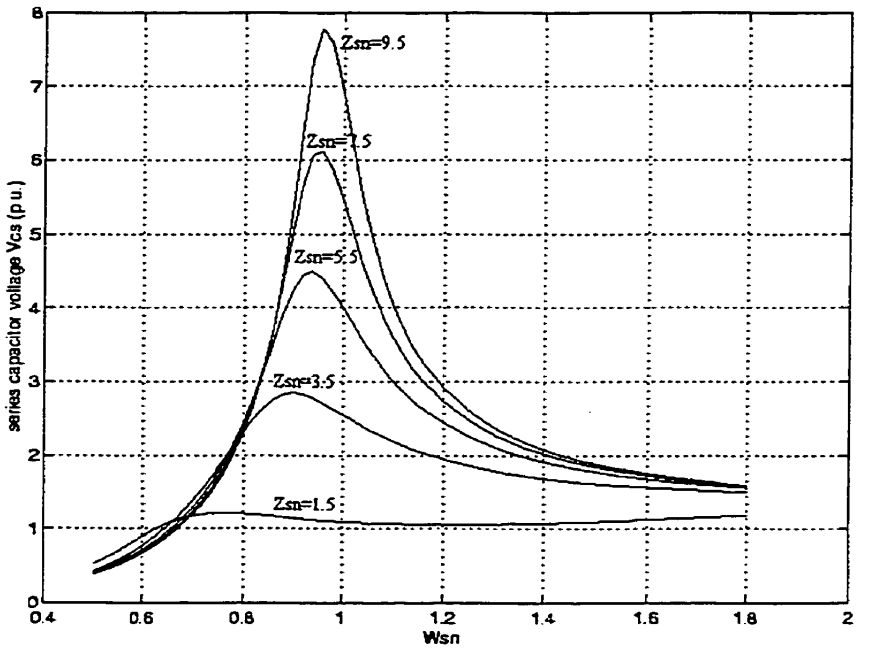

(a)

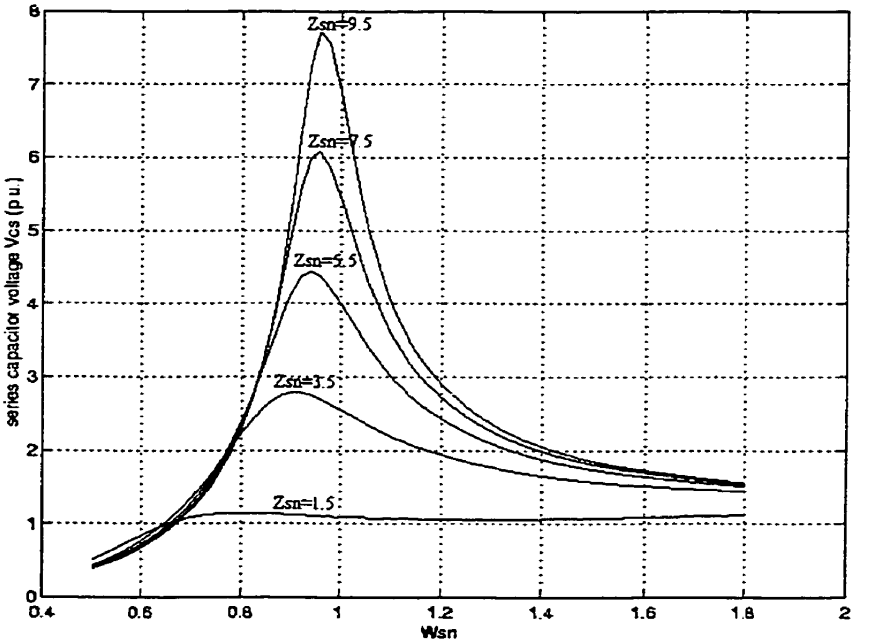

(b)

Figure 4.20: Peak capacitor voltage, v_{cs} versus normalized frequency, ω_{sn}

$\delta = 120^{\circ}$, X_{Lsepn}=0.4p.u., X_{Ltn}=0.2p.u.

(a) Z_{pn}=3.5, (b) Z_{pn}=4.5

4.3 Design Procedure

The discussions in the previous section suggest that the resonant circuit parameters should be within the following ranges for proper operation of the converter.

$$1.5 < Z_{sn} < 5.5$$

$$1.5 < Z_{pn} < 3.5$$

$$< \omega_{sn} < 1.3$$

The choice of the pulse width at which the converter is operated depends on the magnitude of the input voltage and the requirement of the output. For a given output voltage, a lower value of pulse width is used if a higher value of the input voltage is specified. Although the converter will operate successfully for any combination of resonant circuit parameters which are within the ranges established above, the choice of suitable values of the resonant circuit parameters is based on minimizing the KVA/KW ratio of the resonant circuit. Thus the KVA/KW is used as the primary criteria to arrive at the values of the resonant parameters for specified converter conditions. The procedure requires the specifications of four main conditions, namely

The input voltage magnitude, V_{in}

The output voltage magnitude, V_o

The switching frequency, f_s

The converter output power, P_o

The following design steps lead to the determination of the resonant circuit parameters for an assumed transformer leakage inductance.

1. Choose suitable values of Z_{sn} and Z_{pn}. Typically Z_{sn} is chosen to be 3.5p.u. and Z_{pn} is chosen to be 1.5p.u.

2. From the KVA/KW curves, determine ω_{sn} and ω_{pn} at which the minimum KVA/KW occurs for the Z_{sn} and Z_{pn} values selected in step 1.

3. From the values of ω_{sn}, ω_{pn}, Z_{sn}, and Z_{pn} calculate the actual values of L_s, C_s, L_p, and C_p.

4. Calculate the turns ratio of the high frequency transformer from the voltage transfer ratio, M.

The above steps are illustrated in the following design examples.

4.4 Design Examples

Two design exmples are outlined to illustrate the use of the design steps described in the previous section.

Example 1: Three-winding high frequency transformer.

Input voltage, V_{in}: 60 V

Output voltage, V_o: 5 V

Switching Frequency, f_s: 128 kHz

Output power, P_o 500 W

The output current is obtained as

$$I_o = P_o / V_o = 500/5 = 100\,A$$

Assume the leakage inductance is 0.2p.u. and the tertiary winding inductance is 0.2p.u. From Figure 4.3 with Z_{sn}=3.5, Z_{pn}=1.5, the minimum KVA/KW value occurs at ω_{sn}=1.22. From Figure 4.12, the M value that corresponds to ω_{sn}=1.22, Z_{sn}=3.5, and Z_{pn}=1.5 is 0.47p.u.

The series resonant frequency is calculated as

$$f_{rs} = f_s \cdot \omega_{sn} = 128 \times 1.22 = 156.16kHz$$

The turns ratio is obtained as

$$N = M \cdot V_{in}/V_o = 0.47 \cdot 60/5 = 5.6$$

The actual value of the series inductor is obtained as

$$\begin{aligned} L_s &= \frac{Z_{sn} \cdot R_b}{2 \cdot \pi \cdot f_s \cdot \omega_{sn}} \\ &= \frac{(3.5) \cdot (1.53)}{(2) \cdot (3.14) \cdot (128 \times 10^3) \cdot (1.22)} \\ &= 5.60 \mu H \end{aligned}$$

The actual value of the series capacitor is obtained as

$$\begin{aligned} C_s &= \frac{1}{(2 \cdot \pi \cdot f_s \cdot \omega_{sn})^2 \cdot L_s} \\ &= \frac{1}{((2) \cdot (3.14) \cdot (128 \times 10^3) \cdot (1.22))^2 \cdot (5.60 \times 10^{-6})} \\ &= 0.18 \mu F \end{aligned}$$

The actual value of the parallel inductor is obtained as

$$\begin{aligned} L_p &= \frac{Z_{pn} \cdot R_b}{2 \cdot \pi \cdot f_s \cdot \omega_{pn}} \\ &= \frac{(1.5) \cdot (1.53)}{(2) \cdot (3.14) \cdot (128 \times 10^3) \cdot (1.22)} \\ &= 2.38 \mu H \end{aligned}$$

The actual value of the parallel capacitor is obtained as

$$\begin{aligned} C_s &= \frac{1}{(2 \cdot \pi \cdot f_s \cdot \omega_{pn})^2 \cdot L_p} \\ &= \frac{1}{((2) \cdot (3.14) \cdot (128 \times 10^3) \cdot (1.22))^2 \cdot (2.38 \times 10^{-6})} \\ &= 0.45 \mu F \end{aligned}$$

The actual value of the leakage inductance is obtained as

$$L_{se} = \frac{X_{Lsepn} \cdot R_L}{2 \cdot \pi \cdot f_s} = \frac{(0.2) \cdot (0.05)}{(2) \cdot (3.14) \cdot (128 \times 10^3)} = 0.012 \mu H$$

Following the design steps, several other converters with different input conditions are designed. Table 4.1 shows the design results for V_{in}=60V, $\delta = 120°$, and various leakage inductance.

Table 4.1: Design results for the three-winding high frequency transformer

$\delta = 120°$, X_{Ltn}=0.2p.u.

Z_{pn}=1.5 Z_{sn}=3.5	X_{Lsepn} = 0.05 p.u.	X_{Lsepn} = 0.10 p.u.	X_{Lsepn} = 0.15 p.u.	X_{Lsepn} = 0.20 p.u.	X_{Lsepn} = 0.25 p.u.	X_{Lsepn} = 0.30 p.u.
KVA/KW (p.u.)	7.10	7.17	6.79	6.66	6.54	6.43
ω_{sn} (p.u.)	1.12	1.14	1.18	1.22	1.22	1.24
M (p.u.)	0.59	0.56	0.50	0.46	0.46	0.44
i_s (p.u.)	0.73	0.68	0.60	0.54	0.52	0.49
V_p (p.u.)	0.91	0.88	0.81	0.76	0.76	0.75
Turnsratio	7.08	6.72	6.21	5.6	5.50	5.28
L_s (μH)	9.74	8.62	6.90	5.6	5.37	4.89
C_s (μF)	0.13	0.14	0.16	0.18	0.19	0.21
L_p (μH)	4.17	3.69	2.96	2.38	2.30	2.10
C_p (μF)	0.30	0.32	0.38	0.45	0.45	0.48

Example 2: Two-winding high frequency transformer.

Input voltage, V_{in}: 40 V

Output voltage, V_o: 5 V

Switching Frequency, f_s: 128 kHz

Output power, P_o 500 W

The output current is obtained as

$$I_o = P_o / V_o = 500 / 5 = 100A$$

Assume the leakage inductance is 0.05p.u. and the two-winding high frequency transformer is used. From Figure 4.21 with Z_{sn}=3.5, Z_{pn}=1.5, the minimum KVA/KW value occurs at ω_{sn}=1.08. From Figure 4.22, the M value that corresponds to ω_{sn}=1.08, Z_{sn}=3.5, and Z_{pn}=1.5 is 0.72p.u.

The resonant frequency is obtained as

$$f_{rs} = f_s \cdot \omega_{sn} = 128 \times 1.08 = 138.24kHz$$

The turns ratio is obtained as

$$N = M \cdot V_{in} / V_o = 0.72 \cdot 40 / 5 = 5.7$$

The actual value of the series inductor is obtained as

$$\begin{aligned} L_s &= \frac{Z_{sn} \cdot R_b}{2 \cdot \pi \cdot f_s \cdot \omega_{sn}} \\ &= \frac{(3.5) \cdot (1.52)}{(2) \cdot (3.14) \cdot (128 \times 10^3) \cdot (1.08)} \\ &= 6.4 \mu H \end{aligned}$$

The actual value of the series capacitor is obtained as

$$\begin{aligned} C_s &= \frac{1}{(2 \cdot \pi \cdot f_s \cdot \omega_{sn})^2 \cdot L_s} \\ &= \frac{1}{((2) \cdot (3.14) \cdot (128 \times 10^3) \cdot (1.08))^2 \cdot (6.4 \times 10^{-6})} \\ &= 0.20 \mu F \end{aligned}$$

The actual value of the parallel inductor is given by

$$L_p = \frac{Z_{pn} \cdot R_b}{2 \cdot \pi \cdot f_s \cdot \omega_{pn}}$$
$$= \frac{1.5 \cdot 1.52}{(2) \cdot (3.14) \cdot (128 \times 10^3) \cdot (1.08)}$$
$$= 2.79\,\mu H$$

The actual value of the parallel capacitor is given by

$$C_p = \frac{1}{(2 \cdot \pi \cdot f_s \cdot \omega_{pn})^2 \cdot L_p}$$
$$= \frac{1}{((2) \cdot (3.14) \cdot (128 \times 10^3) \cdot (1.22))^2 \cdot (2.79 \times 10^{-6})}$$
$$= 0.45\,\mu F$$

The actual value of the leakage inductance is given by

$$L_{se} = \frac{X_{Lsepn} \cdot R_L}{2 \cdot \pi \cdot f_s} = \frac{(0.05) \cdot (0.05)}{(2) \cdot (3.14) \cdot (128 \times 10^3)} = 0.003\,\mu H$$

Following the design steps, several other converters with different input conditions are designed. Table 4.2 shows the design results for V_{in}=40v, $\delta = 175°$, and various leakage inductance.

Table 4.2: Design results for the two-winding high-frequency transformer

$$\delta = 175°$$

Z_{pn}=1.5 Z_{sn}=3.5	X_{Lsepn} = 0.05 p.u.	X_{Lsepn} = 0.10 p.u.	X_{Lsepn} = 0.15 p.u.	X_{Lsepn} = 0.20 p.u.	X_{Lsepn} = 0.25 p.u.	X_{Lsepn} = 0.30 p.u.
KVA/KW (p.u.)	7.19	7.06	6.95	6.85	6.76	6.67
ω_{sn} (p.u.)	1.08	1.14	1.16	1.16	1.20	1.22
M (p.u.)	0.72	0.64	0.60	0.58	0.55	0.54
i_s (p.u.)	0.89	0.78	0.71	0.69	0.64	0.61
V_p (p.u.)	1.14	1.04	1.00	1.00	0.96	0.96

Turnsratio	5.70	5.10	4.78	4.66	4.42	4.30
L_s (μH)	6.40	4.99	4.27	4.07	3.57	1.74
C_s (μF)	0.20	0.24	0.27	0.28	0.30	0.50
L_p (μH)	2.79	2.14	1.83	1.74	1.53	1.49
C_p (μF)	0.45	0.56	0.62	0.66	0.71	0.58

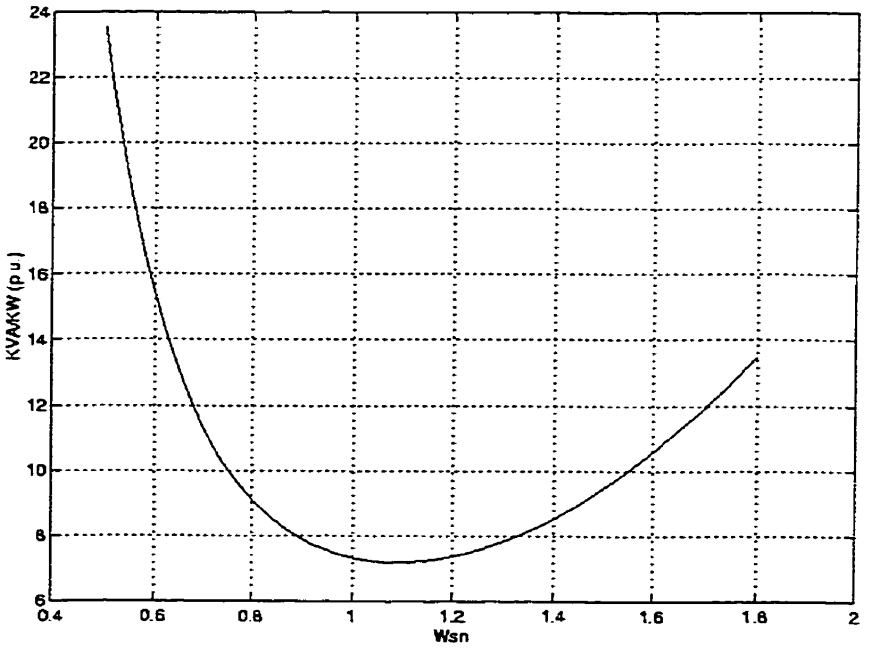

Figure 4.21: KVA/KW rating versus normalized frequency, ω_{sn}

$\delta = 175^{\circ}$, X_{Lsepn}=0.05p.u., Z_{pn}=1.5, Z_{sn}=3.5

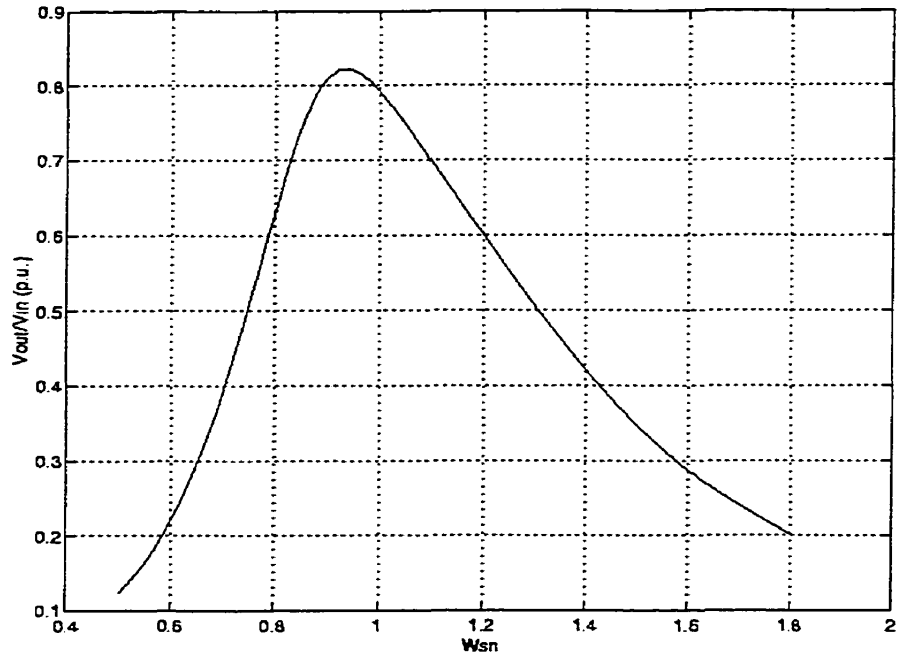

Figure 4.22: Voltage transfer ratio, M versus normalized frequency, ω_{sn}

$\delta = 175°$, X_{Lsepn}=0.05p.u., Z_{pn}=1.5, Z_{sn}=3.5

4.5 Design Verifications Using Pspice

The two design examples are verified using Pspice simulation. Tables 4.3 and 4.4 show the comparison between the predicted values and the Pspice simulation values of the voltages and currents of each circuit. V_{csm}, V_{pm}, and I_{sm} represent the peak values of v_{cs}, v_p, and i_s.

Table 4.3: Predicted and simulated values of the design example using three-winding high frequency transformer

Specifications and Values of Circuit Components	V_{in}=60V, $\delta = 120°$, L_{sc}=0.012 μH, L_τ=0.012 μH, N=5.6 L_s=5.6 μH, C_s=0.18 μF, L_p=2.38 μH, C_p=0.45 μF	
Method	EDF	Pspice
V_{csm}	139.02 V	149.35 V
V_{pm}	45.39 V	49.56 V

I_{sm}	20.76 A	21.80 A
V_o	5 V	5 V
I_o	100 A	100 A

Table 4.4: Predicted and simulated values of the design example using two-winding high frequency transformer

Specifications and Values of Circuit Components	V_{in}=40V, δ=175°, L_{se}=0.003 μH, N=5.7 L_s=6.4 μH, C_s=0.2 μF, L_p=2.79 μH, C_p=0.45 μF	
Method	EDF	Pspice
V_{csm}	135.71 V	142.35 V
V_{pm}	46.15 V	48.62 V
I_{sm}	23.50 A	24.75 A
V_o	5 V	5 V
I_o	100 A	100 A

4.6 Summary

A design approach for series-parallel resonant dc/dc converters that is based on minimum KVA/KW rating of the resonant parameters has been proposed in the chapter. Design examples have been presented to illustrate the procedure. It has been shown that using the minimum KVA/KW rating criteria, the resonant circuit parameters and the transformer parameters can be easily determined to meet the output specification. The tabular results also show that the procedure can be implemented in a computer-based design of the converter. Pspice simulation results of the two design examples presented in the chapter validate the proposed design procedure.

Chapter 5

Conclusion

In this thesis, the generalized analysis and design models of the series-parallel resonant converter are presented taking the leakage inductance of the high frequency transformer into consideration. A new set of design criterions has been developed with a view aiming to minimizing the KVA/KW ratio, i.e. the cost and size of the converter. It is shown that both the analysis model and the design model can predict the results accurately.

5.1 Summary

The main contributions of this thesis can be summarized as follows:

1. The generalized state-space large-signal model for the analysis of series-parallel resonant converters has been developed, taking into account the effect of the leakage inductance of the high-frequency transformer on the performance of the converter.

2. The state-space large-signal model of the series-parallel resonant converter using the extended describing function (EDF) concept, and the steady-state performance of the same has been developed and investigated.

3. Generalized small-signal model of the series-parallel resonant converter based on the extended describing function method has been developed.

4. Generalized design curves of the series-parallel resonant converter have been developed.

5. A design procedure for selecting the resonant components and high-frequency transformer has been proposed. It has been shown that the procedure can be easily automated in a computer based design program for any given transformer leakage inductance.

6. Both the models and proposed procedure design of the converter have been verified using PSPICE.

The results of the work presented in the thesis show that the proposed approach provides both simplicity and accuracy in getting easy-to-use large and small signal models that are readily applicable to the design of resonant converters. This advantage gives the extended describing function method good prospects in industrial applications such as performance evaluation, cost estimation, and cost reduction during the design phase of the development of resonant converters.

5.2 Recommendations for Future Work

The analysis method used in the thesis provides both qualitative and quantitative insight into the steady-state performance and design of the converter. However, it does not provide the transient analysis. Particularly, this model is not able to predict the response time, which is important in some industry applications. Since the model only

considers the fundamental component of the state variables, the error could be very large under certain operating conditions. The effects of the harmonics on the performance of the converter need to be investigated.

The design procedure presented in this thesis is based on minimizing the cost and size of the resonant components of the converter. The criterion for this procedure is KVA/KW ratio. However, the cost and size are not only determined by the KVA/KW ratio, but also determined by the limitations of the circuit components such as the maximum voltage that a capacitor can withstand. It is anticipated that the cost and size of the converter can be described by one or a set of non-linear equations. In order to reach an absolute minimum cost and size, these issues need further investigation.

The developed small-signal model of the converter needs further investigation to determine the dynamic behavior of the converter. Studies on the stability of the converter need to be carried out.

References

[1] Ned Mohan, Tore M. Undeland and William P. Robbins, "Power Electronics, Converters, Applications, and Design". 2nd edition, John Wiley & Sons, Inc. 1995.

[2] John G. Kassakian, Martin F. Schlecht, and George C. Verghese, "Principles of Power Electronics", Addison-Wesley Publishing Company, 1991.

[3] Marian K. Kazimierczuk, Dariusz Czarkowski, "Resonant Power Converter", John Wiley & Sons, Inc. 1995.

[4] Richard Tymerski, "Application of the Time-varying Function for Exact Small-signal Analysis", *IEEE Trans. Power Electronics*, Vol. 9, No. 2, Mar. 1994, pp 196-205.

[5] Yan-Fei Liu and Paresh C. Sen, "A General Unified Large Signal Model for Current Programmed DC-to-DC Converters", *IEEE Trans. Power Electronics*, Vol. 9, No. 4, July 1994, pp 414-424.

[6] R. D. Middlebrook, "Modeling Current-programmed Buck and Boost Regulartors", *IEEE Trans. Power Electronics*, Vol. 4, No.1, Jan. 1989, pp 36-52.

[7] Brad Lehman and Richard M. Bass, "Extensions of Averaging Theory of Power Electronic Systems", *IEEE Trans. Power Electronics*, Vol. 11, No. 4, July 1996, pp 542-553.

[8] Brad Lehman and Richard M. Bass, "Switching Frequency Dependent Averaged Models for PWM DC-DC Converters", *IEEE Trans. Power Electronics*, Vol. 11, No. 1, Jan. 1996, pp 89-98.

[9] Frank H. F. Leung and Peter K. S. Tam, "Large-signal Modeling of Regulated Switching DC-DC Converters Using a Grid-Point Approach", *IEEE Trans. Ind. Electron.* Vol. 43, No. 1, Feb. 1996, pp 238-240.

[10] William McMurray, "Selection of Snubbers and Clamps to Optimize the Design of Transistor Switching Converters", *IEEE Trans. Ind. Appli.*, Vol. 1A-16. No.4, July 1980.

[11] Vlatkovic and Vlatko, "Small-signal Analysis of Phase-shifted PWM Converter", *IEEE Trans. Power Electronics*, Vol. 7, No. 2, Apr. 1992, pp 128-135.

[12] R. D. Middlebrook, Slobodan Cuk, "A General Unified Approach to Modeling Switching Converter Power Stages". *IEEE PESC. Rec.*, 1976, pp. 18-34.

[13] Richard Tymerski, Duwang Li, "Extended Ripple Analysis of PWM DC-to-DC Converters", *IEEE Trans. Power Electronics*, Vol. 8, No. 5, Oct 1993, pp 588-595.

[14] M. M. Jovanovic, W. A. Tabisz, and F. C. Lee, "High Frequency Off-Line Power Conversion Using Zero Voltage Switching Qasiresonant And Multi-Resonant Techniques", *IEEE Trans. Power Electronics*, Vol. 4, No. 5, Oct. 1989, pp. 459-469.

[15] R. J. King and T. A. Stuart, "Small-signal Model for the Series Resonant Converter", *IEEE Trans. Aerosp. Electron. Syst.*, Vol. AES-21, No.3, May. 1985, pp 301-319.

[16] Wen-Jian Gu and Koosuke Harada, "A Circuit Model for the Class E Resonant DC-DC Converter Regulated at a Fixed Switching Frequency", *IEEE Trans. Power Electronics*, Vol. 7, No.1, Jan. 1992, pp 99-110.

[17] Yan-Fei Liu and Paresh C. Sen, "A Novel Resonant Converter Topology for DC-to-DC Power Supply", *IEEE Trans. Aerosp. Electron. Syst.*, Vol. 31, No. 4, Oct. 1995, pp 1301-1312.

[18] K. D. T. Ngo, "Analysis of a Series Resonant Converter Pulse-width Modulated or Current-Controlled for Low Switching Loss", *IEEE Trans on Power Electronics*, Vol. 3, No. 1, Jan. 1998, pp 55-63.

[19] W. A. Tabisz and F. C. Lee, "Zero Voltage Switching Multi-resonant Techniques – a Novel Approach to Improve Performance of High Frequency Quasi-Resonant Converters", *IEEE Trans. Power Electronics*, Vol. 4, No. 5, Oct 1989, pp 450-458.

[20] Praveen K. Jain, Andre St-Martin and Gary Edwards, "Asymmetrical Pulse-Width-Modulated Resonant DC/DC Converter Topologies". *IEEE Trans. Power Electronics.*, Vol. 11, No. 3, May 1996. pp 413-422.

[21] Marian K. Kazimierczuk and Abdulkarim Abdulkarim, "Current-Source Parallel-Resonant DC/DC Converter", *IEEE Trans. Ind. Electron.*, Vol. 42, No. 2, Apr. 1995, pp 199-208.

[22] R. Oruganti and T. C. How, "Resonant-tank Control of Parallel Resonant Converter", *IEEE Trans. Power Electronics*, Vol. 8, No. 2, Apr. 1993, pp 127-134.

[23] A. K. S. Bhat and M. M. Swamy, "Analysis, Design and Optimization of a Secondary-side Resonant Converter Operating in the Discontinuous Capacitor Voltage Mode", *IEEE Trans. Ind. Electron.*, Vol. 40, No. 3, Jun. 1993, pp 334-346.

[24] S. D. Johnson and R. W. Erickson, "Steady-Static Analysis and Design of the Parallel Resonant Converter", *IEEE Trans. Power Electronics*, Vol. 3, No. 1, Jan. 1988, pp 93-104.

[25] V. T. Ranganathan, P. D. Ziogas, and V. R. Stefanovic, "A Regulated DC-DC Voltage Source Converter Using a High Frequency Link", *IEEE Trans. Ind. Appli.* Vol. 1A-18, No. 3, May. 1982, pp 279-287.

[26] Young-Goo Kang and Anand K. Upadhyay, "Analysis and Design of a Half-Bridge Parallel Resonant Converter", *IEEE Trans. Power Electronics*, Vol. 3, No. 3, July 1988, pp 254-265.

[27] S. Deb, A. Joshi, and S. Doradla, "A Novel Frequency-Domain for a Parallel Resonant Converter". *IEEE Trans. Power Electronics*. Vol. 3. No. 2. Aprl. 1988. pp 208-215.

[28] Pankaj Jain, "Fixed Frequency Series-Parallel DC/DC Resonant Converters", 1993, M.Eng thesis, *Memorial University of Newfoundland.*

[29] Pankaj Jain, John E. Quaicoe, and Praveen Jain, "Modeling and Analysis of Fixed Frequency Phase-Shift Modulated Tertiary-Side Parallel-Tuned Resonant DC/DC Converters", *1993 IEEE IAS Rec.*, Oct, 1993, pp 180-185.

[30] Praveen Jain, "A Constant Frequency Resonant DC/DC Converter With Zero Switching Losses", *IEEE Trans Power Electronics*, 1991, pp 1067-1073.

[31] E. X. Yang, F. C. Lee, and M. M. Jovanovic, "Small-Signal Modeling of Power Electronic Circuits by Extended Describing Function Concept". *Proc. VEPC Seminar* 1991, pp. 167-178.

[32] Eric X. Yang, F.C. Lee, and M.M. Jovanovic, "Small-Signal Modeling of Series and Parallel Resonant Converters". *IEEE APEC Rec.*, 1992, pp162-169.

[33] R. Steigerwald, "A Comparison of Half-bridge Resonant Converter Topologies". *IEEE Trans. Power Electronics*, Vol. 3. No. 2, Apr. 1988, pp 174-182.

[34] A. K. S. Bhat, "A Fixed-frequency Modified Series-Resonant Converter: Analysis, Design and Experimental Results", *IEEE Trans. Power Electronics*, Vol. 10, No. 6, Nov. 1995, pp 766-775.

[35] Siu-Chung Wong, and Andrew D. Brown, "Analysis, Modeling and Simulation of Series-Parallel Resonant Converter Circuits", *IEEE Trans. Power Electronics*, Vol. 10, No. 5, Sept. 1995, pp 605-614.

[36] G. S. N. Raju and Seshagirirao Doradla, "An LCL Resonant Converter with PWM Control - Analysis, Simulation and Implementation", *IEEE Trans. Power Electronics*, Vol. 10, No. 2, Mar. 1995, pp 164-174.

[37] Vivek Agarwal and A. K. S. Bhat, "Large Signal Analysis of the LCC-type Parallel Resonant Converter Using Discrete Time Domain Modeling", *IEEE Trans. Power Electronics*, Vol. 10, No. 2, Mar. 1995, pp 222-238.

[38] A. K. S. Bhat, "Analysis and Design of a Series-Parallel Resonant Converter", *IEEE Trans. Power Electronics*, Vol. 8, No. 1, Jan. 1993, pp. 1-11.

[39] The MathWorks Inc. "The Student Edition of MATLAB, Version 4, User's Guide", published by Prentice Hall Inc., 1995

[40] Franz Monssen, "MicroSim Pspice with Circuit Analysis", 2nd edition, Prentice-Hall Inc. 1998.

Appendix A

Frequency Domain Analysis of the Series-Parallel Resonant DC/DC Converter

The frequency domain analysis approach represents the inverter output voltage, v_s, and the primary current, i_p, as the sum of harmonics. A harmonic equivalent circuit excited by the voltage and current harmonics yields state variables that can be represented as the sum of the responses of each individual harmonic component. Figure A.1 shows the nth harmonics equivalent circuit.

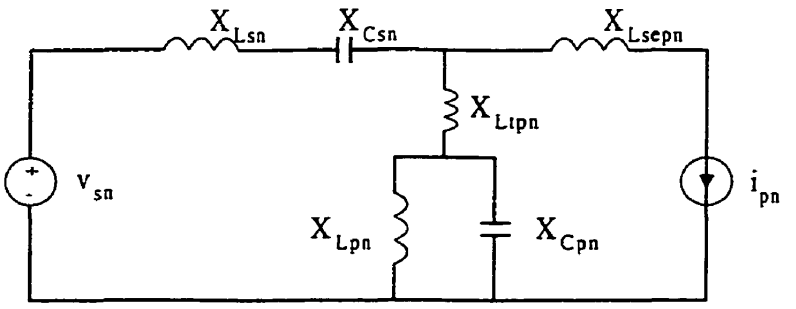

Figure A.1: Nth harmonics equivalent circuit of the series-parallel resonant converter

The Fourier series representation of the nth harmonic component of input voltage v_s is given by

$$v_{sn} = \frac{4V_i}{n\pi}\sin\left(\frac{n\pi}{2}\right)\sin\left(\frac{n\delta}{2}\right)\sin(n\omega_s t) \qquad (A.1)$$

The Fourier series representation of the nth harmonic component of the primary current i_p is given by

$$i_{pn} = \frac{8I_{op}}{n^2\pi\mu}\sin\left(\frac{n\mu}{2}\right)\sin\left[n\left(\omega t - \phi - \frac{\mu}{2}\right)\right] \qquad (A.2)$$

where I_{op} is the constant output current referred to the primary.

Assuming ideal lossless resonant circuit parameter, the nth harmonic total impedance of the series branch is given by

$$Z_{sn} = j(X_{Lsn} - X_{Csn}) \qquad (A.3)$$

The nth harmonic total impedance of the parallel branch is given by

$$Z_{pn} = j\left(X_{Lipn} - \frac{X_{Lpn} X_{Cpn}}{X_{Lpn} - X_{Cpn}} \right) \qquad (A.4)$$

The total nth harmonic input impedance is given by

$$Z_{in} = Z_{sn} + Z_{pn} \qquad (A.5)$$

The nth harmonic resonant current i_{sn} is obtained by applying superposition theorem as

$$\begin{aligned} i_{sn} = & \frac{4V_i}{n\pi Z_{in}} \sin\left(\frac{n\pi}{2}\right) \cos(n\omega_s t) + \ldots \\ & + \frac{8I_{op}}{n^2 \pi \mu} \sin\left(\frac{n\mu}{2}\right) \sin\left[n\left(\omega t - \phi - \frac{\mu}{2} \right) \right] \frac{Z_{pn}}{Z_{in}} \end{aligned} \qquad (A.6)$$

The nth harmonic transformer primary side voltage v_{pn} is obtained as

$$\begin{aligned} v_{pn} = & \frac{4V_i Z_{pn}}{n\pi Z_{in}} \sin\left(\frac{n\pi}{2}\right) \sin\left(\frac{n\delta}{2}\right) \cos(n\omega_s t) + \ldots \\ & + \frac{8I_{op}}{n^2 \pi \mu} \sin\left(\frac{n\mu}{2}\right) \cos\left[n\left(\omega t - \phi - \frac{\mu}{2} \right) \right] \frac{Z_{pn} Z_{sn}}{Z_{in}} \end{aligned} \qquad (A.7)$$

Since all the waveforms have odd-symmetry (Figure 2.5), the input voltage, v_s, the resonant current i_s, the transformer primary current i_p, and the transformer primary voltage v_p can be obtained by summing the n odd harmonics.

$$v_s = \sum_{n=1,3,\ldots}^{\infty} v_{sn} \qquad (A.8)$$

$$i_s = \sum_{n=1,3,\ldots}^{\infty} i_{sn} \qquad (A.9)$$

$$v_p = \sum_{n=1,3,\ldots}^{\infty} v_{pn} \qquad (A.10)$$

$$i_p = \sum_{n=1.3.\cdots}^{\infty} i_{pn} \qquad (A.11)$$

In order to obtain the output values, three equations are needed to achieve a unique solution for ϕ, $\mu$and I_o. The first equation is obtained from the condition that v_p=0 at $\omega_s t = \phi$(Figure 2.5). Equation A.7 gives the condition

$$\sum_{n=1.3.\cdots}^{\infty} \frac{4V_i Z_{pn}}{n\pi Z_{in}} \sin\left(\frac{n\pi}{2}\right)\sin\left(\frac{n\delta}{2}\right)\cos(n\omega_s t)+\cdots + \sum_{n=1.3.\cdots}^{\infty} \frac{8I_{op}}{n^2\pi\mu} \sin\left(\frac{n\mu}{2}\right)\cos\left[n\left(\omega t-\phi-\frac{\mu}{2}\right)\right]\frac{Z_{pn}Z_{sn}}{Z_{in}}=0 \qquad (A.12)$$

The second equation is obtained from the condition that the output voltage is equal to the average of v_p over the interval $\phi+\mu/2$ to $\phi+\pi$, i.e.

$$V_o = \frac{1}{\pi}\int_{\phi+\mu/2}^{\phi+\pi} v_p \, t \qquad (A.13)$$

which from equation A.7 gives

$$= \sum_{n=1.3.\cdots}^{\infty} \frac{4}{n^2\pi^2} \sin\left(\frac{n\pi}{2}\right)\sin\left(\frac{n\delta}{2}\right)\frac{Z_{pn}}{Z_{in}}\cdots \left[\cos\left(n(\phi+\mu)\right)+\cos(n\phi)\right] \qquad (A.14)$$

The third equation is obtained by assuming that the primary voltage, v_p, is sinusoidal. Then, the commutation angle μcan be obtained as

$$\cos(\mu) = 1 - \frac{2X_{Lsepn}I_{on}}{V_{pm}} \qquad (A.15)$$

Generally, a numerical method, for example FSOLVE() in MATLAB, must be employed to solve equations (A.12)-(A.15).

Waveforms of the Series-Parallel Resonant DC/DC Converter Using Two-Winding HF Transformer

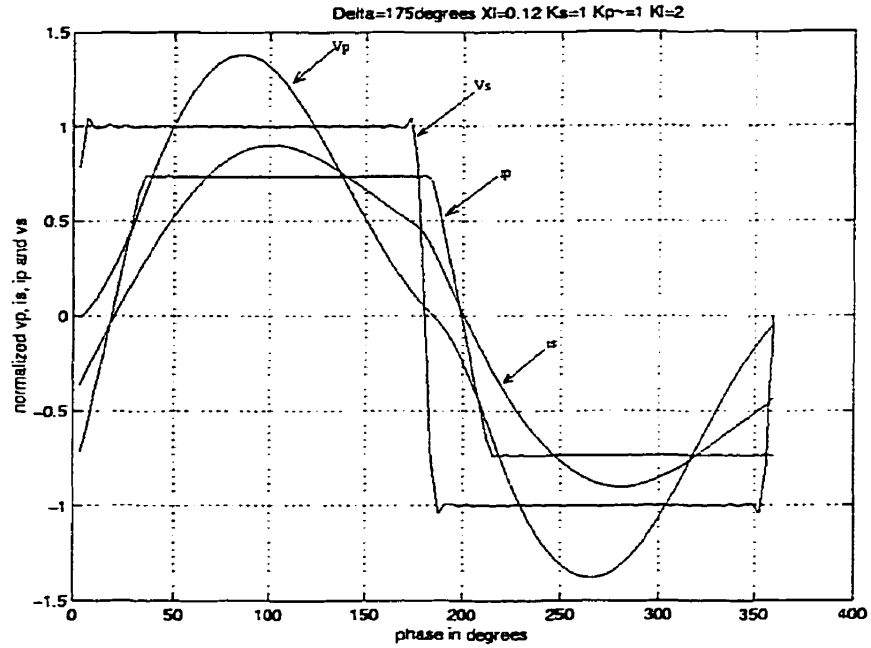

Figure 0.1: Simulated waveforms of the converter with tuned series and parallel branch using two-winding HF transformer, K_l=2

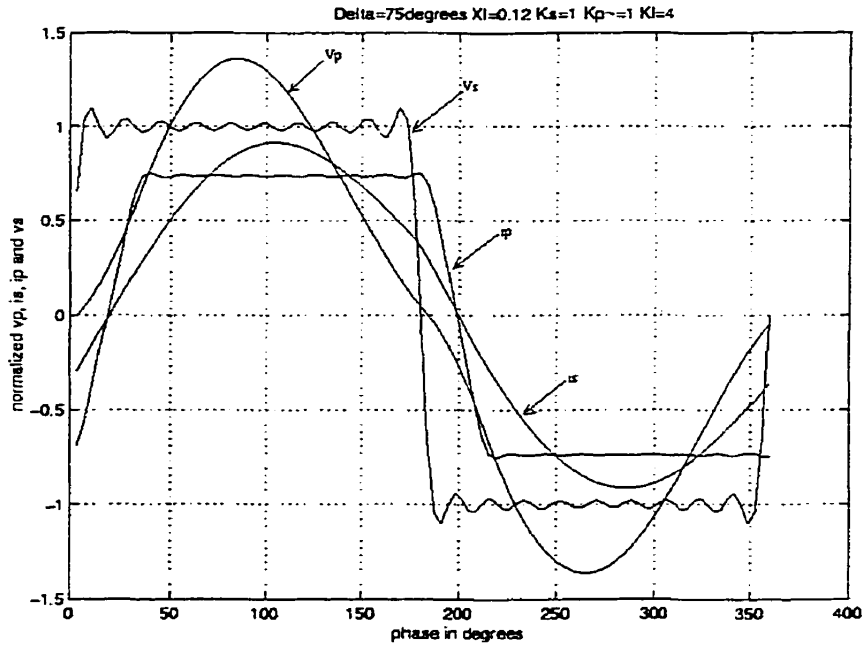

Figure 0.2: Simulated waveforms of the converter with tuned series and parallel branch using two-winding HF transformer, K_l=4

Design Plots of the Series-Parallel Resonant DC/DC Converter with $\delta = 175^{\circ}$

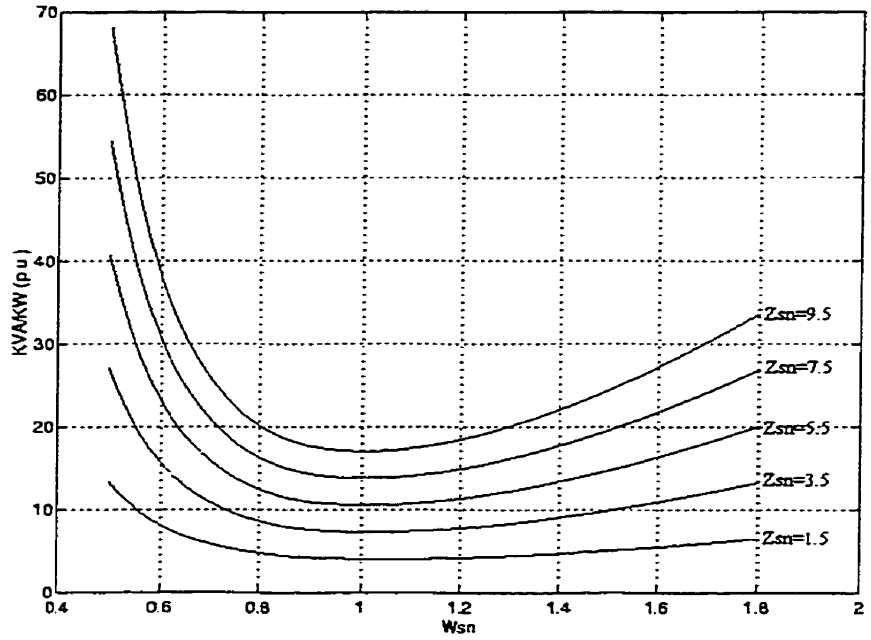

(a)

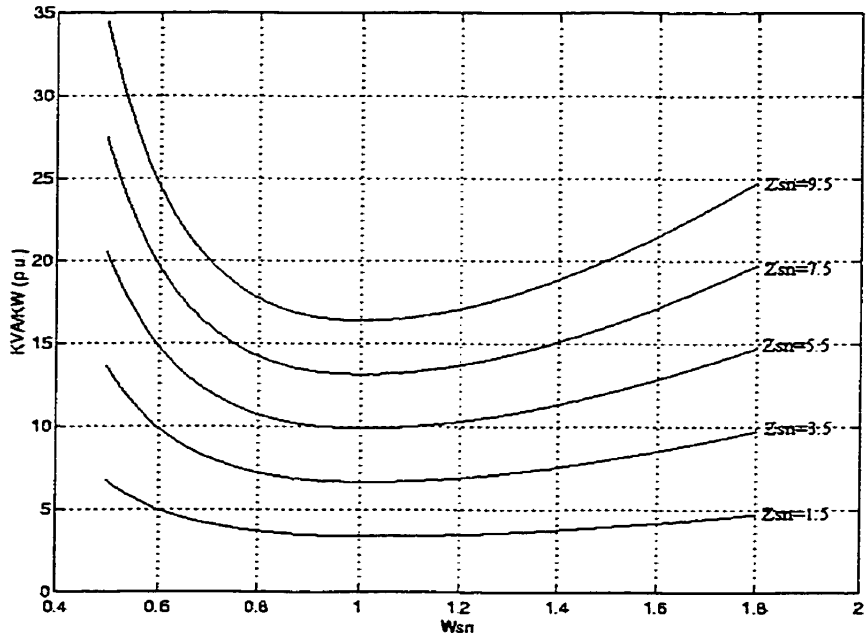

(b)

Figure 0.1: KVA/KW rating versus normalized frequency, ω_{sn}

$\delta = 175°$, $X_{Lsepn}=0$, $X_{Lm}=0.2$p.u.

(a) $Z_{pn}=1.5$, (b) $Z_{pn}=2.5$

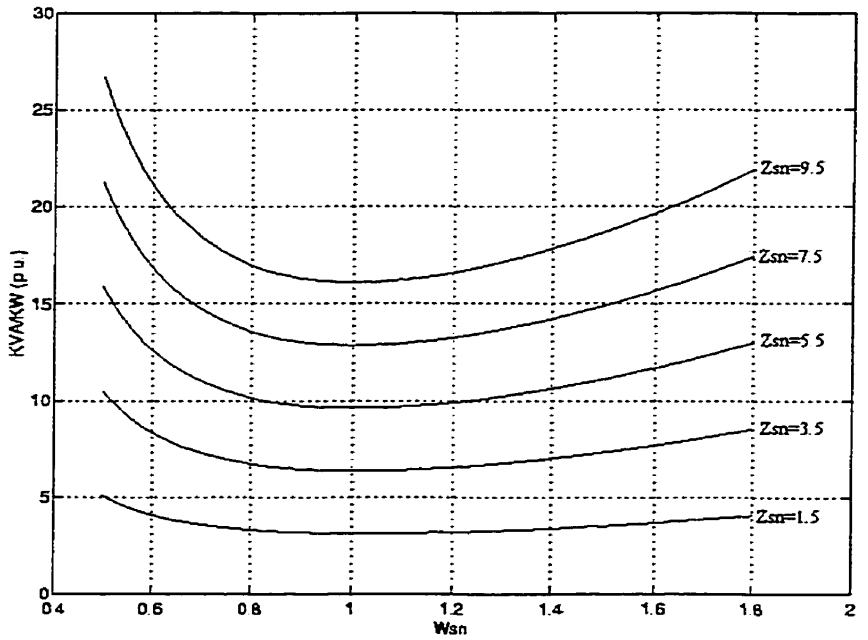

(a)

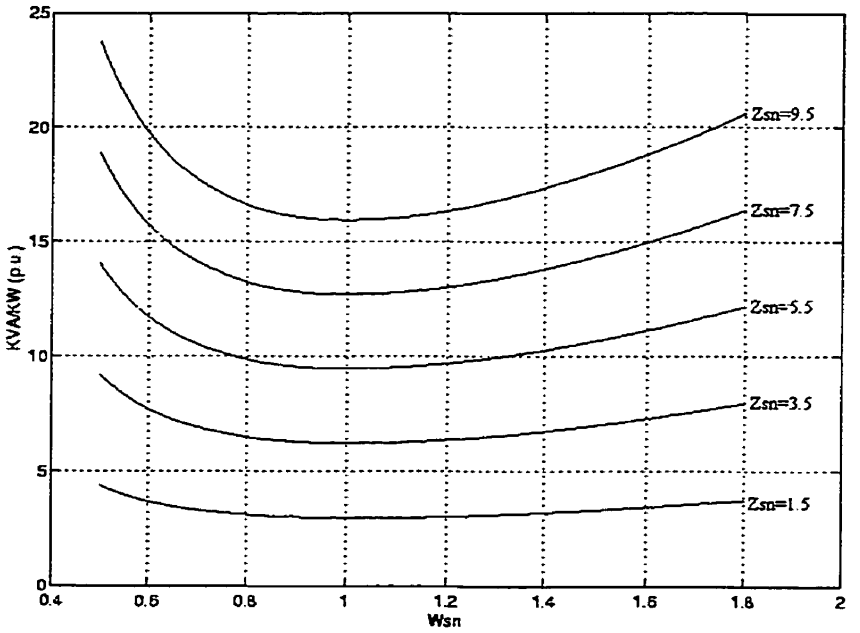

(b)

Figure 0.2: KVA/KW rating versus normalized frequency, ω_{sn}

$\delta = 175^{\circ}$, $X_{Lsepn}=0$, $X_{Lm}=0.2$p.u.

(a) $Z_{pn}=3.5$, (b) $Z_{pn}=4.5$

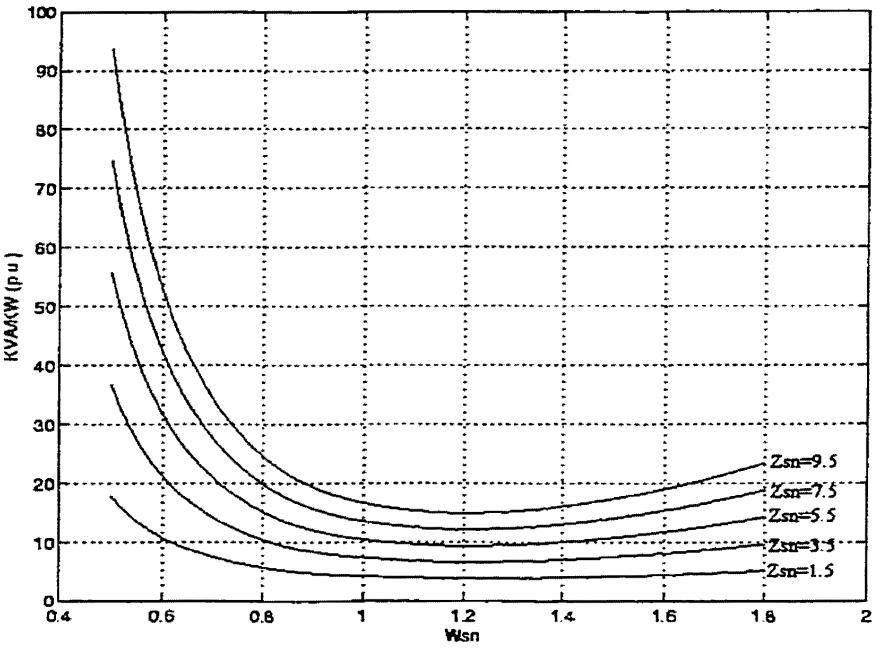

(a)

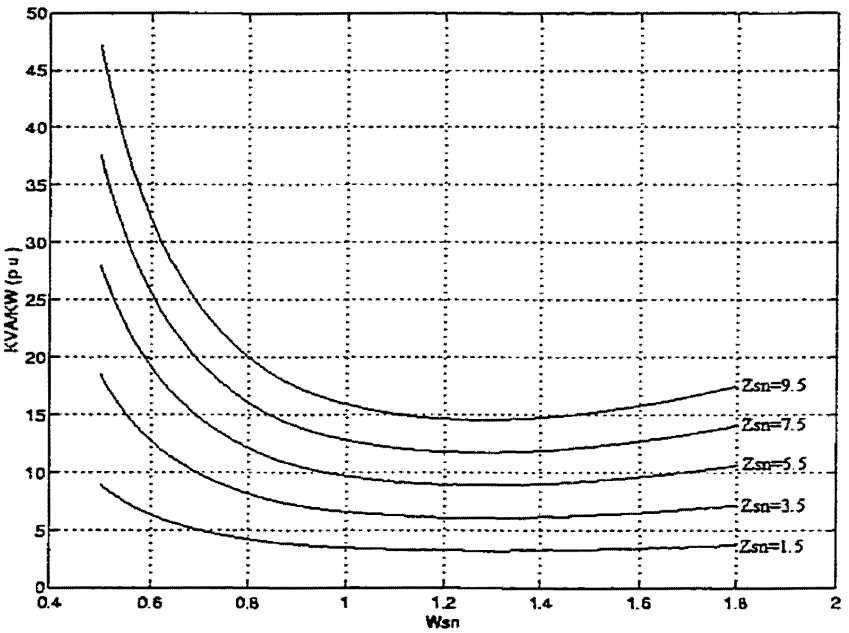

(b)

Figure 0.3: KVA/KW rating versus normalized frequency, ω_{sn}

$\delta = 175^{\circ}$, X_{Lsepn}=0.2p.u., X_{Ltn}=0.2p.u.

(a) Z_{pn}=1.5, (b) Z_{pn}=2.5

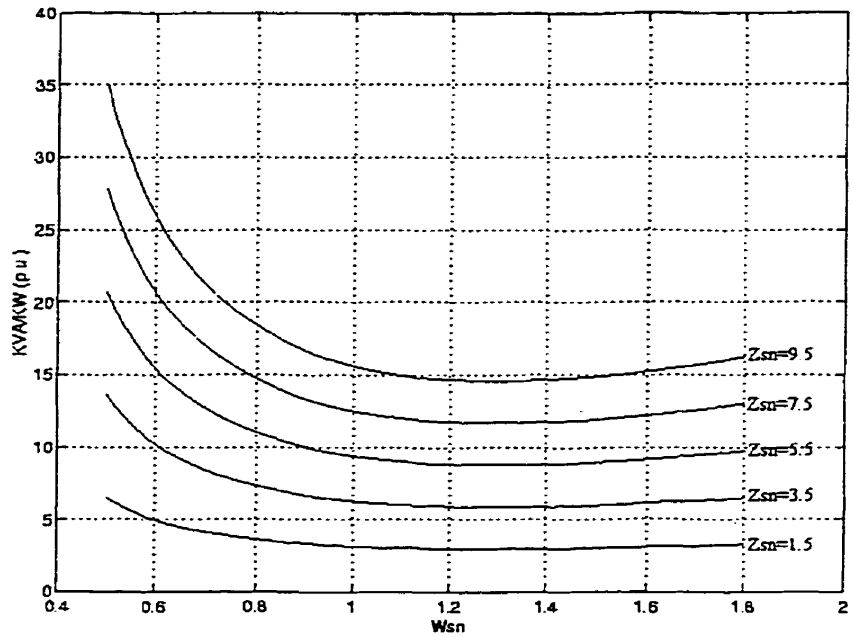

(b)

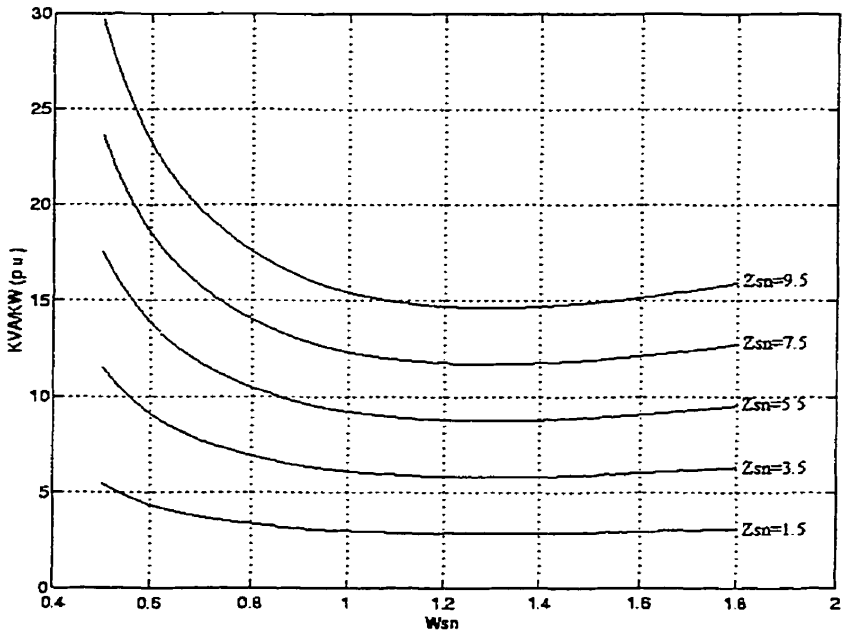

(b)

Figure 0.4: KVA/KW rating versus normalized frequency, ω_{sn}

$\delta = 175°$, X_{Lsepn}=0.2p.u., X_{Ltn}=0.2p.u.

(a) Z_{pn}=3.5, (b) Z_{pn}=4.5

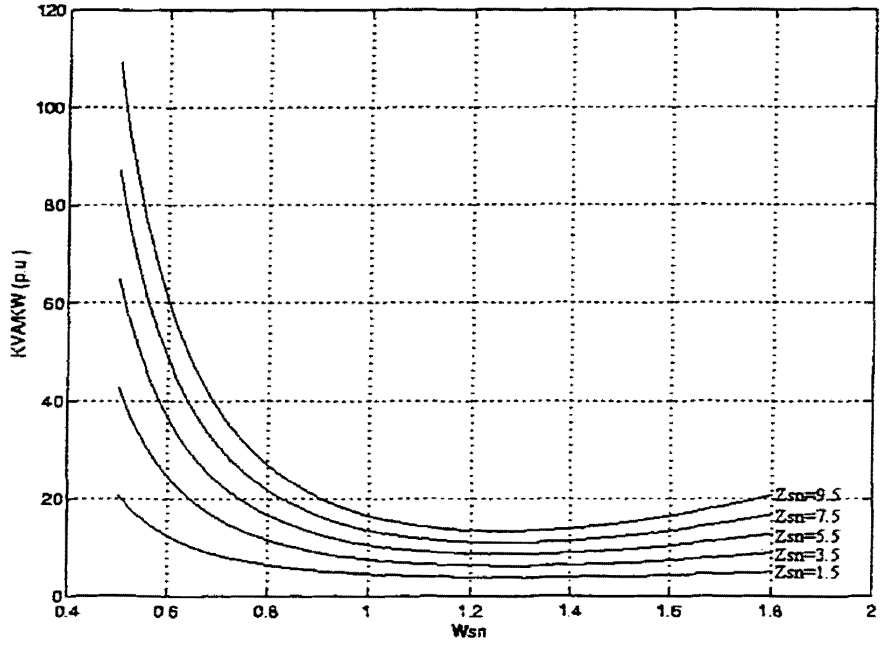

(a)

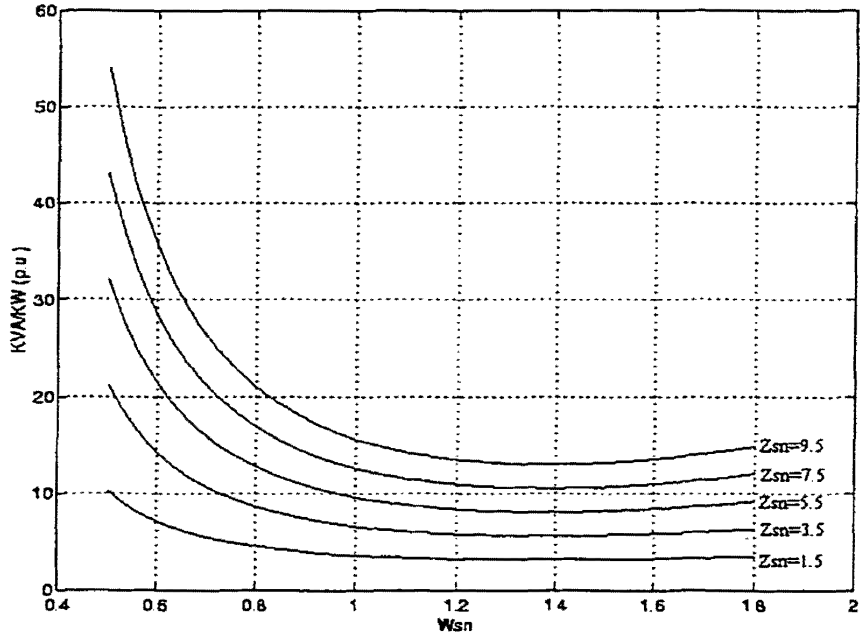

(b)

Figure 0.5: KVA/KW rating versus normalized frequency, ω_{sn}

$\delta = 175°$, X_{Lsepn}=0.4p.u., X_{Ltn}=0.2p.u.

(a) Z_{pn}=1.5, (b) Z_{pn}=2.5

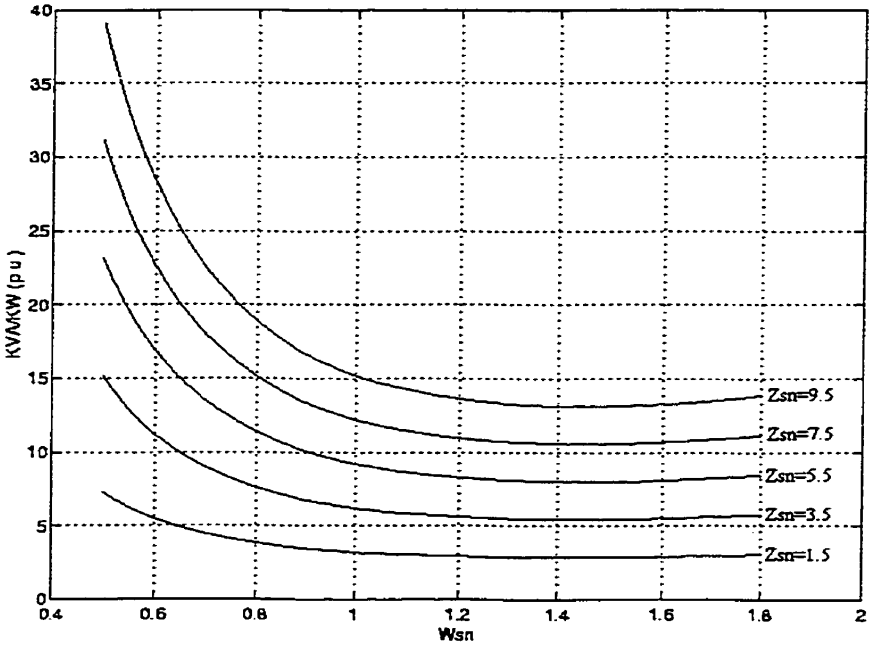

(a)

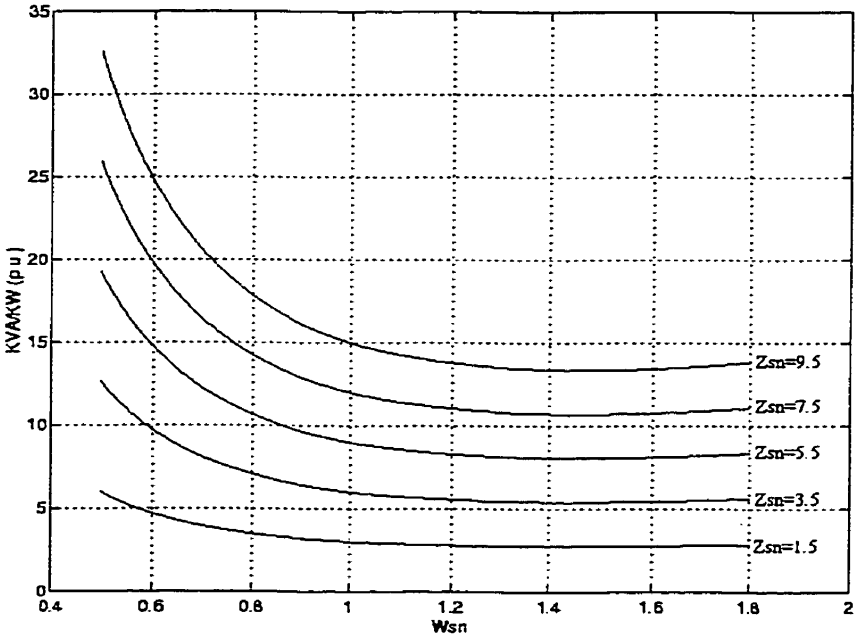

(b)

Figure 0.6: KVA/KW rating versus normalized frequency, ω_{sn}

$\delta = 175^{\circ}$, X_{Lsepn}=0.4p.u., X_{Ltn}=0.2p.u.

(a) Z_{pn}=3.5, (b) Z_{pn}=4.5

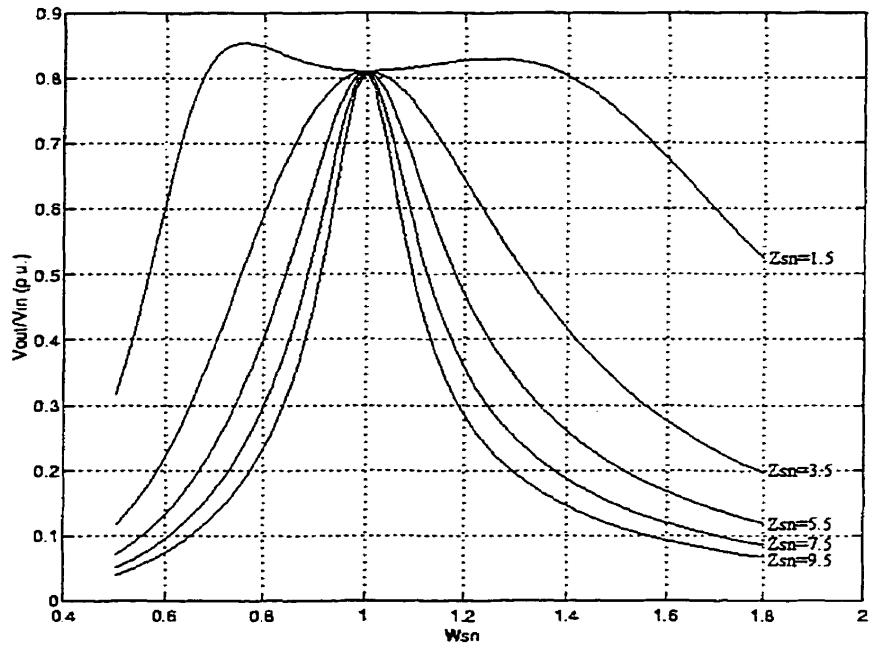

(a)

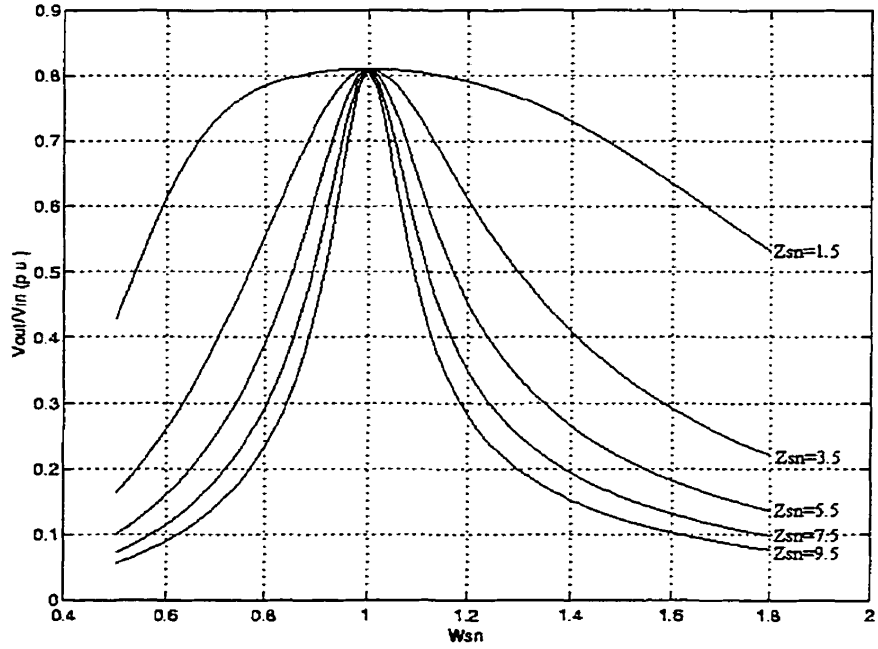

(b)

Figure 0.7: Voltage transfer ratio, M versus normalized frequency, ω_{sn}

$\delta = 175°$, $X_{Lsepn}=0$, $X_{Lm}=0.2$p.u.

(a) $Z_{pn}=1.5$, (b) $Z_{pn}=2.5$

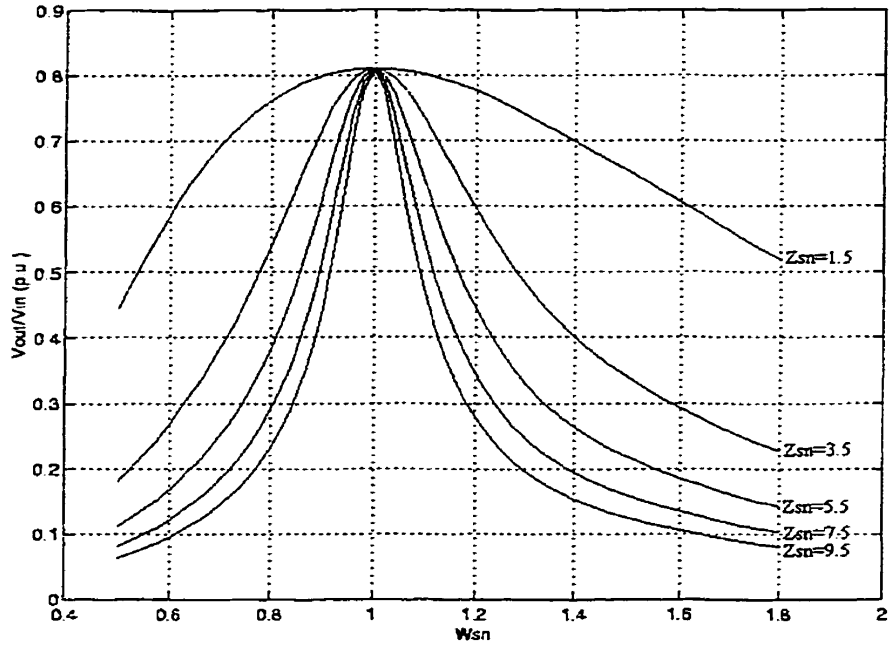

(a)

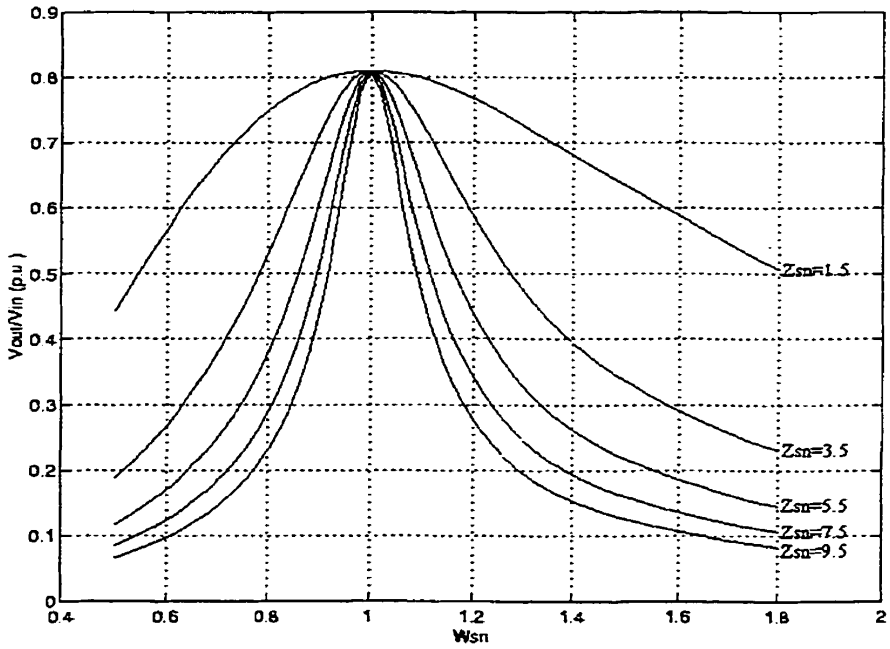

(b)

Figure 0.8: Voltage transfer ratio, M versus normalized frequency, ω_{sn}

$\delta = 175^{\circ}$, $X_{Lsepn}=0$, $X_{Ltn}=0.2$p.u.

(a) $Z_{pn}=3.5$, (b) $Z_{pn}=4.5$

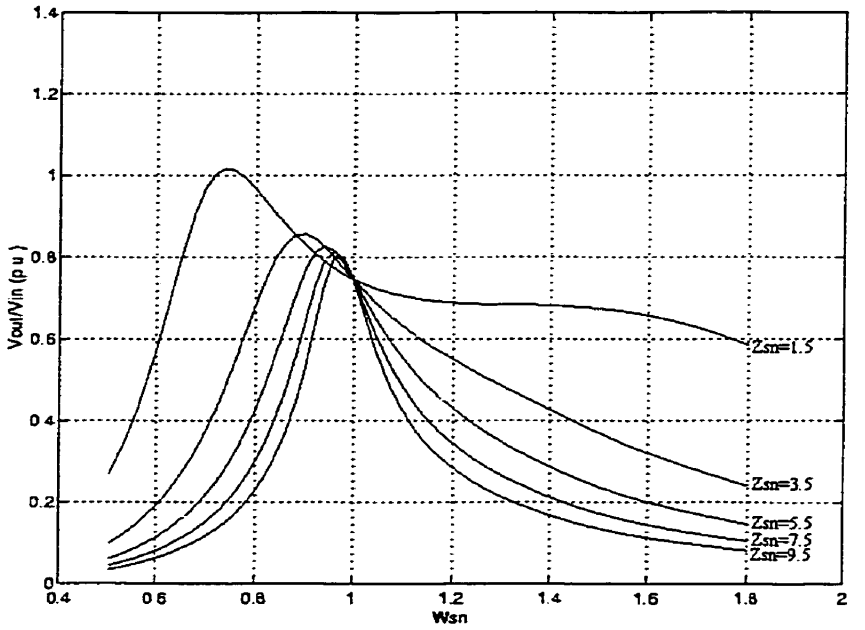

(a)

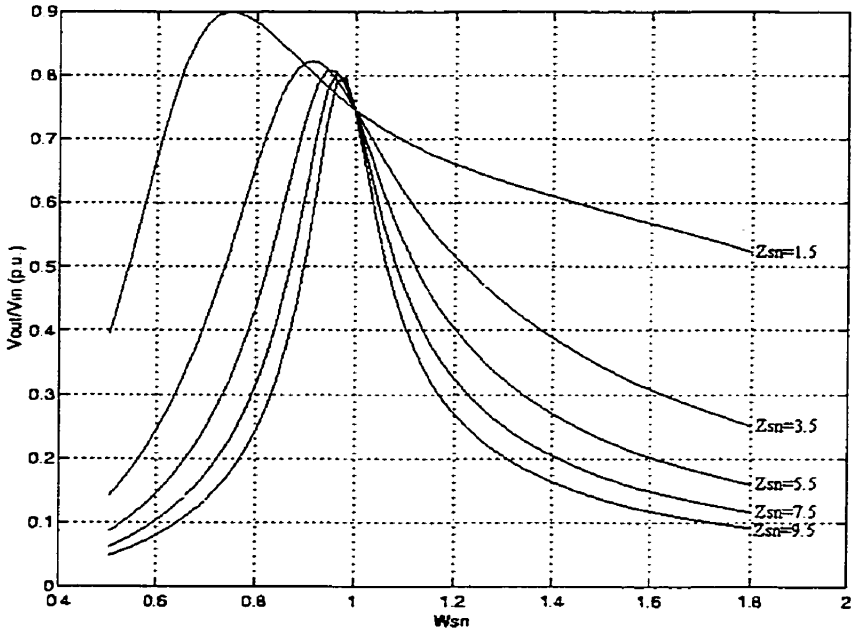

(b)

Figure 0.9: Voltage transfer ratio, M versus normalized frequency, ω_{sn}

$\delta = 175^{\circ}$, X_{Lsepn}=0.2p.u., X_{Ltn}=0.2p.u.

(a) Z_{pn}=1.5, (b) Z_{pn}=2.5

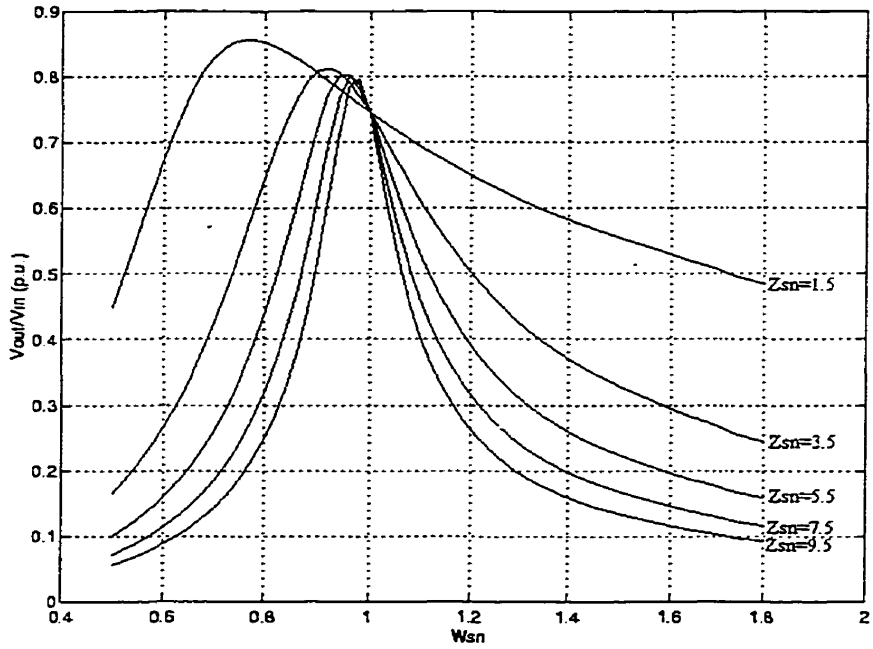

(a)

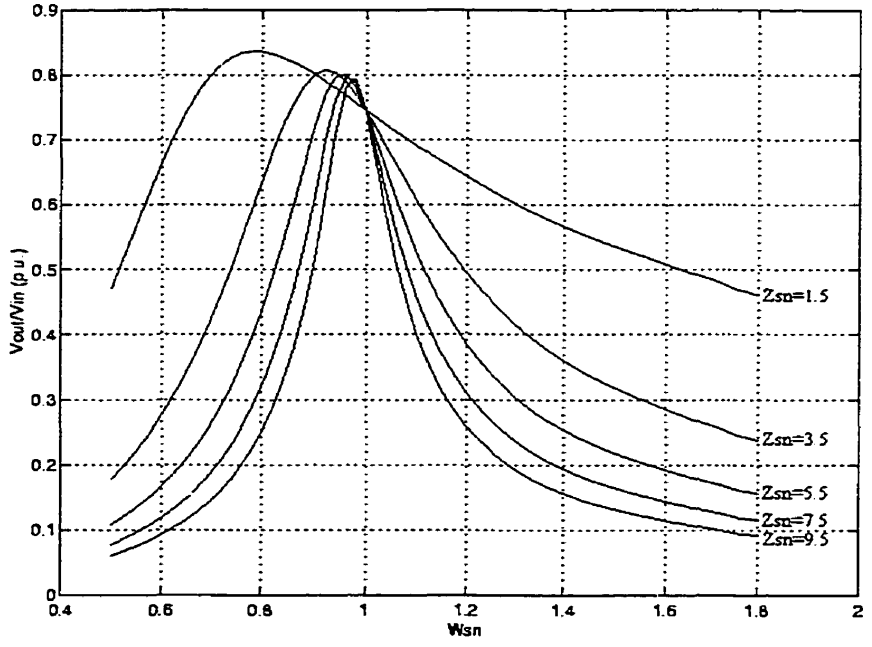

(b)

Figure 0.10: Voltage transfer ratio, M versus normalized frequency, ω_{sn}

$\delta = 175^{\circ}$, X_{Lsepn}=0.2p.u., X_{Lm}=0.2p.u.

(a) Z_{pn}=3.5, (b) Z_{pn}=4.5

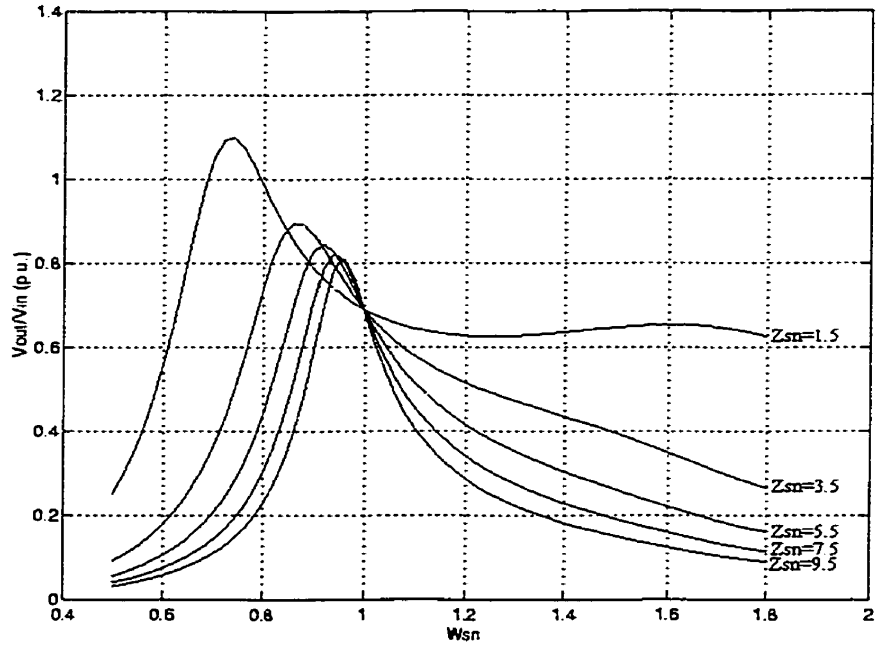

(a)

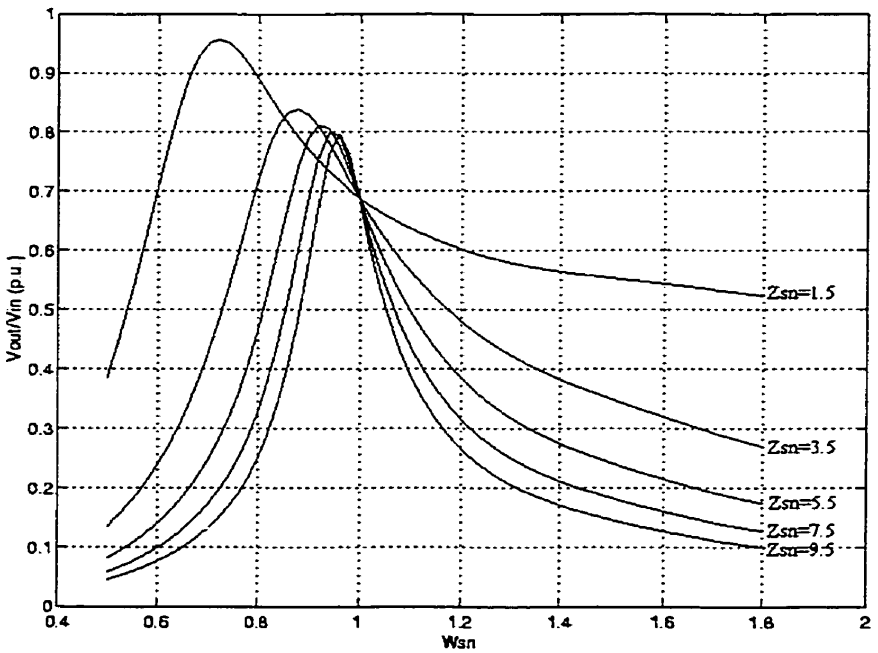

(b)

Figure 0.11: Voltage transfer ratio, M versus normalized frequency, ω_{sn}

$\delta = 175^{\circ}$, X_{Lsepn}=0.4p.u., X_{Ltn}=0.2p.u.

(a) Z_{pn}=1.5, (b) Z_{pn}=2.5

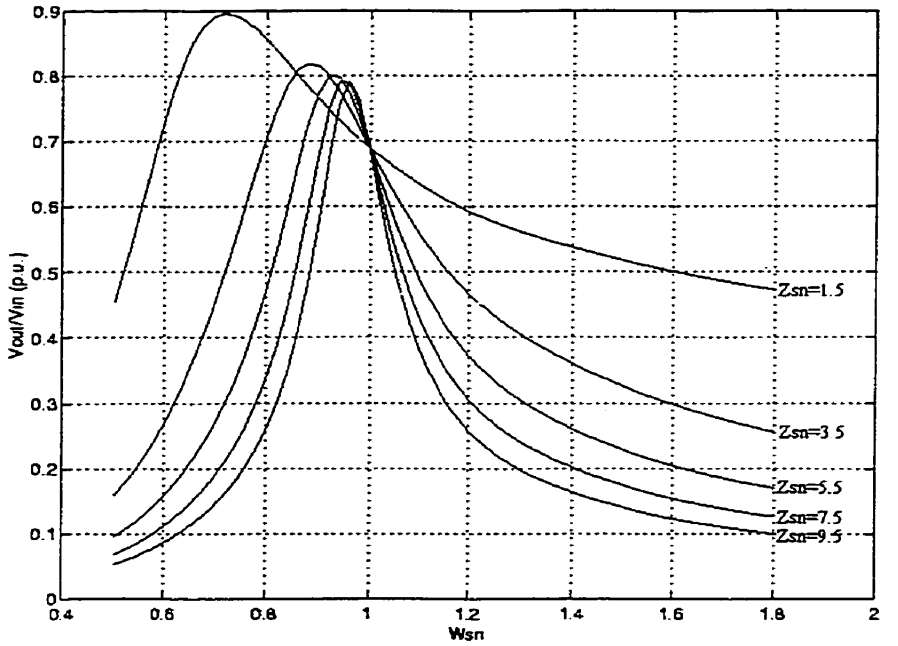

(a)

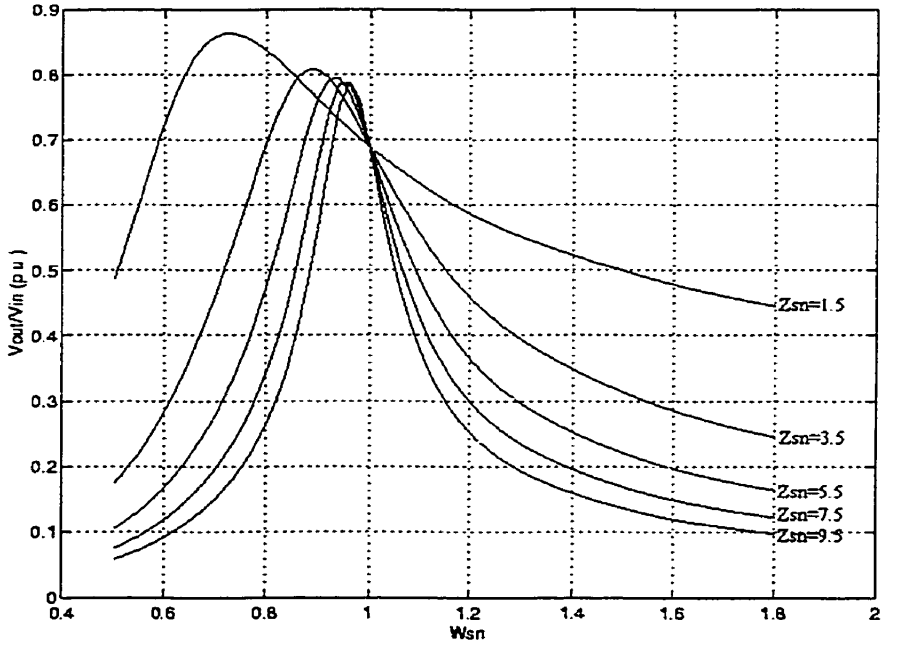

(b)

Figure 0.12: Voltage transfer ratio, M versus normalized frequency, ω_{sn}

$\delta = 175^{\circ}$, X_{Lsepn}=0.4p.u., X_{Ltn}=0.2p.u.

(a) Z_{pn}=3.5, (b) Z_{pn}=4.5

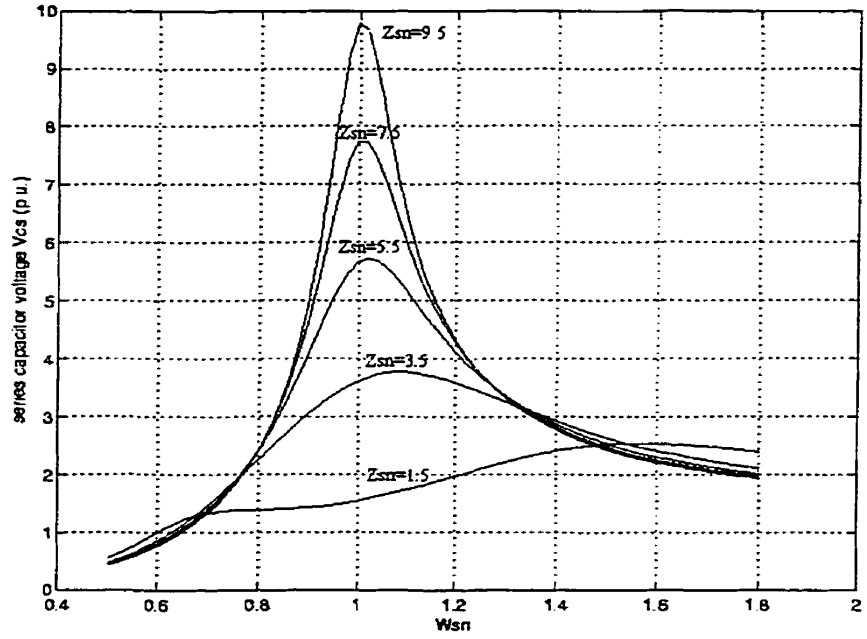

(a)

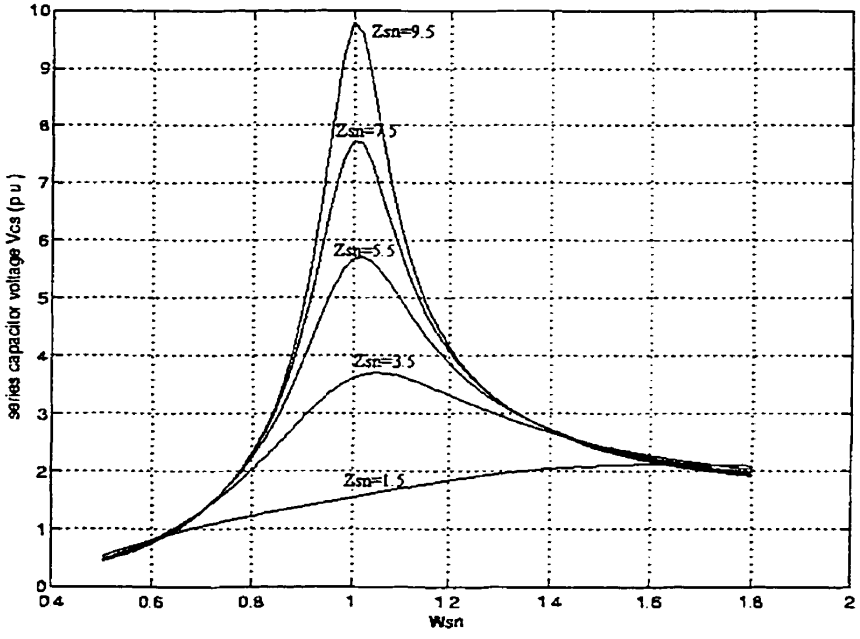

(b)

Figure 0.13: Peak capacitor voltage, v_{cs} versus normalized frequency, ω_{sn}

$\delta = 175°$, $X_{Lsepn}=0$, $X_{Ltn}=0.2$p.u.

(a) $Z_{pn}=1.5$, (b) $Z_{pn}=2.5$

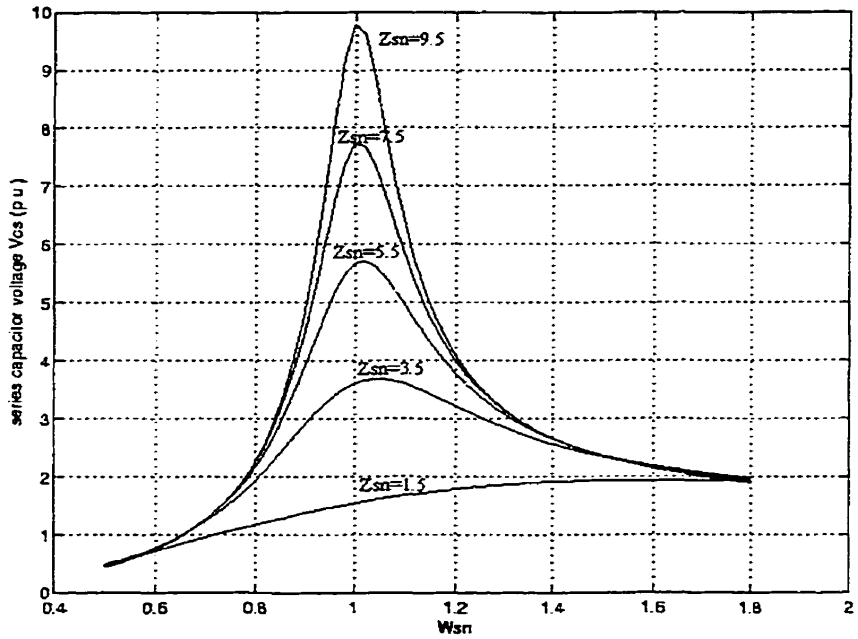

(a)

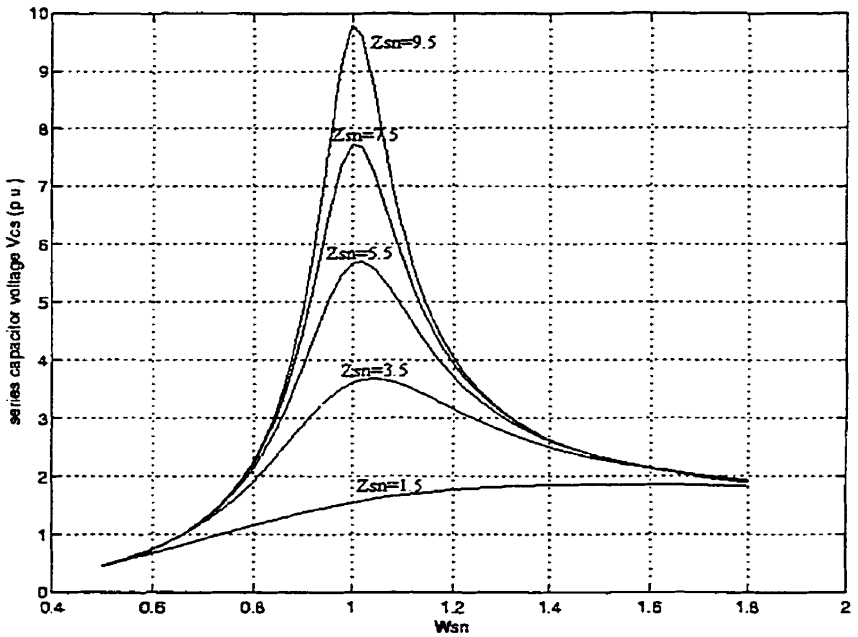

(b)

Figure 0.14: Peak capacitor voltage, v_{cs} versus normalized frequency, ω_{sn}

$\delta = 175^{\circ}$, $X_{Lsepn}=0$, $X_{Ltn}=0.2$p.u.

(a) $Z_{pn}=3.5$, (b) $Z_{pn}=4.5$

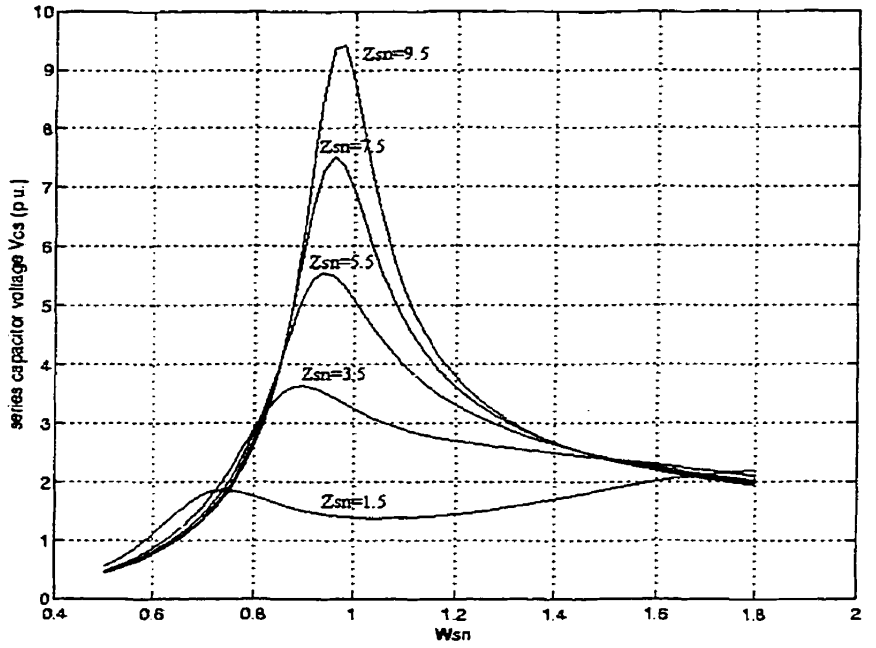

(a)

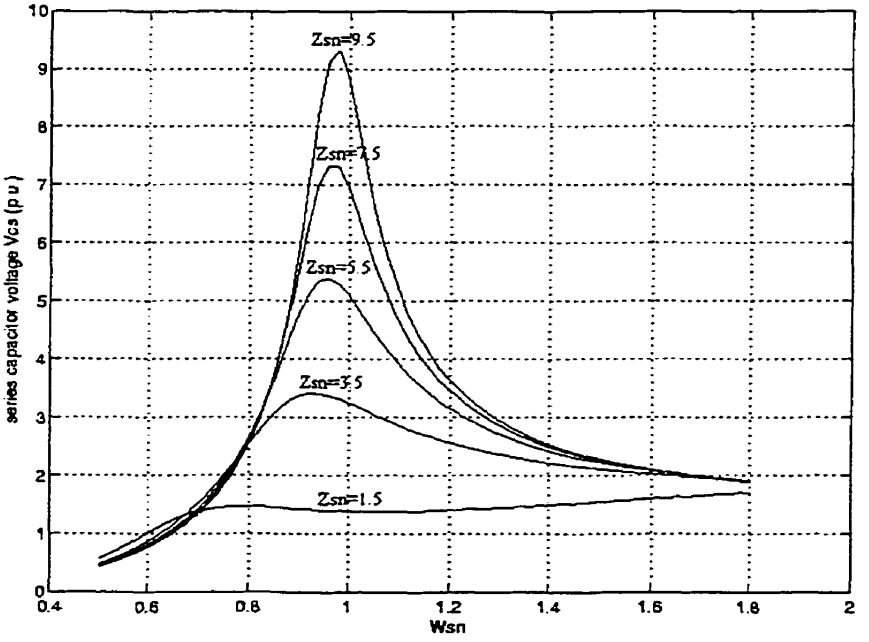

(b)

Figure 0.15: Peak capacitor voltage, v_{cs} versus normalized frequency, ω_{sn}

$\delta = 175^{\circ}$, X_{Lsepn}=0.2p.u., X_{Ltn}=0.2p.u.

(a) Z_{pn}=1.5, (b) Z_{pn}=2.5

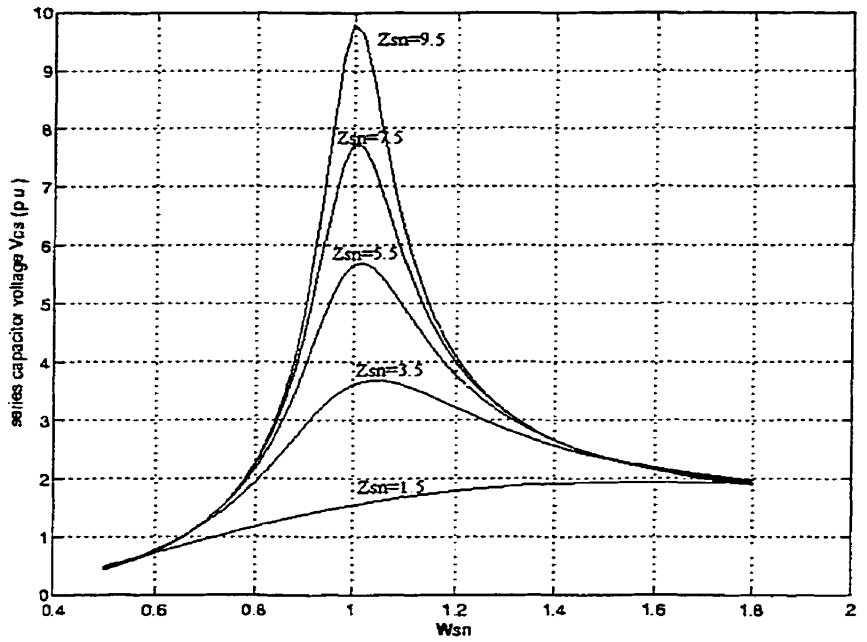

(a)

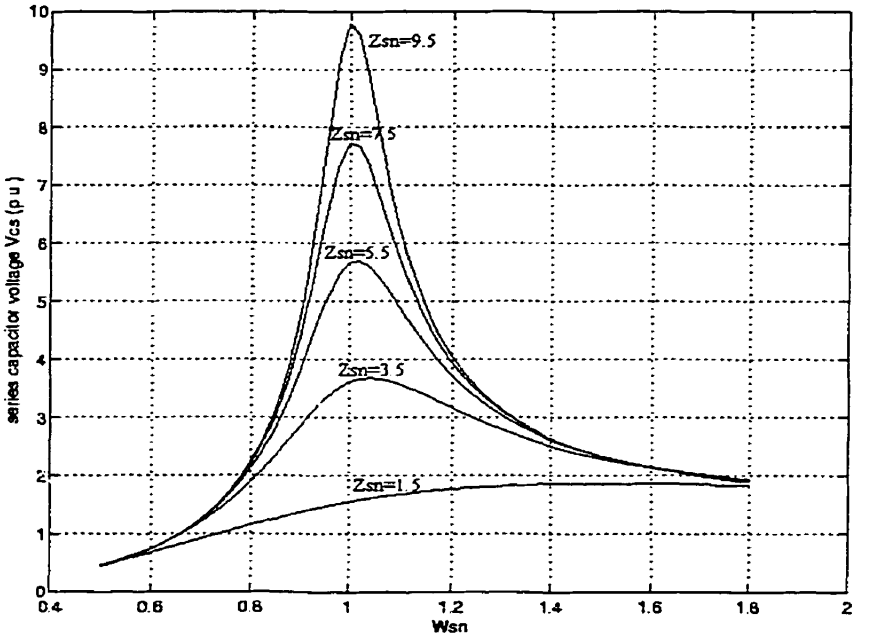

(b)

Figure 0.16: Peak capacitor voltage, v_{cs} versus normalized frequency, ω_{sn}

$\delta = 175^{\circ}$, X_{Lsepn}=0.2p.u., X_{Ltn}=0.2p.u.

(a) Z_{pn}=3.5, (b) Z_{pn}=4.5

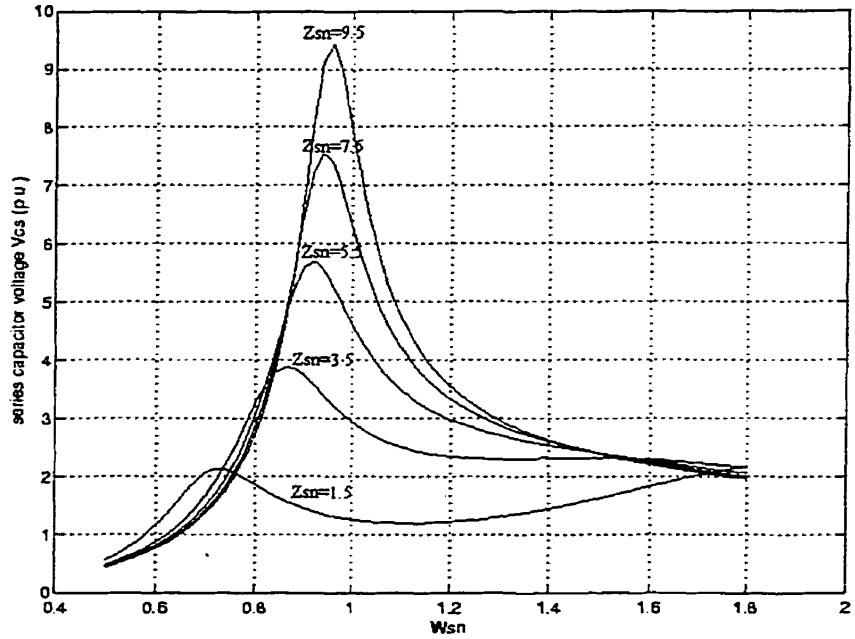

(a)

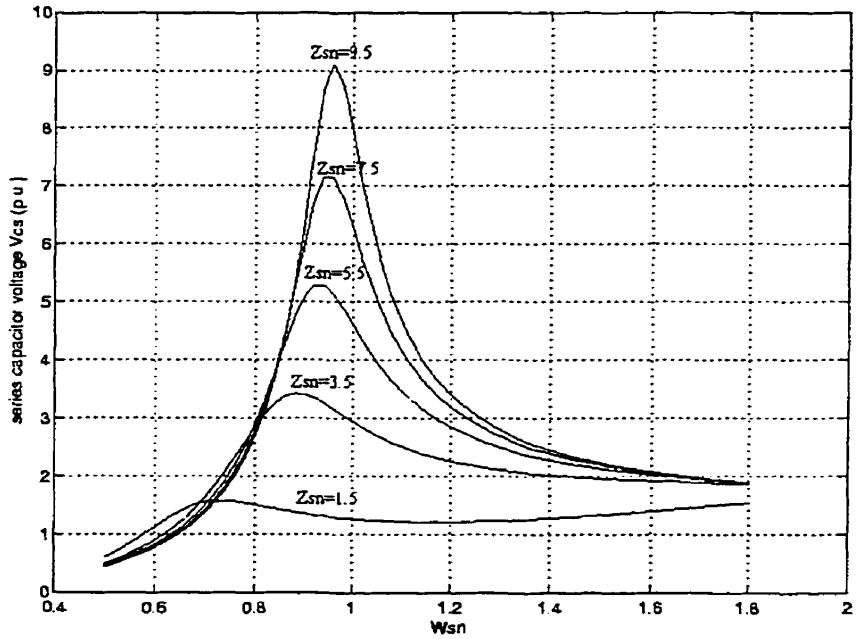

(b)

Figure 0.17: Peak capacitor voltage, v_{cs} versus normalized frequency, ω_{sn}

$\delta = 175^{\circ}$, X_{Lsepn}=0.4p.u., X_{Lin}=0.2p.u.

(a) Z_{pn}=1.5, (b) Z_{pn}=2.5

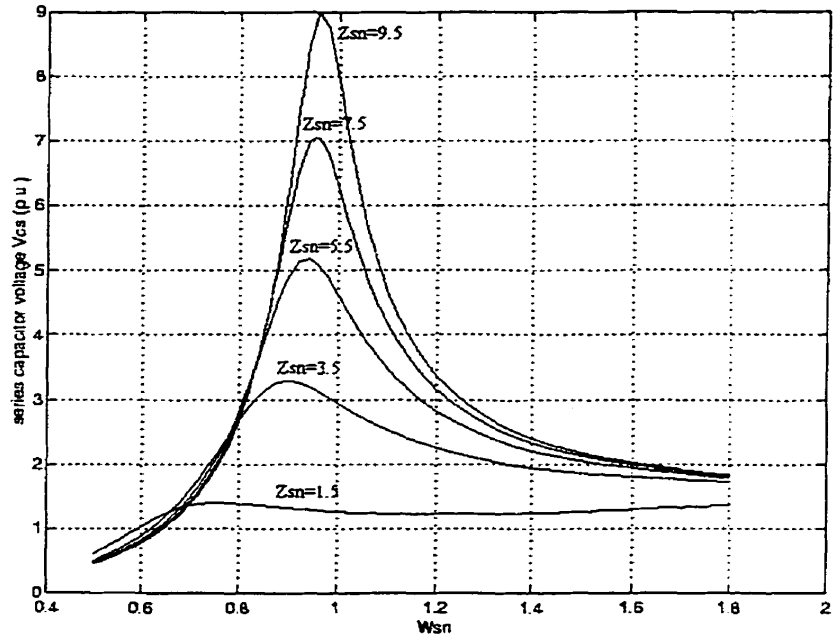

(a)

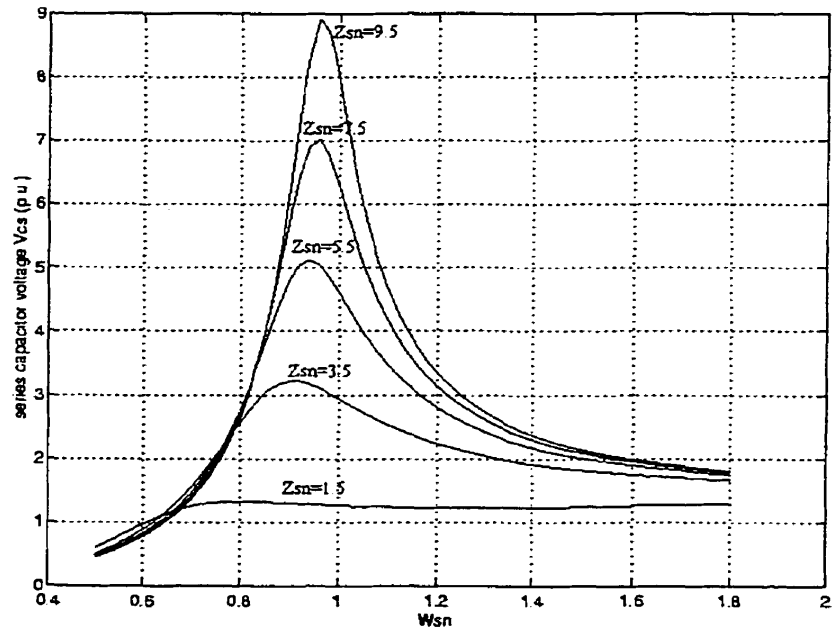

(b)

Figure 0.18: Peak capacitor voltage, v_{cs} versus normalized frequency, ω_{sn}

$\delta = 175^{\circ}$, X_{Lsepn}=0.4p.u., X_{Ltn}=0.2p.u.

(a) Z_{pn}=3.5, (b) Z_{pn}=4.5